STRUCTURAL AND BIOCHEMICAL STUDY OF VPS4

by

Han Han

A dissertation submitted to the faculty of
The University of Utah
in partial fulfillment of the requirements for the degree of

Doctor of Philosophy

Department of Biochemistry

The University of Utah

May 2014

ProQuest LLC.
789 East Eisenhower Parkway
P.O. Box 1346
Ann Arbor, MI 48106 - 1346

The University of Utah Graduate School

STATEMENT OF DISSERTATION APPROVAL

The dissertation of **Han Han**

has been approved by the following supervisory committee members:

Christopher P. Hill	, Chair	**Feb 4th, 2014** Date Approved
Wesley I. Sundquist	, Member	**Feb 4th, 2014** Date Approved
Michael S. Kay	, Member	**Feb 4th, 2014** Date Approved
Markus Babst	, Member	**Feb 5th, 2014** Date Approved
David P. Goldenberg	, Member	**Feb 5th, 2014** Date Approved

and by **Christopher P. Hill**, Chair/Dean of

the Department/College/School of **Biochemistry**

and by David B. Kieda, Dean of The Graduate School.

ABSTRACT

Vps4 is an AAA ATPase that functions in the ESCRT-mediated membrane fission process. Vps4 can use the energy from ATP hydrolysis to disassemble the ESCRT-III complexes. However, the mechanism of ESCRT-III disassembly by Vps4 is not clear. I have tried to address two major questions of Vps4 mechanism: how do monomers form the functional oligomer, and how does the functional Vps4 oligomer process its substrate ESCRT-III proteins. In Chapter 2, which was published recently, we reported that the functional state of Vps4 is a hexamer, and that the interface mediating hexamer formation has been conserved in highly diverse species. Chapter 3 describes my attempts to crystallize an assembled Vps4 hexamer. Despite considerable effort, I was not successful in obtaining crystals of assembled Vps4 that diffract to high resolution, although some preliminary crystals that appear to contain a complex of Vps4 hexamer and the substrate peptide were obtained and may serve as a guide for future efforts. In Chapter 4, I report that residues in helix5 of the Vps2/ESCRT-III protein form a secondary Vps4 binding site, and show that they bind to the pore loops of an asymmetric Vps4 hexamer in a 1:1 peptide:Vps4 hexamer stoichiometry. I further demonstrate that this interaction is negatively regulated by the N-terminal MIT domain of Vps4. These findings support a model of ESCRT-III disassembly in which the Vps4 hexamer pulls the C-terminal helix5 of ESCRT-

III into/through the central pore of the asymmetric Vps4 hexamer. In Chapter 5, I suggest future experiments that could be pursued to confirm this model and further advance understanding of the Vps4 mechanism.

TABLE OF CONTENTS

LIST OF TABLES

CHAPTER 1

INTRODUCTION

Overview of the ESCRT machinery

The endosomal sorting complexes required for transport (ESCRT) machinery was first identified in the multivesicular bodies (MVBs) biogenesis process[1; 2; 3; 4; 5]. Later, the ESCRT machinery was found to be required for other biological processes, such as HIV-1 budding[6; 7; 8; 9], mammalian cytokinesis[10; 11], and cell division in Crenarchaeal species[12; 13] (Figure 1.1 A). All of these processes entail membrane fission of the same topology[14]. Proteins that drive membrane fission reside within the thin membrane necks before membrane fission finishes [14](Figure 1.1 B, left). This is in contrast to the topology of clathrin-mediated endocytosis, in which dynamin mediates membrane fission from the outside face of the thin membrane tubes[15] (Figure 1.1 B, right). Different proteins/protein complexes of ESCRT machinery function sequentially. Early acting complexes are responsible for cargo sorting, recruiting late acting proteins/complexes, and/or membrane deformation[14]. Late acting proteins/complexes are responsible for membrane fission[14]. In this chapter I will summarize how the ESCRT machinery functions in different biological processes, including MVB biogenesis, mammalian cytokinesis, HIV-1 budding,

A:

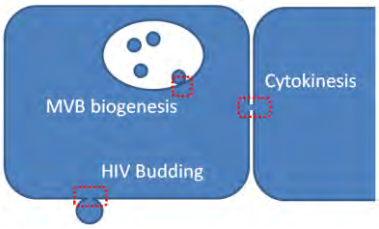

B:

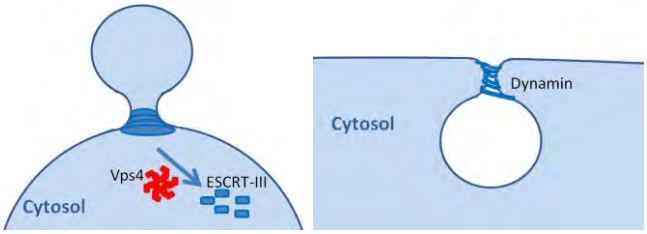

Figure 1.1 ESCRT mediated membrane fission.
A: Different biological processes require the ESCRT machinery for membrane fission.
B: Two different topologies of membrane fission. Left: ESCRT-III mediated membrane fission. ESCRT-III resides on the inside face of the thin tube during membrane fission for events that bud away from the cytosol. Right: Dynamin mediated membrane fission. Dynamin resides on the outside face of the thin tube for events that bud into the cytosol.

exosome budding, and Crenarchaeal cell division, and then review the current understanding of how ESCRT-III and Vps4 drive late stages of the pathway.

ESCRT and MVB biogenesis

The ESCRT machinery was first identified in MVB biogenesis [16]. MVBs are created during the sorting of various membrane proteins into intraluminal vesicles (ILVs) [16]. Modification of cargo proteins by ubiquitin provides a signal for them to enter into the MVB, and fusion of MVBs with lysosome can lead to their degradation [16].

Multiple ESCRT complexes function in different steps of MVBs biogenesis. The ESCRT proteins in yeast MVB biogenesis pathway will be outlined in this section, and they are conserved in higher eukaryotes, albeit with more variations.

ESCRT-0, which is comprised of a 1:1 complex HRS and STAM, functions in the recruitment of cargo proteins [14; 16; 17] (Figure 1.2 A). This heterodimer contains several ubiquitin binding motifs that can recognize ubiquitylated cargoes for recruitment [14]. HRS also contains a FYVE domain that can bind PI(3)P and promote membrane association [18]. Additionally, HRS contains a PSAP motif, which can bind to the ubiquitin E2 variant (UEV) domain of the ESCRT-I protein Vps23(TSG101), thereby recruiting the downstream ESCRT-I [19] (Figure 1.2 B).

A

B

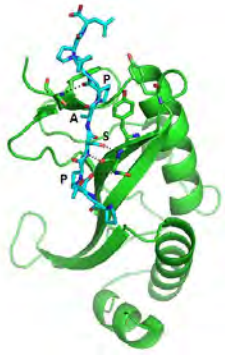

Figure 1.2. ESCRT-0 related protein complexes.
A: Structure of the coiled-coil complex formed by the helical domains of HRS (Cyan) and STAM (Magenta) (PDB ID: 3F1I).
B: Structure of the TSG101 UVE domain (Green) bound with PSAP motif from HRS (Cyan) (PDB ID: 3OBQ).

ESCRT-I comprises four different proteins: Vps23(TSG101), Vps28, Vps37, and MVB12 [14]. Its core forms an elongated structure of ~18nm, which can be divided into a headpiece part and a stalk part [20] (Figure 1.3 A). The headpiece contains fragments from all four proteins and the stalk contains Vps23 (TSG101), Vps37, and MVB12 [20] (Figure 1.3 A). The UEV domain of Vps23(TSG101), which can bind both the HRS PSAP motif [19] and ubiquitin [14], is linked to one end of the stalk. The C terminal domain of Vps28, which is linked to the headpiece, can bind the GLUE domain of the Vps36 ESCRT-II subunit, and thereby recruit ESCRT-II [21] (Figure 1.3 B).

A

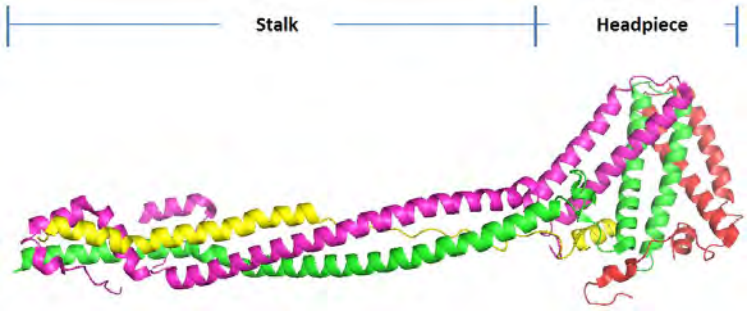

B

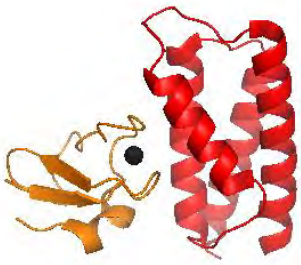

Figure 1.3. ESCRT-I related protein complexes.
A: Structure of ESCRT-I heterotetramer core composed of Vps23 (TSG101) (green), Vps28 (red), Vps37 (magenta), and MVB12 (yellow) (PDB ID: 2P22).
B: Structure of Vps28 C terminal domain (red) bound with Vps36 GLUE domain (orange) (PDB ID: 2J9U).

ESCRT-II is a Y-shape heterotetramer comprising one copy of Vps36, one copy of Vps22, and two copies of Vps25 [22] (Figure 1.4 A). The two copies of Vps25 form the two arms of the Y-shape structure, which can bind to two copies of Vps20, one of the ESCRT-III proteins [23] (Figure 1.4 B). In addition to binding ESCRT-I/Vps28 [21], the Vps36 GLUE domain forms yet another ESCRT ubiquitin-binding domain [14].

In vitro studies using purified ESCRT proteins and giant unilamellar vesicles (GUVs) indicated that ESCRT-I and ESCRT-II complexes can deform the membrane to project a nascent bud, which remains attached to the membrane, into the GUV [24]. ESCRT-I and ESCRT-II recruit ESCRT-III, which drives fission to sever the neck connecting the bud to the GUV [24; 25].

There are four core ESCRT-III proteins in yeast: Vps20, snf7, Vps24, and Vps2 [16]. Vps20 can be recruited by Vps25 of ESCRT-II [23] (Figure 1.4B). Vps20 then recruits Snf7, the most abundant subunit in assembled ESCRT-III complexes, which can form large polymers on the membrane [26; 27]. Snf7 in turn recruits Vps24 and Vps2 [26]. Vps24 functions as a capping protein to limit Snf7 polymerization [26; 27]. Vps2 can recruit the Vps4 ATPase complex, which disassembles ESCRT-III complexes and may function directly in membrane fission [26; 28].

Vps4, the only ATPase in the ESCRT machinery, provides energy for progression through the pathway. Vps4 contains an N-terminal MIT domain that binds with the C-terminal MIM motif of ESCRT-III proteins [28; 29; 30]. This is followed by a ~40 Residue linker and an AAA+ ATPase cassette [31]. The AAA+

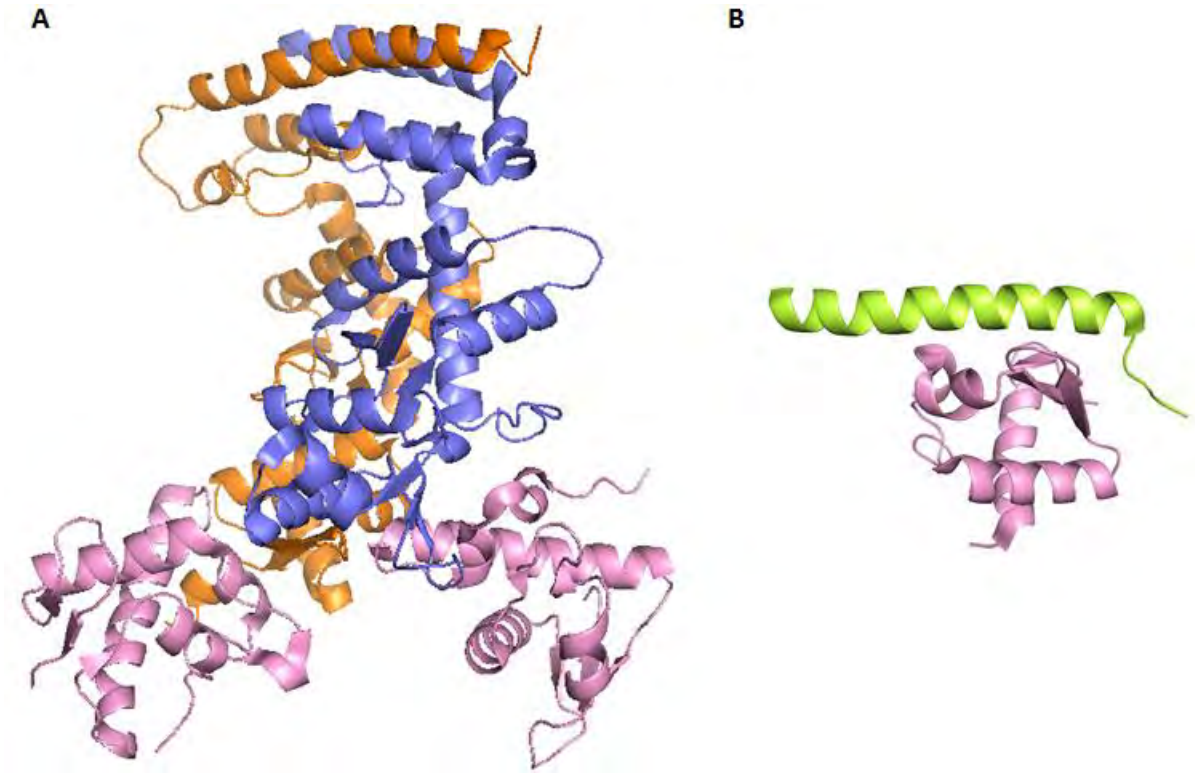

Figure 1.4. ESCRT-II related protein complexes.
A: Structure of ESCRT-II heterotetramer core composed of Vps36 (orange), Vps22 (blue), and two copies of Vps25 (pink) (PDB ID: 2ZME).
B: Structure of hVps25 (EAP20) C terminal domain WH2 domain (pink) bound with helix 1 of hVps20 (CHMP6) (green) (PDB ID: 3HTU).

ATPase proteins typically function as oligomers [32; 33], and Vps4 appears to be functional as a hexamer in the presence of ATP (see Chapter 2). Vps4 uses the energy from ATP hydrolysis to disassemble ESCRT-III complexes and may also function directly in the membrane fission event [34]. Disassembly of ESCRT-III complexes may lead to recycling of ESCRT-III protein, although the mechanism is not clear yet [24; 25]. ESCRT-III and Vps4 drive fission and recycling; they are the most fundamental of ESCRT components and are required for all known ESCRT-dependent processes[14].

ESCRT and HIV-1 budding

Many different classes of viruses use the ESCRT machinery to egress cells, with the most extensively studied being HIV-1[35; 36]. HIV is a retrovirus whose virion displays a membrane that is derived from the plasma membrane of the host cells [35; 36]. To be released from the host cells, an ESCRT-driven membrane fission step is necessary to 'cut' the linkage between the budding virion and the host membrane [35; 36]. ESCRT machinery was recruited to the budding site by the HIV Gag protein, which is the major structural polyprotein of the virus and includes a C-terminal p6 domain that contains two different late (L) domains that recruit early-acting ESCRT protein/complexes [6; 37]. There are two different late domain motifs in p6: PTAP and YPXL [6; 37].

The Gag/p6 PTAP (proline-threonine-alanine-proline) motif binds to a hydrophobic groove on the ubiquitin E2 variant (UVE) domain of the TSG101 subunit of ESCRT-I [19] (Figure 1.5 A). This interaction mimics the interaction between the TSG101 UVE domain and the PSAP motif of the ESCRT-0 subunit HRS (Figure 1.2 B) [19], thereby explaining how HIV-1 can be recruited as an ESCRT pathway substrate [6].

The YPXL (tyrosine-proline-x-leu; x refers to any 1 or 3 residue(s)) motif binds the V domain of the cellular protein ALIX [38; 39]. ALIX contains an N-terminal Bro1 domain, followed by a V domain and a C-terminal proline-rich C-terminal domain (PRD) [38]. The YPXL motif binds to arm-2 of the V domain, with the bulky side-chain of the tyrosine inserted into a hydrophobic pocket on the V domain and the downstream leucine making contact with a hydrophobic surface near the

A:

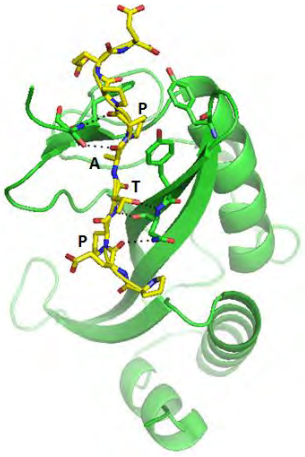

B:

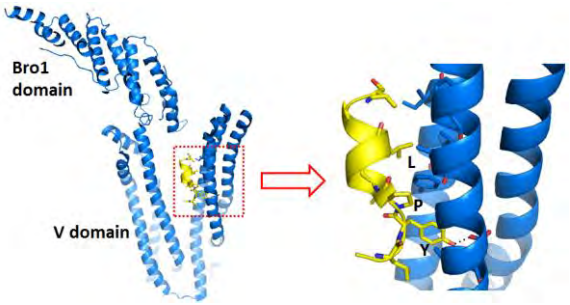

Figure 1.5. Recruitment of ESCRT machinery by HIV late domain.
A: Structure of the complex formed by HIV PTAP motif (yellow) and TSG101 UVE domain (green) (PDB ID: 3OBU).
B: Structure of the complex formed by HIV YPXL motif (yellow) and Alix (blue) (PDB ID: 2R02).

pocket [38; 39] (Figure 1.5 B). Recently, this interaction was found to mimic the interation between the YPXL motif of human syntenin and ALIX [40]. Thus, both of the ESCRT interacting motifs on HIV Gag mimic the existing ESCRT interacting motifs in human cells to recruit ESCRT machinery. Following ALIX and/or ESCRT-1 complexes, the late ESCRT proteins including ESCRT-III and Vps4 are recruited to the virus budding sites.

ESCRT-III and Vps4 are the executors of the membrane fission step during HIV budding [36]. Despite extensive study, it is still not clear how TSG101 recruits ESCRT-III [36]. ESCRT-II complex bridges ESCRT-I and ESCRT-III in MVB biogenesis, but it seems not to be necessary for the HIV budding process based on RNAi knock down studies [41]. However, in vitro studies using GUV and purified proteins indicate that ESCRT-II co-localizes with ESCRT-I and the Gag protein [42]. Thus, whether ESCRT-II or some other protein(s) bridging ESCRT-1 and ESCRT-III during HIV budding remains an open question.

How the alternative YPXL-ALIX pathway recruits ESCRT-III proteins is relatively clear [36]. The N-terminal Bro1 domain of ALIX binds the CHMP4 ESCRT-III subunits [43] (Figure 1.6). The C-terminal residues of CHMP4 proteins form an amphipathic helix, with its hydrophobic surface binding to the concave surface of the banana-shaped Bro1 domain [43] (Figure 1.6). Thus, ALIX can bridge the HIV Gag protein and the ESCRT-III complexes, with its V domain binding to the YPXL motif of Gag protein and its Bro1 domain binding to the C-terminal helix of CHMP4 proteins, respectively.

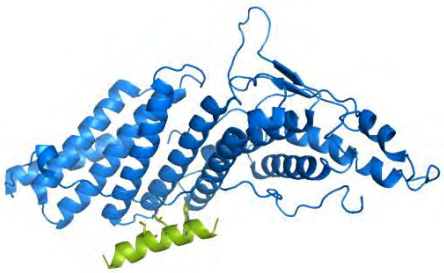

Figure 1.6. Recruitment of ESCRT-III by ALIX.
Structure of the complex formed by ALIX Bro1 domain (blue) and the C-terminal helix of CHMP4B (green) (PDB ID: 3C3Q).

The ESCRT-III proteins recruited by ALIX induce membrane fission at the neck that connects the HIV virion and the plasma membrane of the host cell. There are 12 ESCRT-III proteins in human cells: the charged multivesicular protein (CHMP) variants 1A, 1B, 2A, 2B, 3, 4A, 4B, 4C, 5, 6, and 7, and IST1 [16]. Of these ESCRT-III proteins, only CHMP2 and CHMP4 proteins are necessary for the HIV budding process [44]. CHMP2A and CHMP4B bind each other in an interaction that is necessary for HIV budding [44]. While the C-terminal residues of CHMP4 bind ALIX, the C-terminal residues of CHMP2 proteins contain an MIM1 motif that binds the MIT domain at the N-terminus of Vps4 [29].

There are two Vps4 isoforms in human cells, VPS4A&B [16]. Knocking down both VPS4A and VPSB can inhibit HIV budding, and this inhibition can be rescued by expressing VPS4B alone [30]. Thus, it seems VPSB alone is sufficient for accomplishing HIV budding.

ESCRT and cytokinesis

The last step of cytokinesis is abscission, by which one cell is split topologically into two daughter cells [45; 46]. This step is mediated by ESCRT machinery [46]. Immediately prior to abscission, the two daughter cells are connected by a structure known as the midbody [45]. Different ESCRT proteins/complexes are recruited to the midbody [46]. Similar to the HIV budding process, TSG101 and ALIX are the early-acting ESCRT machinery recruited to the membrane fission site [10; 46; 47].

The midbody protein CEP55 is responsible for recruiting the ESCRT machinery [10; 47]. CEP55 contains an ESCRT- and ALIX-binding region (EABR) (160-217) to recruit the ESCRT-1 subunit TSG101 and ALIX [47]. Two copies of EABR form a coiled-coil dimer that contains one binding site for TSG101 or ALIX [47] (Figure 1.7). The proline-rich tail of ALIX contains a $GPPX_3Y$ motif that binds to the EABR of CEP55 [47] (Figure 1.7). The $GPPX_3Y$ motif wraps around the protruding side chain of Tyrosine187 of the EABR motif of CEP55 [47] (Figure 1.7). The two proline residues on the $GPPX_3Y$ motif form a hydrophobic interface with the side chains of Tryptophan184 and Tyrosine187 of the EABR motif [47] (Figure 1.7). The side chain of the C-terminal $GPPX_3Y$ Tyrosine also contributes to the binding to EABR by (1) inserting between the two bulky side chains of Tyrosine187 and Tryptophan194 of the EABR and (2) forming a hydrogen bond to the side chain of Glutamate192 of EABR [47] (Figure 1.7). The ESCRT-I subunit TSG101 also contains a $GPPX_3Y$ motif, which can compete with ALIX for binding to EABR [47]. This indicates that one copy of EABR dimer can only bind to one ALIX or one TSG101 [47].

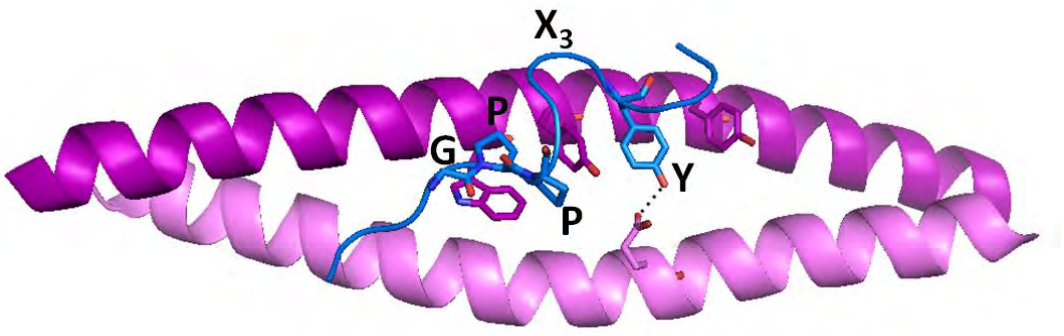

Figure 1.7. Recruitment of ESCRT machinery by CEP55.
Structure of the complex formed by CEP55 EABR dimer (purple) and $GPPX_3Y$ motif of ALIX (blue) (PDB ID: 3E1R).

Similar to the HIV budding process, how ESCRT-III is recruited by ESCRT-I for cytokinesis is not clear, and ESCRT-II appears not to be required [10]. Also similar to HIV budding, ALIX appears to recruit the ESCRT-III subunit CHMP4 [43].

Besides Vps4, another AAA ATPase called spastin is also recruited to the midbody [48]. Like Vps4, spastin contains an MIT domain, which is known to interact with the C-terminal MIM tail of CHMP1B [48]. This interaction is important for the recruitment of spastin to the midbody, which permits the spastin to cleave the microtube at the abscission site, accomplishing a vital aspect of cytokinesis [48].

ESCRT and exosome budding

Exosomes are a class of secreted extracellular vesicles containing molecules involved in cell-cell communication [40]. Cargo molecules are attached to the membrane of endosomes and the membrane buds into the intro lumen to from MVBs with the help of the ESCRT machinery [40]. Recruitment of the ESCRT machinery during this step is accomplished by the syndecans-syntenin-ALIX bridge [40]. Finally, exosomes are released to the outside of cells by fusion of MVBs with plasma membrane [40].

Syndecans are ubiquitous transmembrane proteins that are important for exosome biogenes, which contain a short cytoplasmic domain which can bind to Syntenin [40]. Syntenin contains a 100-amino acid N-terminal domain, two PDZ domains, and a C-terminal domain [40]. The N-terminal domain contains three $LYPX_nL$ motifs which can bind to the V domain of ALIX. ALIX will then recruit the ESCRT-III proteins [40]. The $LYPX_nL$ motif has been identified in the late domain of

the HIV Gag protein, which also recruits ALIX during the HIV budding process [37; 38; 39]. So, HIV uses a sequence motif from syntenin to hijack the ESCRT machinery to complete the membrane fission step of the virion budding process.

ESCRT in Crenarchaea

Homologs of components of the ESCRT machinery have also been identified in some Crenarchaeal species [49; 50]. It has been shown to be involved in the cell division process and to be hijacked by the virus of archaeal species [12; 13; 51]. This indicates that the ESCRT machinery is conserved during evolution. Three genes cdvA, cdvB, and cdvC, which are under the same operon, constitute the ESCRT machinery in Crenarchaea [52].

CdvA was predicted to contain an N-terminal beta-barrel domain followed by an alpha-helix-rich region and a C-terminal tail [53]. CdvA can interact with the lipid membrane, and the membrane binding motif(s) exist in the C-terminal region including the helix-rich region and the C-terminal tail [53]. The C-terminal tail of CdvA can interact with the C-terminal winged-helix (wH)-like domain of CdvB (Figure 1.8 A), which is necessary to recruit CdvB to the membrane [53]. The C-terminal tail was named E3B (ESCRT-III binding) [53].

EM study of purified CdvA from *Metallospherae sedula* indicated that it can form double helical filaments with diameter ranges from 8 to 11 nm in vitro [53]. This structure can be stabilized by DNA, which is similar to the known bacterial DNA partitioning proteins [53]. The biological significance of these double helical filaments is not clear yet.

Figure 1.8. ESCRT complexes from Crenarchaea.
A: Structure of a complex formed by C-terminal tail of CdvA (purple) and C-terminal wH-like domain of CdvB (green) (PDB ID: 2XVC). B: Structure of a complex formed by CdvB MIM motif (green) and CdvC MIT domain (cyan) (PDB ID: 2W2U).

CdvB is the paralog of ESCRT-III protein [52]. It contains an ESCRT-III core fold on the N-terminus, a MIM2 motif which can interact with the MIT domain of CdvC (Vps4)[12], and a C-terminal wH-like domain which can interact with the C-terminal tail of CdvA [53]. Three other ESCRT-III like proteins have also been discovered in *S. solfataricus*, but their implication in cell division is not clear yet [12].

Purified N-terminal ESCRT-III core fold of CdvB can form filaments in vitro, which is similar to the eukaryotic ESCRT-III proteins [52]. The MIM2 motif following the ESCRT-III core fold can bind to the groove between helix 1 and helix 3 of the MIT domain of CdvC [12] (Figure 1.8 B), which is very similar to the interaction between the MIM2 of hCHMP6 and MIT of Vps4A.

The C-terminal winged-helix region of CdvB contains a “broken” wing (Figure 1.8A). The classic wH fold usually contains three beta strands. The C-terminal wH fold of CdvB contains only two beta strands, and E3B region from CdvA binds between the two beta strands of CdvB to form the third beta strands [53] (Figure 1.8 A). So, the C-terminal region of CdvB and the C-terminal E3B tail of

CdvA form a classic wH-fold together [53]. This interaction is necessary for recruiting CdvB to the membrane as the CdvB cannot bind to the membrane by itself [53].

CdvC is the paralog of Vps4 in Crenarchaeal species [52]. It is structurally similar to eukaryotic Vps4 (see Chapter 2). It consists of an N-terminal MIT domain, a linker region, and a C-terminal AAA+ ATPase cassette. The MIT domain is a three-helix-bundle, which can interact with the MIM2 motif of CdvB (Figure 1.8 B). We determined the structure of the C-terminal AAA+ ATPase cassette recently, which is very similar to the structure of Eukaryotic Vps4 (see Chapter 2). Like eukaryotic Vps4, CdvC also forms a ring-like oligomer, which is thought to be the active form [52]. Consistent with their living environment, CdvC from thermophilic Crenarchaeal species can hydrolyze ATP only under high temperature [52].

ESCRT-III mediated membrane fission

ESCRT-III proteins are required for all of the identified ESCRT-involved biological events, as they execute the membrane fission step [14]. There are seven different ESCRT-III proteins in yeast and 12 different subunits in human cells [16]. The sequence similarity among these proteins is low, but their 3D structures are quite similar based on the solved structure of some ESCRT-III proteins and secondary structure predictions [14; 54; 55; 56]. The N-terminal four helices form the core structure of ESCRT-III, and the 5th helix fold back onto the helix 1 and helix

2 of the core [54; 55; 56](Figure 1.9). Some ESCRT-III proteins contain an MIM (MIT interacting Motif) on their C-terminus [28; 29; 30; 57].

ESCRT-III proteins have two different states: monomer in the solution and large polymers when they bind to the membrane [14; 16]. In the monomeric state, the fifth helix of ESCRT-III proteins folds back onto the N-terminal helix core to inhibit the assembly of ESCRT-III proteins [54] (Figure 1.9). Removal of the fifth helix or site-directed mutagenesis to disrupt the interaction between fifth helix and the N-terminal helix core will favor the assembly of ESCRT-III proteins in vitro [54]. However, recent EM reconstructions of lipid-associated Ist1/CHMP1 copolymers indicate helix 5 may play important roles in bridging different subunits within the ESCRT-III polymer (unpublished data from Dr. Frost), which seems consistent to our model that helix 5 is the Vps4-ATPase cassette binding motif and binding of helix 5 to Vps4 induces ESCRT-III disassembly (see Chapter 4).

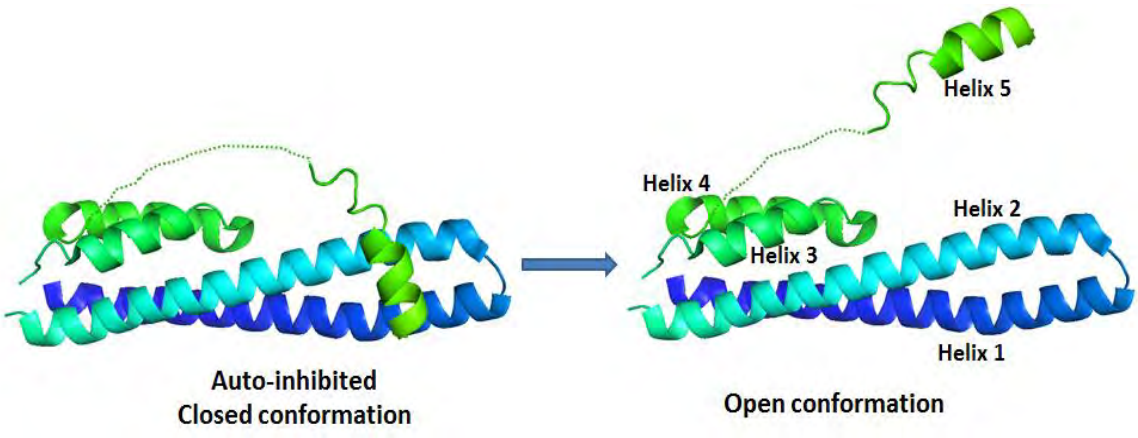

Figure 1.9. Structure of ESCRT-III protein.
Two different conformations of ESCRT-III proteins, represented by structures of CHMP3 (adapted from PDB files 3FRT and 3FRV). Left: autoinhibited conformation which favors the soluble, monomeric state. Right: open conformation induced by membrane binding, which favors the polymerization.

Assembled ESCRT-III proteins have been observed in both cultured cells and in vitro assays [14]. Overexpressed CHMP4 protein, one of the ESCRT-III subunits, can assemble into ~5 nm filaments which form circular arrays on the cytoplasmic face of the plasma membrane [58]. When co-overexpressed with the hydrolysis-defective mutant of Vps4B, the CHMP4 filaments can deform the membrane to protrude toward the outside of the cell [58]. Similar protrusions can also be observed when only overexpressing the N-terminal core domain of CHMP4A (1-116) [58]. Helical filaments of 17 nm diameters were also observed around the membrane abscission site during cytokinesis, which was speculated to be or contain ESCRT-III proteins because the filaments cannot be observed in CHMP2A-depleted cells [59]. Purified ESCRT-III proteins can assemble into filaments or tubes in vitro, which can be disassembled by Vps4 in the presence of ATP [34]. The ESCRT-III tubes formed in the presence of lipid membrane contain cone-shape ends, which were proposed to induce membrane fission [34].

In vitro studies with GUV and purified ESCRT proteins indicate that ESCRT-III proteins can finish the membrane fission process as long as there is enough ESCRT-III supply [25]. Three of the four core ESCRT-III proteins are sufficient for one round of membrane fission: Vps20, snf7, and Vps24 [25]. Vps20 can be recruited to the membrane fission site by ESCRT-II complexes, then recruits snf7 [25]. Adding Vps24 can make the membrane fission step much more efficient [25]. Vps2 is in charge of recruiting Vps4, which is implied to recycle ESCRT-III proteins for further usage with the energy from ATP hydrolysis [25]. In vivo studies, however, indicate that Vps4 may actively participate in the fission step [60; 61; 62].

Several different models have been proposed for the mechanism of membrane fission induced by ESCRT-III and Vps4 [14]. The spiraling dome model is one leading model among them [14]. According to the dome model, ESCRT-III proteins can form spirals when they bind to the membrane [14]. These spirals will form a dome-like structure at the membrane fission site [14]. Opposing membranes bound to the top end of the dome will be pulled together, which will constrict the membrane neck and finally lead to membrane fission [14].

Vps4

Vps4 is an AAA+ ATPase that disassembles ESCRT-III complexes with the energy from ATP hydrolysis [34]. It is the only ATPase in the ESCRT machinery to provide energy for membrane fission.

Vps4 contains an MIT domain on the N-terminus, an AAA+ ATPase cassette on the C-terminus, and a linker region between them [14; 16] (Figure 1.10). The N-terminal MIT domain is a three-helix bundle, which can selectively recognize the MIM motifs on the C-terminal of ESCRT-III proteins [28; 29; 57] (Figure 1.10). Two different MIM motifs have been identified to bind to the Vps4 MIT domain: MIM1 which binds to the groove between the 2nd and 3rd helix of MIT domain and MIM2 which binds to the groove between the 1st and 3rd helix of MIT [28; 29; 30] (Figure 1.10). The C-terminal AAA+ ATPase cassette contains the large ATPase domain and the small ATPase domain, which form the ATP binding/hydrolysis pocket together [31; 63; 64; 65]. For Eukaryotic Vps4, there is a beta domain inserted into the small ATPase domain, which serves as the binding site

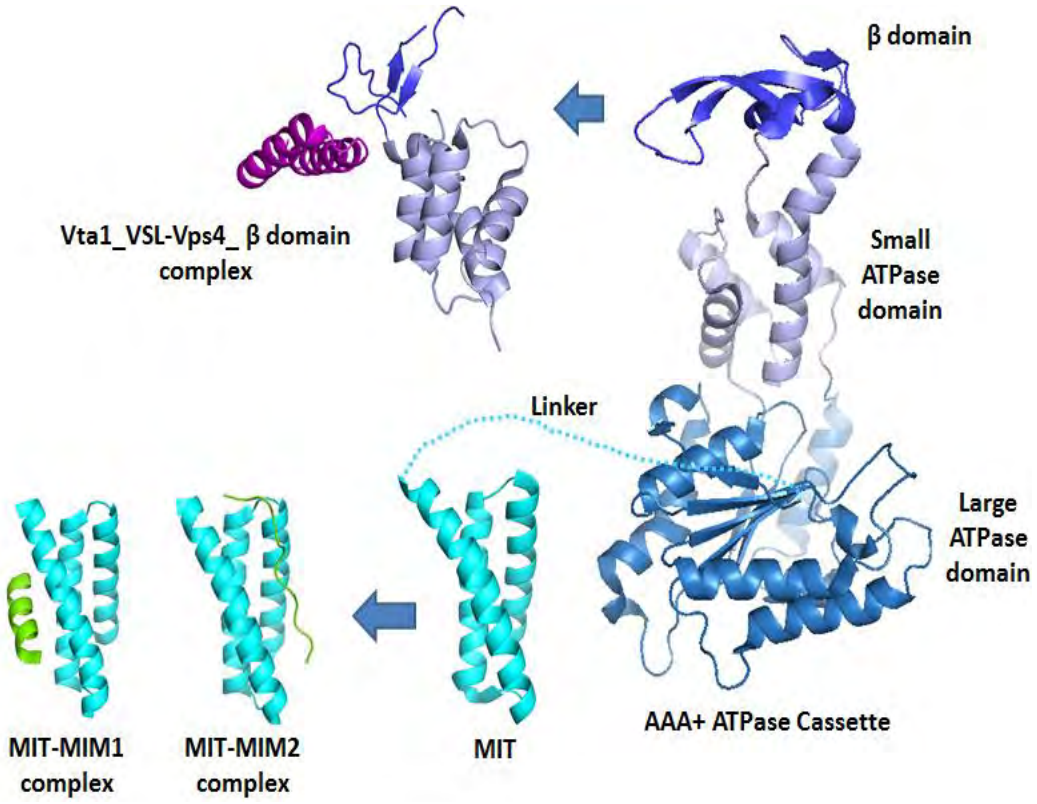

Figure 1.10. Structure of Vps4.
Right: Structures of the MIT domain (PDB ID: 2JQH) and the monomeric AAA+ ATPase Cassette (PDB ID: 1XWI) of human VPS4B.
Bottom left: Structures of the complex formed by MIT domain (VPS4A) and MIM1 motif (CHMP1A) (2JQ9) and the complex formed by MIT domain (VPS4B)-MIM2 motif (CHMP6) (2K3W).
Top left: Structure of the complex formed by Vta1p VSL domain and a fragment containing the β domain and small ATPase domain of *Saccharomyces cerevisiae* Vps4p (3MHV).

for the VSL domain of the Vps4 activator Vta1 (LIP5 in human cells) which can stabilize Vps4 oligomer [31] [66](Figure 1.10). Several structures of the Vps4 AAA+ ATPase cassette from different species have been determined by crystallography and these structures can be superimposed to each very well, which indicates the 3D structure of AAA+ ATPase cassette of Vps4 is very well conserved through evolution [31; 63; 64; 65; 67].

Similar to other AAA+ ATPases, the active form of Vps4 is an oligomer [68]. Several EM or Cryo-EM studies indicate that the Vps4 oligomer is a double-ring structure in the presence of ATP, which contains 12 or 14 subunits [69; 70; 71]. Two of these three EM or Cryo-EM reconstructions of Vps4 oligomer were using a Vps4p mutant containing the E to Q mutation on the Walker B motif, which can still bind ATP but cannot hydrolyze ATP [69; 71]. Recently, our group found that the wild type Vps4p is in an equilibrium between hexamer and dimer in the presence of ATP (see Chapter 2), which indicates that the functional form of Vps4 is a hexamer.

A hexamer model of Vps4 has been proposed based on the D1 ring of p97, a closely-related AAA ATPase [31] (Figure 1.11). This model was proven to be largely valid based on two observations. First, the predicted hexameric interface residues based on the hexamer model were shown to be important for oligomerization and function of Vps4 [31; 64]. Second, the predicted central pore loops are important for the function of Vps4. There are two pore loops lining the central pore of this hexamer model [31; 64] (Figure 1.11). The pore loops of AAA+ ATPases have been shown to be the substrate binding/processing motifs [32; 33; 72; 73; 74]. Human cell VPS4A/B carrying mutations on these pore loops, although they can still assemble into oligomers, cannot support efficient HIV budding, which indicates these pore loops are important for the function of Vps4 [31; 64]. Based on this model, the ATP binding sites are between the two neighbor subunits within one hexamer, and there are six ATP binding sites within one Vps4 hexamer [31; 64].

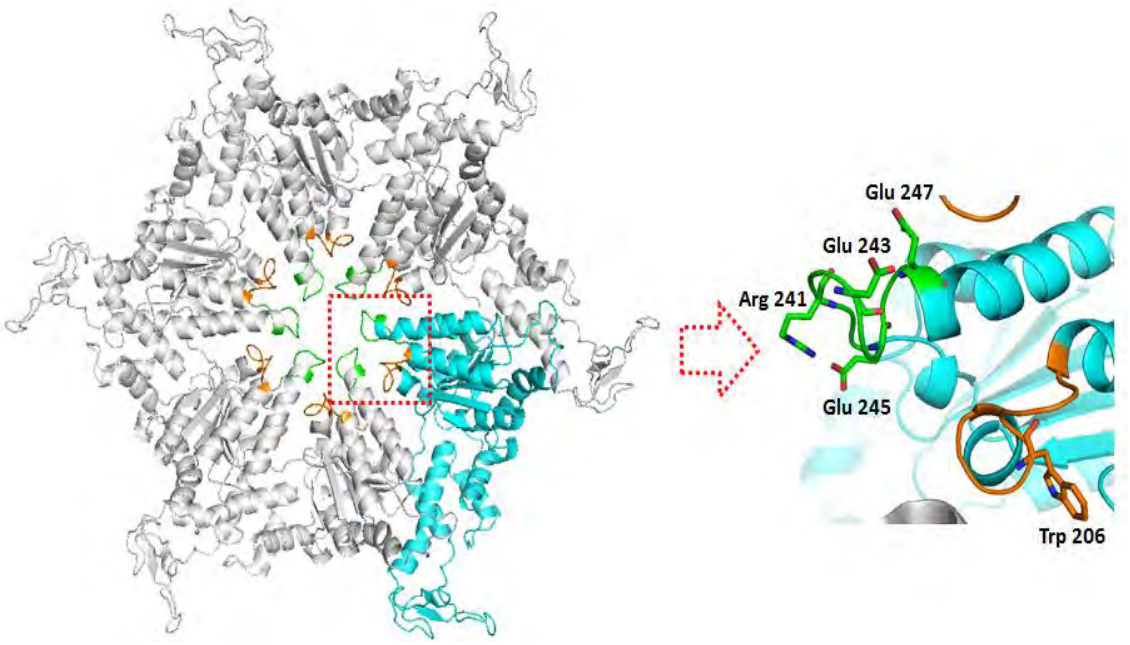

Figure 1.11 : Hexamer model of Vps4.
The p97-like hexamer model of Vps4 built with the structure model of Vps4p ATPase cassette (PDB ID: 3EIH) superimposed on the D1-ring of p97 (PDB ID: 1E32). Important residues of pore loop 1 (orange) and pore loop 2 (green) are shown on the left.

The activity of Vps4 is regulated by several ESCRT proteins, including Vta1/LIP5 and ESCRT-III proteins [75; 76; 77]. Vta1/LIP5 contains a tandem MIT domain on the N-terminus and a VSL (Vta1 SBP1 LIP5) domain on the C-terminus [77]. The MIT domains can bind to the MIM motifs of Did2 and Vps60 [75; 78; 79]. The C-terminal VSL domains can dimerize, which is necessary for the function of Vta1 [77]. The VSL domain is also responsible for binding to the beta domain of Vps4, which can stabilize the Vps4 oligomer [66; 77]. Adding the VSL domain can increase the ATPase activity of Vps4 [75]. Although one structure of the interface between the Vta1-VSL domain and the Vps4-beta domain has been reported [66](Figure 1.10), it is still not clear about how the VSL domain stabilizes the Vps4

oligomer. One model proposed that the VSL domain can crosslink different Vps4 oligomers [66] and the other model stated that the VSL domain crosslinks different subunits within one Vps4 oligomer [67]. There is also a long linker between the MIT domains and the C-terminal VSL domain, which has been indicated to have a regulatory role on the activity of Vps4 [80].

In addition to Vta1, ESCRT-III proteins also play important roles in regulating the activity of Vps4 with different mechanisms.

First, ESCRT-III proteins can regulate the ATPase activity of Vps4 directly. The C-terminal residues of the ESCRT-III proteins CHMP2A, CHMP1B, CHMP3, CHMP4A, CHMP6, and CHMP5 have been shown to stimulate the ATPase activity of VPS4A in a manner that is independent of Vta1/LIP5 [76]. Similar stimulation effect has also been reported for Vps2 [75]. Both the C-terminal MIM motif and the upstream 5th helix of ESCRT-III proteins are necessary to this regulation, but neither of them seems to be able to activate the ATPase activity of full-length Vps4p alone [75; 76]. The 5th helix of ESCRT-III proteins has been reported to form the secondary Vps4 binding site because it can mediate the co-precipitation of overexpressed CHMP2A and Vps4B(E235Q) [81]. We found that the 5th helix can mediate the direct interaction between ESCRT-III and the central pore of Vps4 ATPase cassette, and this interaction can stabilize the Vps4 hexamer, which supports that one mechanism for the stimulation of the ATPase activity of Vps4 is that interacting with ESCRT-III proteins stabilizes the oligomerization of Vps4 (see Chapter 4).

Second, ESCRT-III proteins can also regulate the ATPase activity through Vta1/LIP5. Both Did2 and Vps60 contain MIM motifs binding to the MIT domains of Vta1 [75]. Particularly, the Vps60 contains a very unique MIM5 motif, which is composed of helix 4 and helix 5 of Vps60 [78; 79]. These two helices wrap around the helix bundle of the Vta1_MIT2 domain [78; 79]. Did2 contains a C-terminal tail that binds to the MIT domains of Vta1 [77]. Both Did2 and Vps60 stimulate the ATPase activity of Vps4p in a Vta1-dependent way [75]. The mechanism of this regulation is not yet clear.

In vitro experiments with GUV and purified ESCRT proteins indicate that ESCRT-III proteins are sufficient for membrane fission, and Vps4 functions to recycle ESCRT-III proteins through disassembling ESCRT-III complexes to monomeric ESCRT-III proteins [25]. However, in vivo studies show that Vps4 is recruited to the membrane fission site before membrane fission started [60; 61; 62], which implied that Vps4 may actively participate in the membrane fission process. So, the exact the role of Vps4 in membrane fission is not yet clear. Moreover, how Vps4 disassembles the ESCRT-III complexes is also not yet clear. The published data, as well as our own data, supported the model that Vps4 hexamer disassembles ESCRT-III complexes by pulling the C-terminal region of ESCRT-III subunits into/through the central pore of the Vps4 hexamer [14; 31; 64; 76] (see Chapter 4). More research is still needed to validate this model, especially the high resolution structural information of how ESCRT-III complexes are built and how the active Vps4 hexamer central pore loops interact with the ESCRT-III subunits.

AAA+ ATPase

Vps4 belongs to the AAA+ ATPases (ATPases Associated with diverse cellular Activities) superfamily [1]. AAA stands for ATPases associated with a variety of cellular activities [82]. AAA+ ATPases hydrolyze the gamma phosphate bond of ATP, and utilize the energy from ATP hydrolysis to change the conformation of other biomolecules (substrates) [32; 82]. They act like motors on the molecular level. The AAA ATPases family was first defined for proteins that contain the conserved AAA ATPase module, such as the regulatory subunits (Rpt1-6) of 26S proteasome and NSF which is involved in vesicle fusion [82]. Sequence alignments identified proteins more distantly related to the AAA ATPase family [82]. All of them, including the AAA ATPases, share some distinct structural features, and they are designated the AAA+ ATPases superfamily [32; 33; 82].

The AAA+ ATPase cassette is composed of an N-terminal large ATPase domain and a C-terminal small ATPase domain [32; 33; 82] (Figure 1.12). The large ATPase domain is an alpha-beta-alpha fold, which contains a beta-sheet of 5 parallel strands (beta 1-5) surrounded by five alpha helices (alpha 0-4) [16; 33; 82]. The C-terminal small ATPase domain is a helical bundle of four alpha helices (alpha 5-8) [32; 33; 82]. The ATP binding/hydrolysis pocket is formed between two neighbor subunits of an AAA+ ATPase oligomer, and both of the large and small ATPase domain are required [32; 33]. There are six important structural features of the AAA+ ATPase cassette: Walker A, Walker B, Sensor 1, Sensor 2, Arginine finger, and Pore loop [32; 33].

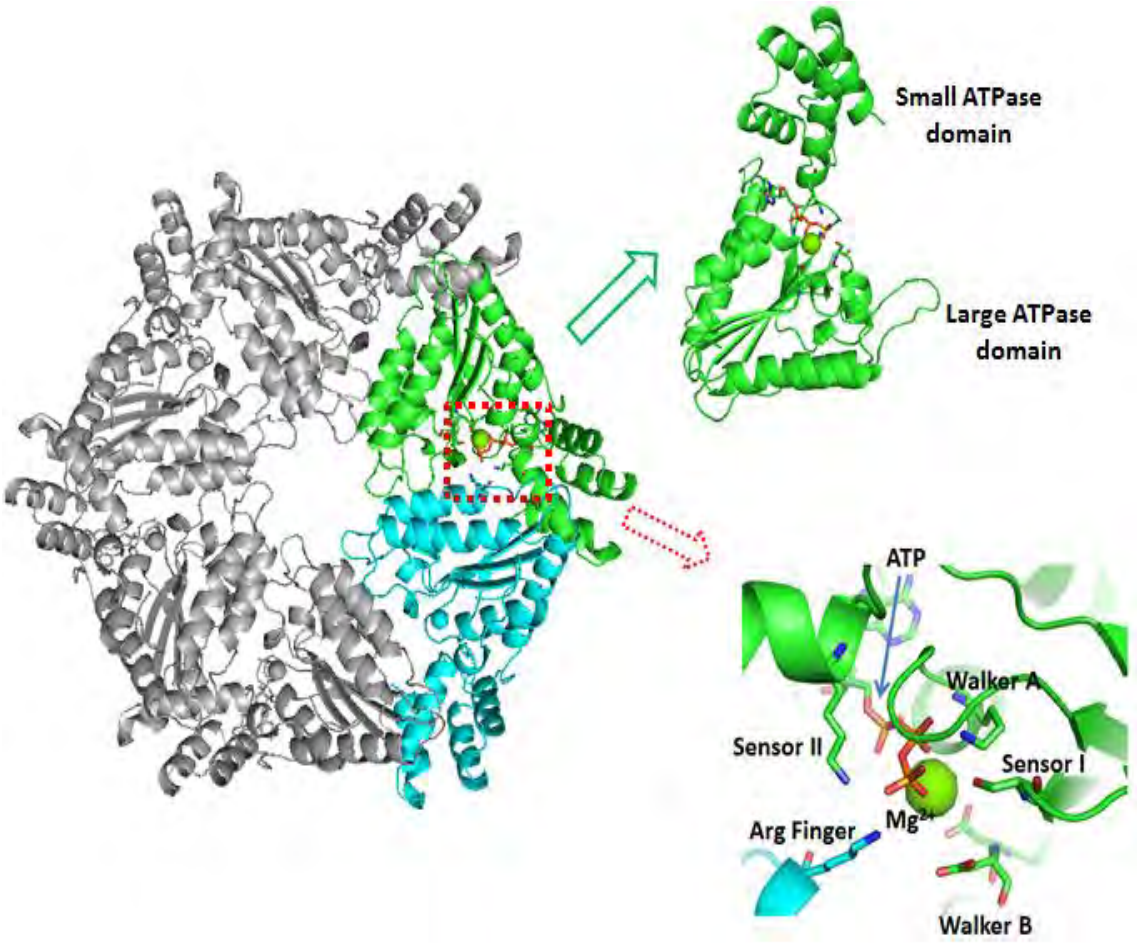

Figure 1.12. Structure features of AAA+ ATPases.
The structure of NSF hexamer is shown (PDB ID: 1NSF). Two NSF monomers next to each other within one hexamer are colored green and blue. The important ATP binding and hydrolysis motifs are shown.

The Walker A motif is located between beta1 and alpha1 [32; 33]. The crucial residue is a lysine residue in the consensus Walker A sequence GxxxxGKT/S (x is any amino acid)[32; 33]. AAA+ ATPases with mutation on the conserved K cannot bind ATP [32].

The Walker B motif starts from beta3 to the alpha3 with the consensus sequence hhhhDE (h is hydrophobic residue) [32; 33]. The conserved aspartate

residue coordinates Mg^{2+} which is necessary for ATP hydrolysis [32]. The following glutamate activates a water molecule for ATP hydrolysis [32]. Mutating this glutamate residue to glutamine does not impair ATP binding ability but inactivates the ATPase activity [32].

The sensor II motif is at the beginning of the alpha 7 of the small ATPase domain [32]. It contains a consensus arginine interacting directly with the gamma phosphate of ATP [32].

The sensor I and the arginine figure(s) constitute the second region of homology (SRH) [32]. Sensor I is a polar residue at the end of beta 4, which is usually an asparagine [32]. This polar residue works together with the glutamate of Walker B motif to activate a water molecule to attack the gamma-phosphate of ATP during ATP hydrolysis [32]. The arginine finger is at the end of the alpha 4 [32]. The active form of AAA+ ATPases is oligomer, in which the arginine finger from one subunit and other important elements from the neighbor subunit, including Walker A, Walker B, Sensor I, and Sensor II, cooperate to form one ATP binding and ATP hydrolysis pocket [32] (Figure 1.12).

Another important feature of AAA+ ATPases is the pore loop which points toward the central hole of the AAA+ ATPase oligomer [32]. A conserved motif Ar-Φ-G (Ar: Aromatic residue, Φ: Hydrophobic residue, and G: Glycine) on the loop between beta 2 and alpha 2 constitutes the pore loop [32]. The pore loop is the substrate (not ATP) binding motif [32].

The active forms of AAA+ ATPases are generally highly ordered oligomers [32; 33]. Most reported AAA+ ATPases form ring-like oligomers as the active form [33].

Binding of ATP, substrate, or other factors may be necessary or helpful for the oligomerization [32; 33]. Ring-like ATPase oligomers can use the energy from ATP hydrolysis to perform diverse cellular functions such as DNA or DNA/RNA duplex unwinding and protein unfolding [32; 33; 83]. The mechanisms of ring-like ATPases have been studied extensively, and three models have been proposed: a concerted model, a stochastic model, and a rotary model [83]. The concerted model states that all of the subunits around the ring have the same ATP hydrolysis states [83]. The stochastic model states that the ATP hydrolysis states of different subunits around the ring are randomly distributed [83]. The rotary model is the most favored model, as several structures of AAA+ ATPases or RecA-like ATPases support this model, including F1-ATPase, E.coli Rho helicase, and papillomavirus E1 helicase [74; 84; 85]. According to this model, the different subunits around the ring hydrolyze ATP in a certain sequence, clockwise or counterclockwise [83]. Loops or other motifs projecting towards the central pore of the ring are responsible for binding and reforming or moving of the substrates [83]. The conformation and/or position of these loops of different subunits have different states according to the ATP hydrolysis states of these subunits [83].

Outline of chapters

This introduction is followed by four chapters. Chapters 2-4 document my efforts towards understanding how Vps4 works, while Chapter 5 summarizes my current understanding and envisions the future direction of research on Vps4.

Chapter 2 reports the discovery of Vps4 hexamer as the active form of Vps4 and two structures of AAA+ ATPase cassette of Crenarchaeal Vps4 homologs in collaboration with Dr. Monroe. In contrast to the prevailing double ring models [69; 70; 71], our size exclusion chromatography and analytical ultracentrifugation analyses of wild type Vps4p supported the model that Vps4 is active as a single ring hexamer. We further support the proposal that the Vps4 hexamer resembles the p97 D1-ring structure through mutagenesis of residues as the proposed interface [31; 64]. This chapter also describes the solution association states and crystal structures of the AAA+ ATPase cassettes of two crenarchaeal Vps4 homologs. Both structures are very similar to the AAA+ ATPase cassette of eukaryotic homologs, and although neither crystalize as hexamers, both crystal lattices preserve a packing interface that resembles the hexameric interface of the p97-like Vps4 hexamer model. Finally, we showed that mutation on this interface disrupts oligomerization of Crenarchaeal Vps4 homologs and impairs their ATPase activity, indicating that this interface is conserved through evolution. This chapter was published recently in the Journal of Molecular Biology [67]. Dr. Monroe performed the analysis of the oligomerization of Vps4, and I contributed the two crystal structures of of the AAA+ ATPase cassettes of two Crenarchaeal Vps4 homologs and biochemical characterization of them.

Chapter 3 documents crystallization efforts toward a structure of the Vps4 hexamer. Different strategies were used, including screening Vps4 homologs from different Crenarchaeal species, stabilizing association by fusion with another protein that forms a stable hexamer, stabilizing the Vps4p hexamer by

addition of the Vta1p VSL domain, and stabilizing a functional asymmetric hexamer by use of ADP·AlFx and addition of a substrate peptide. Although a lot of crystal hits were obtained, no crystals that diffracted to sufficient resolution to determine the crystal symmetry were found that could contain a Vps4 hexamer.

Chapter 4 describes characterization of the interaction between the Vps4p hexamer and residues from helix 5 of Vps2, one of the ESCRT-III proteins in *Saccharomyces cerevisiae*. The equivalent region in a homologous ESCRT-III protein had been shown to activate the ATPase activity of Vps4A [76], and the sequence around the helix 5 of the human CHMP2A ESCRT-III subunit was known to be important for co-precipitation of overexpressed CHMP2A and Vps4B(E235Q) [81]. Consistent with these earlier observations, I found that that helix 5 of Vps2 can interact directly with the pore loops of the Vps4p hexamer, and one ΔMIT-Vps4p hexamer can bind one substrate. Furthermore, I demonstrated that the interaction required ADP·AlFx, an ATP analog mimicking ATP, ADP, and the transition state of ATP during ATP hydrolysis. These data indicate that the functional Vps4 hexamer is asymmetric.

We also found that the interaction with the pore loops of the Vps4p hexamer may be limited to residues of helix 5 of the ESCRT-III subunits. In particular, my data indicate that a patch of negatively charged residues adjacent to the N-terminus of helix 5 of Vps2 may serve as a stop translocation signal when they reach a collar of negatively charged residues around the central pore of the Vps4p hexamer. The resulting charge-charge repulsion may function to prevent the N-terminal four helices of ESCRT-III protein from being processed by Vps4.

Finally, Peptide binding to the Vps4p pore loops was found to be autoinhibited by the MIT domain on the N-terminus of Vps4p. Moreover, binding of the C-terminal Vps2p MIM1 motif to the Vps4p MIT domain alleviated this autoinhibition. These data suggest an autoinhibiory regulatory mechanism that functions to prevent processing of nonspecific proteins by Vps4.

This chapter is a manuscript in preparation that reports a detailed characterization of the interaction between peptides derived from ESCRT-III substrates with the AAA ATPase domain of Vps4. I did all of the biochemical analysis of Vps4p-Vps2p interaction; Dr. Joerg Votteler from Prof. Sundquist's Lab confirmed the importance of the pore loop 2 of Vps4 in HIV budding system.

Chapter 5 summarizes all of the biochemical and structural studies on Vps4 in Chapter 2-4 and proposes some possible experiments in three directions for future studies of Vps4, including crystallization of the Vps4 hexamer and ESCRT-III disassembly by Vps4.

References

1. Babst, M., Sato, T. K., Banta, L. M. & Emr, S. D. (1997). Endosomal transport function in yeast requires a novel AAA-type ATPase, Vps4p. *EMBO J* **16**, 1820-31.

2. Katzmann, D. J., Babst, M. & Emr, S. D. (2001). Ubiquitin-dependent sorting into the multivesicular body pathway requires the function of a conserved endosomal protein sorting complex, ESCRT-I. *Cell* **106**, 145-55.

3. Babst, M., Katzmann, D. J., Snyder, W. B., Wendland, B. & Emr, S. D. (2002). Endosome-associated complex, ESCRT-II, recruits transport machinery for protein sorting at the multivesicular body. *Dev Cell* **3**, 283-9.

4. Babst, M., Katzmann, D. J., Estepa-Sabal, E. J., Meerloo, T. & Emr, S. D. (2002). Escrt-III: an endosome-associated heterooligomeric protein complex required for mvb sorting. *Dev Cell* **3**, 271-82.

5. Katzmann, D. J., Stefan, C. J., Babst, M. & Emr, S. D. (2003). Vps27 recruits ESCRT machinery to endosomes during MVB sorting. *J Cell Biol* **162**, 413-23.

6. Pornillos, O., Higginson, D. S., Stray, K. M., Fisher, R. D., Garrus, J. E., Payne, M., He, G. P., Wang, H. E., Morham, S. G. & Sundquist, W. I. (2003). HIV Gag mimics the Tsg101-recruiting activity of the human Hrs protein. *J Cell Biol* **162**, 425-34.

7. Garrus, J. E., von Schwedler, U. K., Pornillos, O. W., Morham, S. G., Zavitz, K. H., Wang, H. E., Wettstein, D. A., Stray, K. M., Cote, M., Rich, R. L., Myszka, D. G. & Sundquist, W. I. (2001). Tsg101 and the vacuolar protein sorting pathway are essential for HIV-1 budding. *Cell* **107**, 55-65.

8. Martin-Serrano, J., Zang, T. & Bieniasz, P. D. (2001). HIV-1 and Ebola virus encode small peptide motifs that recruit Tsg101 to sites of particle assembly to facilitate egress. *Nat Med* **7**, 1313-9.

9. VerPlank, L., Bouamr, F., LaGrassa, T. J., Agresta, B., Kikonyogo, A., Leis, J. & Carter, C. A. (2001). Tsg101, a homologue of ubiquitin-conjugating (E2) enzymes, binds the L domain in HIV type 1 Pr55(Gag). *Proc Natl Acad Sci U S A* **98**, 7724-9.

10. Carlton, J. G. & Martin-Serrano, J. (2007). Parallels between cytokinesis and retroviral budding: a role for the ESCRT machinery. *Science* **316**, 1908-12.

11. Morita, E., Sandrin, V., Chung, H. Y., Morham, S. G., Gygi, S. P., Rodesch, C. K. & Sundquist, W. I. (2007). Human ESCRT and ALIX proteins interact with proteins of the midbody and function in cytokinesis. *EMBO J* **26**, 4215-27.

12. Samson, R. Y., Obita, T., Freund, S. M., Williams, R. L. & Bell, S. D. (2008). A role for the ESCRT system in cell division in archaea. *Science* **322**, 1710-3.

13. Lindas, A. C., Karlsson, E. A., Lindgren, M. T., Ettema, T. J. & Bernander, R. (2008). A unique cell division machinery in the Archaea. *Proc Natl Acad Sci U S A* **105**, 18942-6.

14. McCullough, J., Colf, L. A. & Sundquist, W. I. (2013). Membrane fission reactions of the mammalian ESCRT pathway. *Annu Rev Biochem* **82**, 663-92.

15. Schmid, S. L. & Frolov, V. A. (2011). Dynamin: functional design of a membrane fission catalyst. *Annu Rev Cell Dev Biol* **27**, 79-105.

16. Hanson, P. I. & Cashikar, A. (2012). Multivesicular body morphogenesis. *Annu Rev Cell Dev Biol* **28**, 337-62.

17. Ren, X., Kloer, D. P., Kim, Y. C., Ghirlando, R., Saidi, L. F., Hummer, G. & Hurley, J. H. (2009). Hybrid structural model of the complete human ESCRT-0 complex. *Structure* **17**, 406-16.

18. Misra, S. & Hurley, J. H. (1999). Crystal structure of a phosphatidylinositol 3-phosphate-specific membrane-targeting motif, the FYVE domain of Vps27p. *Cell* **97**, 657-66.

19. Im, Y. J., Kuo, L., Ren, X., Burgos, P. V., Zhao, X. Z., Liu, F., Burke, T. R., Jr., Bonifacino, J. S., Freed, E. O. & Hurley, J. H. (2010). Crystallographic and functional analysis of the ESCRT-I /HIV-1 Gag PTAP interaction. *Structure* **18**, 1536-47.

20. Kostelansky, M. S., Schluter, C., Tam, Y. Y., Lee, S., Ghirlando, R., Beach, B., Conibear, E. & Hurley, J. H. (2007). Molecular architecture and functional model of the complete yeast ESCRT-I heterotetramer. *Cell* **129**, 485-98.

21. Gill, D. J., Teo, H., Sun, J., Perisic, O., Veprintsev, D. B., Emr, S. D. & Williams, R. L. (2007). Structural insight into the ESCRT-I/-II link and its role in MVB trafficking. *EMBO J* **26**, 600-12.

22. Im, Y. J. & Hurley, J. H. (2008). Integrated structural model and membrane targeting mechanism of the human ESCRT-II complex. *Dev Cell* **14**, 902-13.

23. Im, Y. J., Wollert, T., Boura, E. & Hurley, J. H. (2009). Structure and function of the ESCRT-II-III interface in multivesicular body biogenesis. *Dev Cell* **17**, 234-43.

24. Wollert, T. & Hurley, J. H. (2010). Molecular mechanism of multivesicular body biogenesis by ESCRT complexes. *Nature* **464**, 864-9.

25. Wollert, T., Wunder, C., Lippincott-Schwartz, J. & Hurley, J. H. (2009). Membrane scission by the ESCRT-III complex. *Nature* **458**, 172-7.

26. Teis, D., Saksena, S. & Emr, S. D. (2008). Ordered assembly of the ESCRT-III complex on endosomes is required to sequester cargo during MVB formation. *Dev Cell* **15**, 578-89.

27. Saksena, S., Wahlman, J., Teis, D., Johnson, A. E. & Emr, S. D. (2009). Functional reconstitution of ESCRT-III assembly and disassembly. *Cell* **136**, 97-109.

28. Obita, T., Saksena, S., Ghazi-Tabatabai, S., Gill, D. J., Perisic, O., Emr, S. D. & Williams, R. L. (2007). Structural basis for selective recognition of ESCRT-III by the AAA ATPase Vps4. *Nature* **449**, 735-9.

29. Stuchell-Brereton, M. D., Skalicky, J. J., Kieffer, C., Karren, M. A., Ghaffarian, S. & Sundquist, W. I. (2007). ESCRT-III recognition by VPS4 ATPases. *Nature* **449**, 740-4.

30. Kieffer, C., Skalicky, J. J., Morita, E., De Domenico, I., Ward, D. M., Kaplan, J. & Sundquist, W. I. (2008). Two distinct modes of ESCRT-III recognition are required for VPS4 functions in lysosomal protein targeting and HIV-1 budding. *Dev Cell* **15**, 62-73.

31. Scott, A., Chung, H. Y., Gonciarz-Swiatek, M., Hill, G. C., Whitby, F. G., Gaspar, J., Holton, J. M., Viswanathan, R., Ghaffarian, S., Hill, C. P. & Sundquist, W. I. (2005). Structural and mechanistic studies of VPS4 proteins. *EMBO J* **24**, 3658-69.

32. Hanson, P. I. & Whiteheart, S. W. (2005). AAA+ proteins: have engine, will work. *Nat Rev Mol Cell Biol* **6**, 519-29.

33. Erzberger, J. P. & Berger, J. M. (2006). Evolutionary relationships and structural mechanisms of AAA+ proteins. *Annu Rev Biophys Biomol Struct* **35**, 93-114.

34. Lata, S., Schoehn, G., Jain, A., Pires, R., Piehler, J., Gottlinger, H. G. & Weissenhorn, W. (2008). Helical structures of ESCRT-III are disassembled by VPS4. *Science* **321**, 1354-7.

35. Martin-Serrano, J. & Neil, S. J. (2011). Host factors involved in retroviral budding and release. *Nat Rev Microbiol* **9**, 519-31.

36. Votteler, J. & Sundquist, W. I. (2013). Virus budding and the ESCRT pathway. *Cell Host Microbe* **14**, 232-41.

37. Strack, B., Calistri, A., Craig, S., Popova, E. & Gottlinger, H. G. (2003). AIP1/ALIX is a binding partner for HIV-1 p6 and EIAV p9 functioning in virus budding. *Cell* **114**, 689-99.

38. Fisher, R. D., Chung, H. Y., Zhai, Q., Robinson, H., Sundquist, W. I. & Hill, C. P. (2007). Structural and biochemical studies of ALIX/AIP1 and its role in retrovirus budding. *Cell* **128**, 841-52.

39. Zhai, Q., Fisher, R. D., Chung, H. Y., Myszka, D. G., Sundquist, W. I. & Hill, C. P. (2008). Structural and functional studies of ALIX interactions with YPX(n)L late domains of HIV-1 and EIAV. *Nat Struct Mol Biol* **15**, 43-9.

40. Baietti, M. F., Zhang, Z., Mortier, E., Melchior, A., Degeest, G., Geeraerts, A., Ivarsson, Y., Depoortere, F., Coomans, C., Vermeiren, E., Zimmermann, P. & David, G. (2012). Syndecan-syntenin-ALIX regulates the biogenesis of exosomes. *Nat Cell Biol* **14**, 677-85.

41. Langelier, C., von Schwedler, U. K., Fisher, R. D., De Domenico, I., White, P. L., Hill, C. P., Kaplan, J., Ward, D. & Sundquist, W. I. (2006). Human ESCRT-II complex and its role in human immunodeficiency virus type 1 release. *J Virol* **80**, 9465-80.

42. Carlson, L. A. & Hurley, J. H. (2012). In vitro reconstitution of the ordered assembly of the endosomal sorting complex required for transport at membrane-bound HIV-1 Gag clusters. *Proc Natl Acad Sci U S A* **109**, 16928-33.

43. McCullough, J., Fisher, R. D., Whitby, F. G., Sundquist, W. I. & Hill, C. P. (2008). ALIX-CHMP4 interactions in the human ESCRT pathway. *Proc Natl Acad Sci U S A* **105**, 7687-91.

44. Morita, E., Sandrin, V., McCullough, J., Katsuyama, A., Baci Hamilton, I. & Sundquist, W. I. (2011). ESCRT-III protein requirements for HIV-1 budding. *Cell Host Microbe* **9**, 235-42.

45. Chen, C. T., Hehnly, H. & Doxsey, S. J. (2012). Orchestrating vesicle transport, ESCRTs and kinase surveillance during abscission. *Nat Rev Mol Cell Biol* **13**, 483-8.

46. Caballe, A. & Martin-Serrano, J. (2011). ESCRT machinery and cytokinesis: the road to daughter cell separation. *Traffic* **12**, 1318-26.

47. Lee, H. H., Elia, N., Ghirlando, R., Lippincott-Schwartz, J. & Hurley, J. H. (2008). Midbody targeting of the ESCRT machinery by a noncanonical coiled coil in CEP55. *Science* **322**, 576-80.

48. Yang, D., Rismanchi, N., Renvoise, B., Lippincott-Schwartz, J., Blackstone, C. & Hurley, J. H. (2008). Structural basis for midbody targeting of spastin by the ESCRT-III protein CHMP1B. *Nat Struct Mol Biol* **15**, 1278-86.

49. Ellen, A. F., Albers, S. V., Huibers, W., Pitcher, A., Hobel, C. F., Schwarz, H., Folea, M., Schouten, S., Boekema, E. J., Poolman, B. & Driessen, A. J. (2009). Proteomic analysis of secreted membrane vesicles of archaeal Sulfolobus species reveals the presence of endosome sorting complex components. *Extremophiles* **13**, 67-79.

50. Ghazi-Tabatabai, S., Obita, T., Pobbati, A. V., Perisic, O., Samson, R. Y., Bell, S. D. & Williams, R. L. (2009). Evolution and assembly of ESCRTs. *Biochem Soc Trans* **37**, 151-5.

51. Snyder, J. C., Samson, R. Y., Brumfield, S. K., Bell, S. D. & Young, M. J. (2013). Functional interplay between a virus and the ESCRT machinery in archaea. *Proc Natl Acad Sci U S A* **110**, 10783-7.

52. Moriscot, C., Gribaldo, S., Jault, J. M., Krupovic, M., Arnaud, J., Jamin, M., Schoehn, G., Forterre, P., Weissenhorn, W. & Renesto, P. (2011). Crenarchaeal CdvA forms double-helical filaments containing DNA and interacts with ESCRT-III-like CdvB. *PLoS One* **6**, e21921.

53. Samson, R. Y., Obita, T., Hodgson, B., Shaw, M. K., Chong, P. L., Williams, R. L. & Bell, S. D. (2011). Molecular and structural basis of ESCRT-III recruitment to membranes during archaeal cell division. *Mol Cell* **41**, 186-96.

54. Bajorek, M., Schubert, H. L., McCullough, J., Langelier, C., Eckert, D. M., Stubblefield, W. M., Uter, N. T., Myszka, D. G., Hill, C. P. & Sundquist, W. I. (2009). Structural basis for ESCRT-III protein autoinhibition. *Nat Struct Mol Biol* **16**, 754-62.

55. Muziol, T., Pineda-Molina, E., Ravelli, R. B., Zamborlini, A., Usami, Y., Gottlinger, H. & Weissenhorn, W. (2006). Structural basis for budding by the ESCRT-III factor CHMP3. *Dev Cell* **10**, 821-30.

56. Xiao, J., Chen, X. W., Davies, B. A., Saltiel, A. R., Katzmann, D. J. & Xu, Z. (2009). Structural basis of Ist1 function and Ist1-Did2 interaction in the multivesicular body pathway and cytokinesis. *Mol Biol Cell* **20**, 3514-24.

57. Scott, A., Gaspar, J., Stuchell-Brereton, M. D., Alam, S. L., Skalicky, J. J. & Sundquist, W. I. (2005). Structure and ESCRT-III protein interactions of the MIT domain of human VPS4A. *Proc Natl Acad Sci U S A* **102**, 13813-8.

58. Hanson, P. I., Roth, R., Lin, Y. & Heuser, J. E. (2008). Plasma membrane deformation by circular arrays of ESCRT-III protein filaments. *J Cell Biol* **180**, 389-402.

59. Guizetti, J., Schermelleh, L., Mantler, J., Maar, S., Poser, I., Leonhardt, H., Muller-Reichert, T. & Gerlich, D. W. (2011). Cortical constriction during

abscission involves helices of ESCRT-III-dependent filaments. *Science* **331**, 1616-20.

60. Baumgartel, V., Ivanchenko, S., Dupont, A., Sergeev, M., Wiseman, P. W., Krausslich, H. G., Brauchle, C., Muller, B. & Lamb, D. C. (2011). Live-cell visualization of dynamics of HIV budding site interactions with an ESCRT component. *Nat Cell Biol* **13**, 469-74.

61. Elia, N., Sougrat, R., Spurlin, T. A., Hurley, J. H. & Lippincott-Schwartz, J. (2011). Dynamics of endosomal sorting complex required for transport (ESCRT) machinery during cytokinesis and its role in abscission. *Proc Natl Acad Sci U S A* **108**, 4846-51.

62. Jouvenet, N., Zhadina, M., Bieniasz, P. D. & Simon, S. M. (2011). Dynamics of ESCRT protein recruitment during retroviral assembly. *Nat Cell Biol* **13**, 394-401.

63. Xiao, J., Xia, H., Yoshino-Koh, K., Zhou, J. & Xu, Z. (2007). Structural characterization of the ATPase reaction cycle of endosomal AAA protein Vps4. *J Mol Biol* **374**, 655-70.

64. Gonciarz, M. D., Whitby, F. G., Eckert, D. M., Kieffer, C., Heroux, A., Sundquist, W. I. & Hill, C. P. (2008). Biochemical and structural studies of yeast Vps4 oligomerization. *J Mol Biol* **384**, 878-95.

65. Inoue, M., Kamikubo, H., Kataoka, M., Kato, R., Yoshimori, T., Wakatsuki, S. & Kawasaki, M. (2008). Nucleotide-dependent conformational changes and assembly of the AAA ATPase SKD1/VPS4B. *Traffic* **9**, 2180-9.

66. Yang, D. & Hurley, J. H. (2010). Structural role of the Vps4-Vta1 interface in ESCRT-III recycling. *Structure* **18**, 976-84.

67. Monroe, N., Han, H., Gonciarz, M. D., Eckert, D. M., Karren, M. A., Whitby, F. G., Sundquist, W. I. & Hill, C. P. (2013). The oligomeric state of the active Vps4 AAA ATPase. *J Mol Biol*.

68. Babst, M., Wendland, B., Estepa, E. J. & Emr, S. D. (1998). The Vps4p AAA ATPase regulates membrane association of a Vps protein complex required for normal endosome function. *EMBO J* **17**, 2982-93.

69. Yu, Z., Gonciarz, M. D., Sundquist, W. I., Hill, C. P. & Jensen, G. J. (2008). Cryo-EM structure of dodecameric Vps4p and its 2:1 complex with Vta1p. *J Mol Biol* **377**, 364-77.

70. Hartmann, C., Chami, M., Zachariae, U., de Groot, B. L., Engel, A. & Grutter, M. G. (2008). Vacuolar protein sorting: two different functional states of the AAA-ATPase Vps4p. *J Mol Biol* **377**, 352-63.

71. Landsberg, M. J., Vajjhala, P. R., Rothnagel, R., Munn, A. L. & Hankamer, B. (2009). Three-dimensional structure of AAA ATPase Vps4: advancing structural insights into the mechanisms of endosomal sorting and enveloped virus budding. *Structure* **17**, 427-37.

72. Martin, A., Baker, T. A. & Sauer, R. T. (2008). Pore loops of the AAA+ ClpX machine grip substrates to drive translocation and unfolding. *Nat Struct Mol Biol* **15**, 1147-51.

73. Roll-Mecak, A. & Vale, R. D. (2008). Structural basis of microtubule severing by the hereditary spastic paraplegia protein spastin. *Nature* **451**, 363-7.

74. Enemark, E. J. & Joshua-Tor, L. (2006). Mechanism of DNA translocation in a replicative hexameric helicase. *Nature* **442**, 270-5.

75. Azmi, I. F., Davies, B. A., Xiao, J., Babst, M., Xu, Z. & Katzmann, D. J. (2008). ESCRT-III family members stimulate Vps4 ATPase activity directly or via Vta1. *Dev Cell* **14**, 50-61.

76. Merrill, S. A. & Hanson, P. I. (2010). Activation of human VPS4A by ESCRT-III proteins reveals ability of substrates to relieve enzyme autoinhibition. *J Biol Chem* **285**, 35428-38.

77. Xiao, J., Xia, H., Zhou, J., Azmi, I. F., Davies, B. A., Katzmann, D. J. & Xu, Z. (2008). Structural basis of Vta1 function in the multivesicular body sorting pathway. *Dev Cell* **14**, 37-49.

78. Skalicky, J. J., Arii, J., Wenzel, D. M., Stubblefield, W. M., Katsuyama, A., Uter, N. T., Bajorek, M., Myszka, D. G. & Sundquist, W. I. (2012). Interactions of the human LIP5 regulatory protein with endosomal sorting complexes required for transport. *J Biol Chem* **287**, 43910-26.

79. Yang, Z., Vild, C., Ju, J., Zhang, X., Liu, J., Shen, J., Zhao, B., Lan, W., Gong, F., Liu, M., Cao, C. & Xu, Z. (2012). Structural basis of molecular recognition between ESCRT-III-like protein Vps60 and AAA-ATPase regulator Vta1 in the multivesicular body pathway. *J Biol Chem* **287**, 43899-908.

80. Norgan, A. P., Davies, B. A., Azmi, I. F., Schroeder, A. S., Payne, J. A., Lynch, G. M., Xu, Z. & Katzmann, D. J. (2013). Relief of autoinhibition enhances Vta1 activation of Vps4 via the Vps4 stimulatory element. *J Biol Chem* **288**, 26147-56.

81. Shim, S., Merrill, S. A. & Hanson, P. I. (2008). Novel interactions of ESCRT-III with LIP5 and VPS4 and their implications for ESCRT-III disassembly. *Mol Biol Cell* **19**, 2661-72.

82. Neuwald, A. F., Aravind, L., Spouge, J. L. & Koonin, E. V. (1999). AAA+: A class of chaperone-like ATPases associated with the assembly, operation, and disassembly of protein complexes. *Genome Res* **9**, 27-43.

83. Lyubimov, A. Y., Strycharska, M. & Berger, J. M. (2011). The nuts and bolts of ring-translocase structure and mechanism. *Curr Opin Struct Biol* **21**, 240-8.

84. Abrahams, J. P., Leslie, A. G., Lutter, R. & Walker, J. E. (1994). Structure at 2.8 A resolution of F1-ATPase from bovine heart mitochondria. *Nature* **370**, 621-8.

85. Thomsen, N. D. & Berger, J. M. (2009). Running in reverse: the structural basis for translocation polarity in hexameric helicases. *Cell* **139**, 523-34.

CHAPTER 2

THE OLIGOMERIC STATE OF THE ACTIVE VPS4 AAA ATPASE

This chapter is a published article in the Journal of Molecular Biology. I contributed the structures of Crenarchaeal Vps4 and the biochemical analysis of them.

Reprinted from the Journal of Molecular Biology, Volume 426, Issue 3, Nicole Monroe, Han Han, Malgorzata D. Gonciarz, Debra M.Eckert, Mary Anne Karren, Frank G. Whitby, Wesley I. Sundquist, Christopher P. Hill, The Oligomeric State of the Active Vps4 AAA ATPase, Pages 510–525, Copyright (2014), with permission from Elsevier.

The Oligomeric State of the Active Vps4 AAA ATPase

Nicole Monroe, Han Han, Malgorzata D. Gonciarz, Debra M. Eckert, Mary Anne Karren, Frank G. Whitby, Wesley I. Sundquist and Christopher P. Hill

Department of Biochemistry, *University of Utah School of Medicine, 15 North Medical Drive East RM 4100, Salt Lake City, UT 84112-5650, USA*

Correspondence to Wesley I. Sundquist and Christopher P. Hill: *wes@biochem.utah.edu; chris@biochem.utah.edu*
http://dx.doi.org/10.1016/j.jmb.2013.09.043
Edited by T. Yeates

Abstract

The cellular ESCRT (*e*ndosomal *s*orting *c*omplexes *r*equired for *t*ransport) pathway drives membrane constriction toward the cytosol and effects membrane fission during cytokinesis, endosomal sorting, and the release of many enveloped viruses, including the human immunodeficiency virus. A component of this pathway, the AAA ATPase Vps4, provides energy for pathway progression. Although it is established that Vps4 functions as an oligomer, subunit stoichiometry and other fundamental features of the functional enzyme are unclear. Here, we report that although some mutant Vps4 proteins form dodecameric assemblies, active wild-type *Saccharomyces cerevisiae* and *Sulfolobus solfataricus* Vps4 enzymes can form hexamers in the presence of ATP and ADP, as assayed by size-exclusion chromatography and equilibrium analytical ultracentrifugation. The Vta1p activator binds hexameric yeast Vps4p without changing the oligomeric state of Vps4p, implying that the active Vta1p–Vps4p complex also contains a single hexameric ring. Additionally, we report crystal structures of two different archaeal Vps4 homologs, whose structures and lattice interactions suggest a conserved mode of oligomerization. Disruption of the proposed hexamerization interface by mutagenesis abolished the ATPase activity of archaeal Vps4 proteins and blocked Vps4p function in *S. cerevisiae*. These data challenge the prevailing model that active Vps4 is a double-ring dodecamer, and argue that, like other type I AAA ATPases, Vps4 functions as a single ring with six subunits.

Introduction

The ESCRT (*e*ndosomal *s*orting *c*omplexes *r*equired for *t*ransport) pathway mediates multiple cellular membrane remodeling and fission events including the abscission step of cytokinesis [1–3], formation of intraluminal vesicles that bud into the MVB (*m*ulti*v*esicular *b*ody) [4–9], and exosome and shedding microvesicle formation [10–12]. This cellular pathway is exploited by retroviruses and many other enveloped viruses to facilitate budding and release from cells, a process that requires the same membrane topological changes as the endogenous cellular processes [13–18]. The ESCRT pathway has multiple components that act both early and late in vesiculation and membrane fission. The leading model is that ESCRT-III subunits drive the late stages by assembling into polymeric filaments that constrict the neck of the budding virus or vesicle [19–21]. The only core enzyme in the pathway, Vps4 (*v*acuolar *p*rotein *s*orting *4*), also performs an essential role by disassembling ESCRT-III filaments, a process that may be mechanistically coupled with membrane fission [22–25]. Although the ESCRT pathway has been primarily characterized in eukaryotic cells, homologs of Vps4 and its substrates have been identified in archaeal species belonging to the Sulfolobales or Desulfurococcales orders of the large crenarchaeal phylum [26,27], where they mediate cleavage furrow ingression and cytokinesis [28,29]. Thaumarchaea and

certain species of the euryarchaeal phylum also contain ESCRT-III and Vps4 homologs in addition to homologs of the bacterial cell division protein FtsZ [27]. Similar to their eukaryotic counterparts, archaeal ESCRT proteins may also serve as host factors for the release of viruses that infect these organisms [30,31].

Vps4 is a member of the meiotic clade of AAA ATPases [32–34] (*A*TPases *a*ssociated with diverse cellular *a*ctivities). These enzymes typically comprise a variable N-terminal substrate-binding domain followed by either one or two ATPase cassettes (type I and II AAA ATPases, respectively), each of which includes a large N-terminal domain and a smaller C-terminal domain. Vps4 is characterized by the presence of an N-terminal MIT (*m*icrotubule *i*nteracting and *t*rafficking) domain, a canonical ATPase cassette, and a C-terminal helix that packs against the large ATPase domain (Supplementary Fig. 1). MIT domains are three-helix bundles that recognize peptide motifs, termed MIM (*M*IT domain *i*nteracting *m*otifs) located in the C-terminal tails of their ESCRT-III substrates [35–38]. Eukaryotic Vps4 proteins also contain a three-strand insertion (termed the β-domain) following the third helix of the small ATPase domain. This feature contributes to Vta1p/LIP5 binding [39–41], which stimulates Vps4 assembly and ATPase activity *in vitro* [42,43], and promotes Vps4 activity *in vivo* [39,42,44]. Although the Vta1p/LIP5 activator is important in eukaryotes, crenarchaeal Vps4 proteins lack a β-domain [26] and also lack recognizable Vta1/LIP5 proteins.

Eukaryotic Vps4 exhibits an inactive monomer–dimer equilibrium in the absence of nucleotides and forms a functional higher-order oligomer upon binding ATP [40,45–49]. Obligate oligomerization is consistent with other AAA ATPases, which typically function as hexamers [33,50,51]. Thus far, no crystal structures reported for Vps4 show closed rings, but in most cases they show 6-fold packing about a screw axis [40,46,47,49,52]. Models for Vps4 assembly have therefore been guided by studies of its most closely related structural homologs, spastin [53] and p97 [54–57]. We have previously proposed a model for a Vps4 hexamer [40] that was generated by superposition on the D1 ring of the type II AAA ATPase p97 [55] and supported by mutagenesis of proposed interface residues [46].

However, three independent electron microscopy (EM) studies have reported models for the assembled Vps4 protein that do not conform to a single-ring hexamer. All three models feature a double-ring structure with 12 [48,58] or 14 [47] subunits but, otherwise, differ considerably from each other in subunit organization. Owing to the stabilizing effects of nucleotide binding, these structural studies were all performed using either non-hydrolyzable ATP analogs [47] or the Vps4p(E233Q) mutant [48,58]. Equivalent E-to-Q variants are commonly used for studies of AAA ATPases because they bind but do not hydrolyze ATP due to the requirement of the highly conserved glutamate to activate the water molecule that attacks the γ-phosphate [59,60].

To clarify models of Vps4 assembly, we have determined the oligomeric state of the wild-type protein in the presence of nucleotides. Surprisingly, although the *Saccharomyces cerevisiae* Vps4p(E233Q) mutant enzyme can form a dodecamer, as reported previously [40,48], we find that wild-type Vps4p assembles into a hexamer in the presence of nucleotides and remains hexameric when associated with Vta1p. In contrast to an earlier report [26], we also find that the Vps4 enzyme from the crenarchaeon *Sulfolobus solfataricus* displays ATPase activity and can assemble into a hexamer, although dodecameric assemblies can also form under non-physiological conditions. To understand crenarchaeal Vps4 better, we determined crystal structures of the ATPase domains of Vps4 proteins from *S. solfataricus* and *Acidianus hospitalis*. These structures lack β-domains but otherwise closely resemble the eukaryotic proteins, validating their designation as Vps4 homologs. Although these Vps4 proteins did not crystallize as discrete hexamers, they did form lattices with 6-fold screw axes that suggest models for the interfaces in the ring hexamer. Disruption of proposed interfaces prevents hexamerization in solution and abolishes ATPase activity, further supporting the p97-based homology model. Equivalent point mutations indicate that Vps4p hexamerization is required for MVB sorting in yeast, also supporting our model that Vps4 functions as a hexamer that resembles the D1 ring of p97.

Results

Wild-type *S. cerevisiae* Vps4p is a hexamer in the presence of nucleotides

Although wild-type Vps4p has not previously been reported to form stable assemblies, higher-order oligomerization is a prerequisite for Vps4p function [45]. The enzyme is expected to achieve high local concentrations *in vivo* when its MIT domains bind the MIM motifs on the polymeric ESCRT-III filaments, and we therefore reasoned that wild-type Vps4p would oligomerize at high protein concentrations. Indeed, wild-type Vps4p (100 μM, 1 mM ATP) eluted from an analytical size-exclusion column as a complex with an apparent molecular mass (MM) that approximated a hexamer (apparent MM = 245 kDa, calculated MM = 289 kDa; Fig. 1a, panel 1, red curve). The peak was asymmetric, however, and tailed toward smaller species, indicating that multiple Vps4p complexes might be present in rapid exchange. Consistent with this possibility, the retention time of the Vps4p

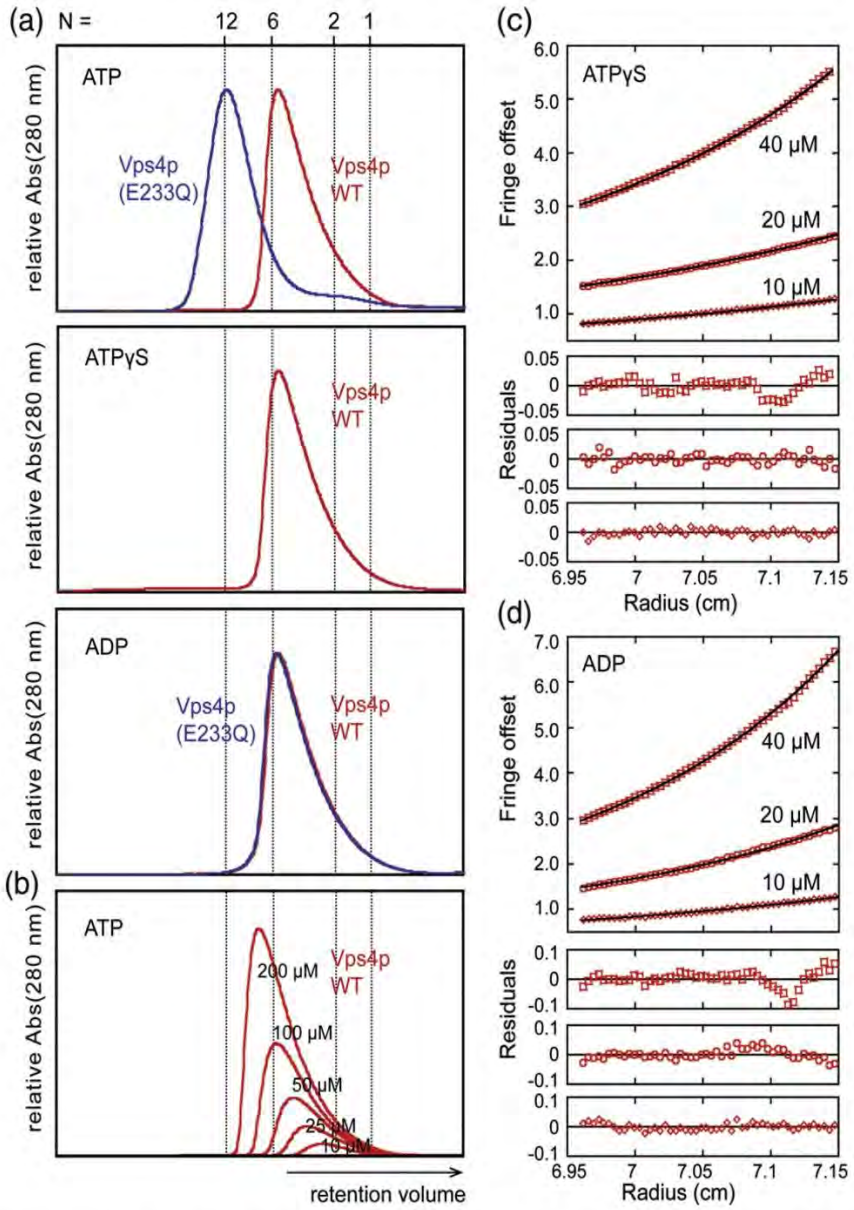

Fig. 1. Oligomerization of *S. cerevisiae* Vps4p proteins. (a) Size-exclusion chromatograms of wild-type Vps4p (red) and Vps4p(E233Q) (blue), injected at a concentration of 100 μM, in the presence of 2 mM magnesium chloride and 1 mM ATP, 0.2 mM ATPγS, or 1 mM ADP. Expected retention volumes for different oligomeric states of Vps4p based on molecular mass standards are indicated with dotted lines. Note that Vps4p(E233Q) elutes as a dodecamer in the presence of ATP but as a hexamer in the presence of ADP, whereas wild-type Vps4p elutes as a hexamer in the presence of ATP, ATPγS, or ADP. (b) Size-exclusion chromatograms of wild-type Vps4p at concentrations ranging from 10 μM to 200 μM in the presence of 1 mM ATP. Note that the complex migrates more slowly at lower concentrations, indicating that Vps4p is in a rapid equilibrium between different oligomeric states. (c and d) Equilibrium AUC at 4 °C indicates that wild-type Vps4p is in a dimer–hexamer equilibrium in the presence of (c) 1 mM ATPγS or (d) 1 mM ADP. The interference signal from sedimentation data at 5000 rpm is plotted *versus* the distance from the axis of rotation (radius) as red symbols. Three different protein concentrations are displayed as follows: 40 μM (upper), 20 μM (middle), and 10 μM (lower). The global fit to data obtained for three concentrations at rotor speeds of 3000 rpm (not shown) and 5000 rpm using a dimer–hexamer model is shown in black with residuals for all three concentrations displayed below.

oligomer increased when the protein concentration was reduced (Fig. 1b). Vps4p also formed hexamer-sized complexes in the presence of the non-hydrolyzable ATP analog ATPγS (100 μM Vps4p, 0.2 mM ATPγS; Fig. 1a, panel 2) and in the presence of ADP (100 μM Vps4p, 1 mM ADP; Fig. 1a, panel 3).

Consistent with previous reports that the hydrolysis-deficient Vps4p(E233Q) mutant dodecamerizes in the presence of ATP [40,48,58], we also found that ATP-bound Vps4p(E233Q) migrated more rapidly than the wild-type protein (Fig. 1a, panel 1, compare red and blue curves). In the presence of ADP, however, both the wild-type and hydrolysis-deficient Vps4p proteins eluted as hexamer-sized complexes (Fig. 1a, panel 3). These observations indicate the following: (1) wild-type yeast Vps4p oligomerizes reversibly into a higher-order complex that migrates primarily as an apparent hexamer on size-exclusion chromatography, (2) hexamerization is favored by high protein concentrations; (3) unlike Vps4p(E233Q), wild-type Vps4p does not form a stable dodecamer under our experimental conditions; and (4) both Vps4p and Vps4p(E233Q) can form hexamer-sized complexes in the presence of ADP.

Equilibrium analytical ultracentrifugation (AUC) experiments were performed to obtain shape-independent estimates of the mass of the nucleotide-bound Vps4p complexes and to determine their relative stabilities (Fig. 1c). The non-hydrolyzable ATP analog, ATPγS, was used in these experiments to avoid complications associated with ATP hydrolysis over the multiday centrifugation period. Importantly, ATPγS-bound and ATP-bound Vps4p have indistinguishable size-exclusion chromatography profiles (Fig. 1a, compare panels 1 and 2). The AUC data could not be adequately fit using single-species models for Vps4p dimers, hexamers, or dodecamers but were adequately described by a dimer–hexamer equilibrium model with an equilibrium dissociation constant of 3.7 nM^2 when subunit concentrations up to 80 μM were used. This dissociation constant implies that there will be equimolar concentrations of dimer and hexamer at a dimer concentration of 61 μM, in reasonable agreement with the size-exclusion chromatography data shown in Fig. 1. At higher concentrations (100–120 μM), the appearance of higher-molecular-mass species led to significant residual bias. Our attempts to globally fit all data using a dimer–dodecamer or a dimer–hexamer–dodecamer equilibrium did not produce satisfactory residuals, but the fits did indicate that the fraction of Vps4p forming higher-molecular-mass species was small under these conditions. Based on the K_D of 3.7 nM^2 estimated from centrifugation, we conclude that the nucleotide-bound Vps4p size-exclusion chromatography peaks represent rapidly equilibrating mixtures that initially consist of an approximately equimolar distribution of Vps4p subunits between hexamers and dimers in a hexamer:dimer ratio of 41:59 at the initial concentration of Fig. 1a, panel 2, and that small amounts of larger species appear at higher concentrations.

We also used equilibrium AUC to analyze the oligomeric state of Vps4p in the presence of ADP to determine if there is a difference in the stability of the complex in the presence of different nucleotides (Fig. 1d). Again, the radial distribution is best described by a dimer–hexamer equilibrium, this time, with a much tighter dissociation constant of 0.04 nM^2. This result challenges the concept that Vps4p oligomers only form in the presence of ATP.

S. cerevisiae Vps4p remains hexameric upon binding of Vta1p

Vta1p stimulates Vps4p ATPase activity *in vitro* at least in part by promoting Vps4p assembly [39]. We therefore tested the effect of adding equimolar concentrations of Vta1p to Vps4p (100 μM, 1 mM ATP). The Vps4p–Vta1p–ATP complex eluted as a single major peak (Fig. 2a, red curve) that contained both proteins (Fig. 2b) and had an apparent molecular mass of 520 kDa. We have previously shown that Vps4p(E233Q) and Vta1p form a stable 12:6 complex [58] (expected MM ≈ 800 kDa). We verified this finding (Fig. 2a, blue curve, apparent MM ≈ 910 kDa), confirming that the ATP-bound complex of wild-type Vps4p–Vta1p is substantially smaller than the ATP-bound complex of Vps4p(E233Q)–Vta1p. These observations indicate that wild-type Vps4p remains hexameric when bound to Vta1p because the complex is significantly smaller than the Vps4p(E233Q)–Vta1p complex.

Our efforts to determine the stoichiometry of the Vps4p–Vta1p complex were complicated by the poor separation of complex and unbound protein. Moreover, the relatively weak affinity of Vta1p for its binding site on Vps4p (K_D = 17 μM [41]), combined with the Vps4p self-association, produced a complicated mixture of species during the size-exclusion chromatography. Therefore, although both elution volume and band intensity suggest a 6:6 stoichiometry, we cannot rule out the possibility that the Vps4p hexamer can bind up to six Vta1p dimers, resulting in a 6:12 subunit stoichiometry [41].

Oligomeric state of crenarchaeal Vps4 homologs

Owing to the complexity of *S. cerevisiae* Vps4p oligomerization, we also examined the oligomerization behavior of simpler Vps4 proteins from the hyperthermophilic crenarchaeal species, *S. solfataricus* (SsoVps4; 36% amino acid identity with human VPS4B, 35% identity with *S. cerevisiae* Vps4p) and *A. hospitalis* (AhosVps4; 36% identity with human VPS4B, 37% identity with *S. cerevisiae* Vps4p). Primary sequences indicate that the crenarchaeal homologs lack a β-domain and do not associate with Vta1/LIP5 activators. Curiously, an earlier study concluded that recombinant SsoVps4 does not oligomerize [26]. This prompted us to consider the possibility that these thermophilic proteins might need to be heated in order to oligomerize. We found that this is indeed the case, and therefore, we incubated the Sso

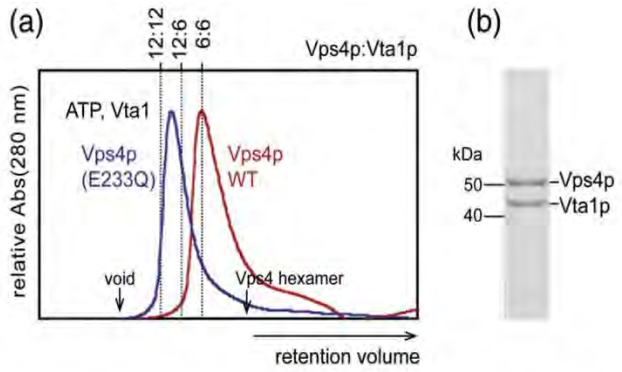

Fig. 2. Wild-type Vps4p remains hexameric and Vps4p(E233Q) remains dodecameric in the presence of Vta1p. (a) ATP-bound wild-type and E233Q Vps4p size-exclusion chromatograms. Calculated retention volumes for 6:6, 6:12, and 12:12 Vps4p–Vta1p complexes are indicated. The void volume and the expected elution volume for the Vps4p hexamer are indicated by arrows. (b) SDS-PAGE analysis of the peak fraction of wild-type Vps4p (48 kDa) in the presence of Vta1p (37 kDa) confirms that the peak represents a complex of both proteins.

and Ahos proteins for 15 min at 75 °C during the purification procedure (see Materials and Methods).

In the absence of nucleotide, both wild-type SsoVps4 and the hydrolysis mutant SsoVps4(E206Q) appeared to be dodecameric as analyzed by size-exclusion chromatography (Fig. 3a, panel 1, compare red and blue traces). This is similar to a report of the Vps4 homolog CdvC from *Metallosphaera sedula*, which forms dodecamer-sized oligomers in the absence of nucleotides [61]. In the presence of ATP or ADP, however, both wild-type and E206Q SsoVps4 eluted as lower-molecular-mass complexes, whose retention times were close to those expected for hexamers (Fig. 3a, panels 2 and 3). SsoVps4(E206Q) eluted slightly earlier than the wild-type protein, and both proteins migrated slightly more rapidly when bound to ADP than ATP. AhosVps4 behaved similarly to SsoVps4, both in the absence and in the presence of nucleotide (Supplementary Fig. 2 and data not shown).

Like *S. cerevisiae* Vps4p, the archaeal proteins eluted in asymmetric peaks, suggesting that the protein is rapidly interconverting between multiple oligomeric states. Consistent with this hypothesis, the retention volume of ATP-bound SsoVps4 decreased as the concentration increased (Fig. 3b, panel 1). Note that the peak maximum shifted to retention volumes of larger apparent molecular mass than a hexamer when concentrations higher than 100 μM were used. Because SsoVps4 will only oligomerize if the protein is exposed to elevated temperatures at least once during the purification procedure, we tested the effect of temperature on the migration behavior of SsoVps4 by performing similar size-exclusion chromatography experiments at room temperature (Fig. 3c, panels 2 and 3). For each concentration analyzed, the protein migrated more rapidly at room temperature than at 4 °C, indicating that oligomerization is entropically driven.

AUC analyses of SsoVps4

AUC was used to obtain shape-independent measures of the sizes and equilibria of SsoVps4. In the absence of nucleotide, the radial distribution fits a single-species dodecamer model (Fig. 4a) for the E206Q mutant. This analysis was also performed in the presence of 1 mM ATP, which was possible because ATPase activity was negligible at 4 °C. The equilibrium distribution of SsoVps4 in the presence of ATP could not be adequately fit by a single-species model, and the best fit was obtained using a dimer–hexamer model with a K_D of 0.01 nM^2 (Fig. 4b). We therefore conclude that the nucleotide-bound SsoVps4 size-exclusion chromatography peaks represent rapidly interconverting mixtures of hexamers and dimers, although in this case, the hexamer predominates because the estimated K_D implies that SsoVps4 subunits partition into a hexamer:dimer ratio of 89:11 at the initial concentration of size-exclusion chromatography (Fig. 3a, panel 2). Thus, despite their evolutionary divergence, Vps4 proteins from both yeast and crenarchaea can form stable dodecamers under some conditions, but in both cases, the wild-type Vps4 enzymes interconvert between dimers and hexamers in the presence of adenosine nucleotides.

We performed similar sedimentation equilibrium experiments on AhosVps4. However, this protein was more polydisperse and tended to form higher-order aggregates, and we were therefore not able to fit to random residuals.

ATPase activity of archaeal Vps4 proteins

Although sequence alignments show the presence of Walker A, Walker B, and sensor 1 motifs that are typical of authentic AAA ATPases (Supplementary Fig. 1), there is a report that SsoVps4 lacks ATPase activity [26]. The results of an ATPase activity assay

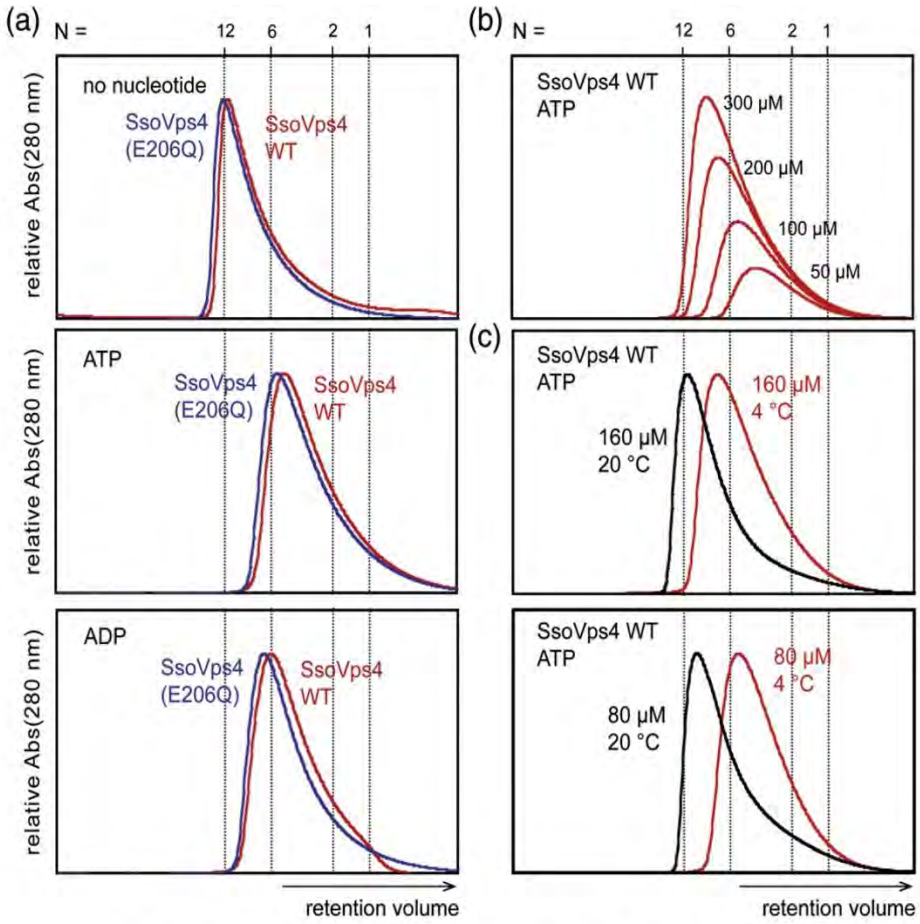

Fig. 3. Characterization of SsoVps4 oligomerization by size-exclusion chromatography. (a) Chromatograms of SsoVps4 (red) and SsoVps4(E206Q) (blue) injected at concentrations of 100 µM. Both proteins eluted as dodecamers in the absence of nucleotide but eluted as hexamers when the buffer was supplemented with 2 mM magnesium chloride and 1 mM ATP or ADP. (b) Chromatograms of different concentrations of SsoVps4. The shift in retention volume following injection at different protein concentrations indicates that SsoVps4 rapidly interconverts between multiple oligomeric states. (c) A shift of temperature from 4 °C (red) to 20 °C (black) reduces the elution volume: 160 µM (upper) and 80 µM (lower). Standard molecular mass markers displayed very similar retention volumes at the two temperatures.

have not been reported for AhosVps4. Our observation that the recombinant Vps4 homologs of *S. solfataricus* and *A. hospitalis* form higher-order oligomers upon heat treatment prompted us to test whether these proteins are functional ATPases at different temperatures. As shown in Fig. 5, ATP hydrolysis was not detected at 4 °C or 37 °C, but both SsoVps4 and AhosVps4 displayed strong ATPase activity at 60 °C. The rate of ATP hydrolysis was 16.8 ATP/min/subunit for SsoVps4 at an enzyme concentration of 0.5 µM and was 67 ATP/min/subunit for AhosVps4 at 0.2 µM. As expected, mutation of the Walker B glutamate abolished enzymatic activity in the point mutants SsoVps4(E206Q) and AhosVps4(E200Q) (Fig. 5). Consistent with our results, a previous study found a maximal ATP hydrolysis rate of 210 ATP/min/subunit (reported as 0.5 µmol ATP/min/mg protein) for the Vps4 homolog from the hyperthermophilic archaeon *M. sedula* [61] at the same temperature. The requirement for high temperature is consistent with the observation that increasing temperature drives oligomerization (above), presumably because these proteins have been evolutionarily optimized to function at elevated temperature [62].

Crystal structures of Vps4 proteins from *S. solfataricus* and *A. hospitalis*

Motivated by the observation that crenarchaeal Vps4 proteins oligomerize more tightly without the requirement for an activator protein, we determined crystal structures of SsoVps4 and AhosVps4 in the absence of nucleotide. Unfortunately, neither structure appears to capture an active arrangement. Data collection and refinement statistics are listed in Table 1. SsoVps4

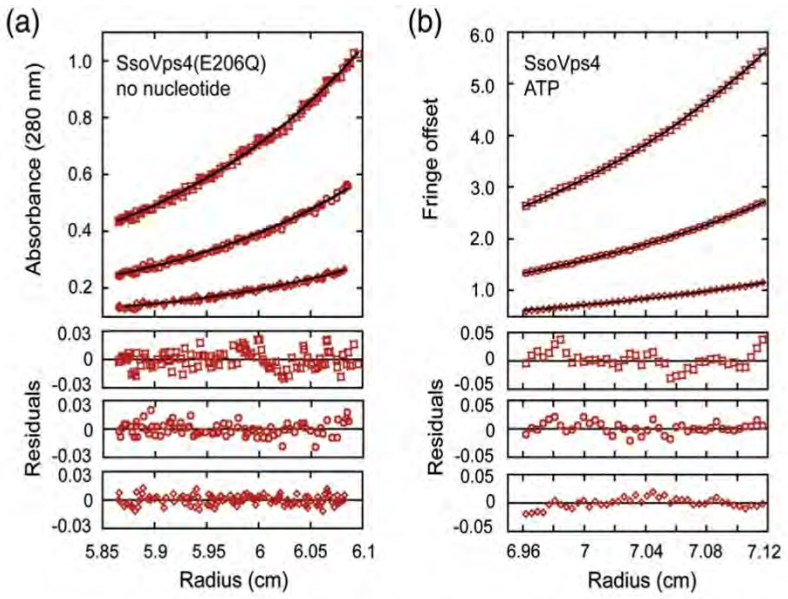

Fig. 4. Characterization of SsoVps4 oligomerization by equilibrium AUC. (a) SsoVps4(E206Q) in the absence of nucleotide. Data are shown from a 3500-rpm spin at three protein concentrations: 10 μM (upper), 5 μM (middle), and 2.5 μM (lower). The black line corresponds to an ideal species fit for dodecameric SsoVps4. Residuals are displayed below. (b) Wild-type SsoVps4 in the presence of 1 mM ATP at 5000 rpm. Three different protein concentrations are displayed as follows: 47 μM (upper), 24 μM (middle), and 12 μM (lower). Interference scans at 3000 rpm for all concentrations were also included in the fit but are not shown here. The fit obtained using a dimer–hexamer model is shown in black.

crystals were grown from a construct spanning the ATPase domain (residues 85–372) containing the E206Q mutation. Diffraction data were collected to a resolution of 2.8 Å, the structure was determined by the single-wavelength anomalous diffraction method,

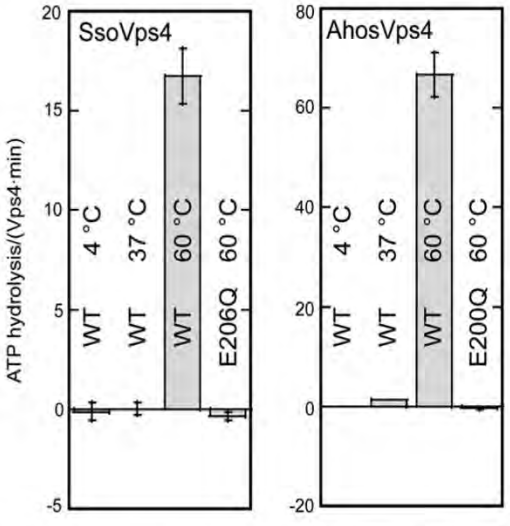

Fig. 5. ATPase activity of SsoVps4 and AhosVps4 at 4 °C, 37 °C, and 60 °C. Both proteins are active at 60 °C. Mutation of the Walker B glutamate in SsoVps4(E206Q) or AhosVps4(E200Q) abolishes ATPase activity.

and the model was refined to an R_{free} value of 25%. Most of the sequence for residues 99–369 is ordered and reveals an AAA ATPase cassette that closely resembles previously reported structures of eukaryotic Vps4 proteins (Fig. 6a). Superposition of the SsoVps4(E206Q) ATPase domain (green) with yeast Vps4p (PDB ID: 3EIE [46], blue) yields a root-mean-square deviation of 1.62 Å on 237 pairs of C^{α} atoms. We also crystallized wild-type, full-length AhosVps4, determined the structure by molecular replacement using our refined SsoVps4 structure as a search model, and refined the model to an R_{free} value of 26% against data to a resolution of 2.1 Å. Although SDS-PAGE analysis of washed crystals confirmed that the crystals contained the intact protein (Supplementary Fig. 3), the MIT domain and linker are not visible in electron density maps, presumably due to disorder. Most of the sequence corresponding to residues 93–362, which covers the ATPase cassette of AhosVps4, is well ordered. Consistent with their 75% amino acid sequence identity, the AhosVps4 and SsoVps4 ATPase cassette structures superimpose closely, with a root-mean-square deviation of 0.49 Å on 206 pairs of C^{α} atoms (Fig. 6b).

All five helices of the eukaryotic large AAA ATPase domain and four helices of the small AAA ATPase domain have counterparts in the crenarchaeal proteins. We found a minor difference, in that the human, mouse, and yeast Vps4 ATPase cassette

Table 1. X-ray data collection and refinement statistics.

	SsoVps4(E206Q, 85–372)	AhosVps4
Data collection		
Beamline	SSRL 7-1	SSRL 11-1
Wavelength (Å)	0.97945	0.9795
Resolution range (Å)	23–2.73 (2.83–2.73)	28–2.1 (2.18–2.1)
Space group	$P6_4$	$P6_5$
Cell parameters (Å)		
a	101.3	96.0
c	64.7	79.5
Total observations	113,696	229,024
Unique observations	19,379	24,622
Completeness (%)	98.6 (92.0)	98.9 (98.4)
$\langle I \rangle / \sigma(I)$	25.2 (7.8)	13.5 (4.5)
R_{sym}	0.073 (0.657)	0.083 (0.673)
Refinement		
R_{work}/R_{free} (%)	21.6/25.1	21.4/25.6
RMSD from ideal geometry		
Bond lengths (Å)	0.008	0.017
Bond angles (°)	1.2	1.4
Average *B*-factor (Å^2)	91.9	46.7
Ramachandran favored (%)	98.7	99.6
Ramachandran outliers (%)	0	0

Values in parentheses refer to the high-resolution shell.

structures each contain six β-strands in the large AAA ATPase domain, whereas both of our archaeal Vps4 structures display only five β-strands, and the residues that correspond to the eukaryotic β′-strand are disordered in archaea. Also, as anticipated from sequence alignments (Supplementary Fig. 1), the ~45-residue β-domain that is inserted between helix 8 and helix 9 in eukaryotic Vps4 proteins is missing from the SsoVps4 and AhosVps4 AAA ATPase cassettes. Instead, the two helices are connected by a well-ordered loop.

Analysis of the crystallographic interface

None of the crystal structures reported to date directly reveals how the active Vps4 oligomer is assembled. We have previously presented mutagenesis data that implicate an interface seen in crystal forms of yeast Vps4p as being important for assembly [46]. Remarkably, this interface, which propagates the crystallographic or non-crystallographic 6_5 screw axis seen in all published yeast Vps4p crystal structures [43,46,47] and all reported structures of human and murine VPS4B [40,52], is also found in SsoVps4 and AhosVps4 crystals, where it propagates 6_4 and 6_5 screw axes, respectively. Despite the difference in helical pitch, the ~600-Å^2 interfaces are highly similar in SsoVps4 and AhosVps4 crystals. The majority of the interface is formed by residues in helix 1 of the large AAA ATPase domain packing against helix 8 of the small AAA ATPase domain, and superposition of 13 pairs of C^α atoms from helices 1 and 8 across the SsoVps4 and AhosVps4 interfaces yields an RMSD of 1.2 Å. The interface residues are highly conserved throughout crenarchaea, and as seen in many functional interfaces [63], central hydrophobic residues are flanked by polar interactions.

Guided by our earlier analysis of yeast Vps4p interfaces and the observation that packing of SsoVps4 and AhosVps4 resembles packing of the closed hexameric ring of p97 D1 when viewed along the screw axis (Fig. 7a), we propose a Vps4 hexamer model that resembles p97 D1. The conserved subunit

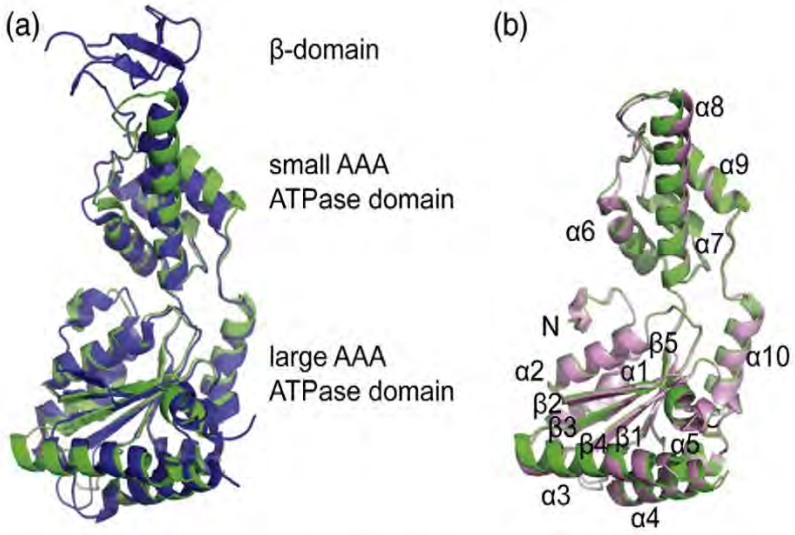

Fig. 6. Crystal structures of the ATPase cassettes of SsoVps4 and AhosVps4. (a) Superposition of SsoVps4 (green) and Vps4p (PDB ID: 3EIE [46], blue) yields an RMSD of 1.62 Å over 237 pairs of C^α atoms. (b) The structures of SsoVps4 (green) and AhosVps4 (pink) overlay with an RMSD of 0.49 Å on 206 pairs of C^α atoms.

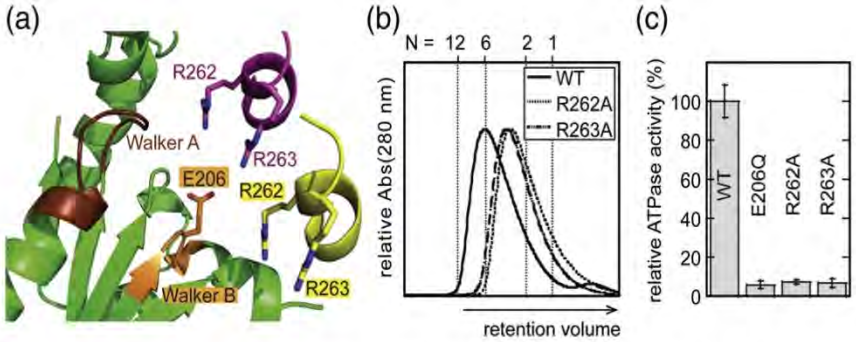

Fig. 8. Arginine finger residues contribute to Vps4 oligomerization and are important for ATPase activity. (a) The nucleotide binding site of SsoVps4 (green) contains the conserved Walker A (brown) and Walker B (orange) motifs. The neighboring subunit in the crystal is shown in yellow, and its position in the p97-like hexamer model is shown in magenta. Glutamate 206 and the potential arginine finger residues 262 and 263 are shown in stick representation. (b) Point mutations R262A and R263A destabilize the oligomer and (c) abolish ATPase activity.

Functional relevance of the p97-like hexamer in *S. cerevisiae*

We have previously described mutations that disrupt higher-order assembly of *S. cerevisiae* Vps4p(E233Q). Specifically, each of the Vps4p(E233Q) L151D, I351A, and I354D point mutant proteins are monomeric [46], and the Vps4p(E233Q, R352A) mutant is dimeric in solution [40]. All of these mutations map to the interface between neighboring subunits in our p97-based model of the assembled Vps4p hexamer [40] (Fig. 9a). As shown in Fig. 9b, we found that the L151D and R352A mutations also disrupted higher-order oligomerization of wild-type Vps4p.

We tested these two hexamerization mutants for the ability to support the ESCRT-dependent sorting of a model green fluorescent protein (GFP)-carboxypeptidase S (CPS) cargo into yeast MVBs [36] (Fig. 9c). When the ESCRT pathway is functional, GFP-CPS is sorted into MVB vesicles and concentrates within the vacuole, and the lumen fluoresces green (Fig. 9c, inset, upper panel). In the absence of ESCRT pathway activity, the GFP-CPS cargo is not sorted into MVB vesicles, resulting in green fluorescent labeling of the limiting vacuolar membrane (Fig. 9c, inset, lower panel). The ESCRT pathway requires Vps4p activity, and these two different phenotypes are therefore observed in yeast cells that either express or lack wild-type Vps4p. Each of the phenotypes was highly penetrant, as reflected in the scoring of 3× 100 cells that either expressed wild-type Vps4p (95.1 ± 2.4% of cells exhibited luminal GFP staining) or lacked Vps4p (1.1 ± 1.9% of cells exhibited luminal staining). To determine the importance of hexamerization, we

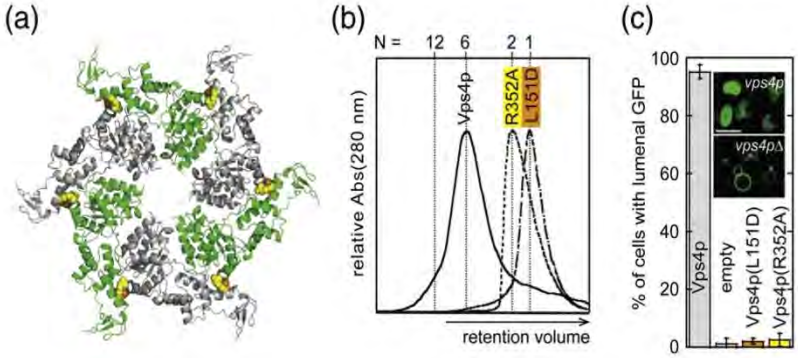

Fig. 9. Mutational analysis of the hexamer interface in yeast Vps4p. (a) L151 (orange spheres) and R352 (yellow spheres) map to the hexamer interface in the p97-like ring. (b) Vps4p(R352A) and Vps4p(L151D) do not form higher-order oligomers as shown by size-exclusion chromatography in the presence of 1 mM ATP. (c) Vacuolar protein sorting of the model cargo CPS-GFP into the vacuole lumen is severely impaired in yeast cells expressing interface mutants Vps4p(L151D) or Vps4p(R352A) as compared to cells containing wild-type Vps4p. Insets show control examples of successful (upper) and unsuccessful (lower) CPS-GFP sorting. Error bars are defined in the text.

scored GFP-CPS sorting in cells that expressed either monomeric Vps4p(L151D) (2.0 ± 1.0% of cells exhibiting vacuolar membrane staining) or dimeric Vps4p(R352A) (2.5 ± 2.1% of cells exhibiting vacuolar membrane staining). The expression level of Vps4p was not significantly affected by the point mutations and was similar to the level of endogenous Vps4p (data not shown). Thus, two different point mutations that disrupt the formation of the p97-like Vps4p hexamer *in vitro* also inhibit Vps4p function in MVB protein sorting in yeast.

Discussion

Vps4 is a key component of the cellular ESCRT pathway. To understand how conformational changes during the ATP hydrolysis cycle translate into remodeling of the ESCRT-III polymer, it is critical to define the quaternary structure of the active Vps4 enzyme. Previous reports have described Vps4p as a double-ring structure because biophysical characterization of the *S. cerevisiae* Vps4p(E233Q) mutant suggested that the assembled enzyme contained 10–14 subunits. This hypothesis was supported by three independent EM reconstructions that all contained two stacked rings with 6-fold [48,58] or 7-fold [47] symmetry, although in other regards, the EM reconstructions were dramatically different from one another. The suggested double-ring structure also differed from other type I AAA ATPases such as spastin, which form a single hexameric ring [53]. Type II AAA ATPases such as p97 do have two stacked rings, but the double-ring architecture results from a hexameric subunit arrangement with each subunit contributing two AAA ATPase domains [57].

The data presented here show that wild-type yeast and archaeal Vps4 proteins exist in equilibrium between oligomeric states, and at sufficiently high concentration in the presence of nucleotide, they assemble into hexamers and other higher-order oligomers. These findings are consistent with the concentration dependence of ATP hydrolysis rates that we and others [39,45,65] have observed *in vitro* and support a model for Vps4 activation in which the high local concentration that results from recruitment to ESCRT-III polymers, together with activation by LIP5/Vta1, drives assembly into an active complex [44,66]. The distribution of oligomeric states that we observe for wild-type Vps4 *in vitro* raises the question: Which one represents the biologically active species? AAA ATPases most commonly function as hexameric assemblies [50,51,67] but can sometimes also exist in oligomeric states other than that of their functional unit. For example, (1) the ClpB AAA ATPase switches from a predominantly heptameric assembly to a hexamer upon nucleotide binding [68], (2) the archaeal proteasome activating nucleosidase PAN exists as a dodecamer when overexpressed in bacteria [69] but functions as a hexamer [70], and (3) RuBisCO activase exists in a concentration-dependent distribution of oligomeric states [71], but a point mutation can convert the enzyme into functional hexamers [72].

In the case of yeast Vps4p, the hydrolysis-deficient protein, Vps4p(E233Q), is dodecameric in the presence of ATP. We suggest that this assembly may be artifactual, however, because the oligomerization behavior of Vps4p(E233Q) in the presence of ATP differs from that of the wild-type protein. Replacing the conserved Walker B glutamate by a glutamine is common in studies of ATPases because it allows ATP binding and assembly while preventing hydrolysis [60]. Indeed, there are no significant differences between the crystal structures of unassembled wild-type and hydrolysis-deficient Vps4p enzymes nor do these proteins differ in dimerization behavior [46]. Moreover, mixed complexes of wild-type Vps4p and Vps4p(E233Q) retain ATPase activity [45,65]. Nevertheless, our data indicate that ATP stabilizes Vps4p(E233Q) in a dodecameric assembly under conditions where the wild-type protein is predominantly hexameric.

Crystal structures of RecA-like and AAA+ hexameric helicases in complex with substrates indicate that ring asymmetry is fundamental to mechanism [73,74]. Similarly, we propose that wild-type Vps4 forms a closed hexameric ring, with ring closure accommodated by different conformations within the subunits around the ring. In this model, the conformational variability results from alternative flexing between large and small ATPase domains that is induced by different ATP/ADP nucleotide binding states and therefore varies throughout the reaction cycle. This hypothesis is supported by crystal structures of Vps4p that suggest a nucleotide-dependent change in the angle between the large and small AAA ATPase domains [46,49]. When ATP is bound to hydrolysis-deficient Vps4p(E233Q), subunits may be forced into the same nucleotide state, thereby artificially restricting its ability to assume the active asymmetric assembly. The resulting aberrant hexamer may present surfaces that stabilize non-native ring stacking. The second acidic residue in the Walker B motif, which corresponds to Glu233 in Vps4p, forms an intersubunit salt bridge in p97 and NSF [75] except when this interaction is displaced by the γ-phosphate of bound ATP. Given the assumption that native assembly requires different nucleotide states, Vps4p(E233Q) may form aberrant assemblies because it cannot adopt the required range of conformations. A requirement for different nucleotide states could also explain why we have not observed dodecamer formation upon binding of non-hydrolyzable ATPγS to the wild-type enzyme. Interestingly, the equivalent mutation does not seem to significantly affect oligomerization in archaeal proteins.

In short, while we cannot fully explain the assembly of Vps4p(E233Q), we have focused our studies on the more relevant wild-type protein.

Our data support the model that the hexamer is the smallest functional unit of the Vps4 enzyme. The following observations support the relevance of a p97-like hexameric ring structure: (1) wild-type Vps4 proteins from *S. cerevisiae, S. solfataricus*, and *A. hospitalis* assemble into hexamers in the presence of nucleotide; (2) wild-type Vps4p remains hexameric in complex with Vta1p activators; and (3) conservation of the hexamer interface is suggested by crystal structures and by analyses of Vps4 point mutations that disrupt assembly *in vitro* and block ESCRT pathway function in yeast cells. Although we have not definitively determined a stoichiometry for the Vps4–Vta1 complex, structural studies indicate that each β-domain associates with a Vta1 dimer [41]. Our data do not indicate that binding of the Vta1 dimer to the β-domains at the periphery of Vps4 rings stabilizes interactions between hexamers as suggested by previous studies [41,43] insofar as we do not observe such assemblies in our size-exclusion chromatography experiments (Fig. 2a). Nevertheless, we cannot exclude the possibility that such clustering of hexamers may occur at the high local concentrations expected at the ESCRT-III lattice.

In addition to hexamers, we also observed a small fraction of larger complexes of *S. cerevisiae* and crenarchaeal wild-type Vps4. We do not know how the hexamers assemble further or whether these structures are biologically relevant. The size of higher-order assemblies continues to increase with increasing protein concentration. One possible explanation for this observation is that non-native ring structures that form in the presence of a single type of nucleotide are prone to stacking interactions and give rise to double-ring structures as described for Vps4p(E233Q). Alternatively, if ring closure cannot be accomplished, subunits may be added to the ends of a spiral that may resemble the helical packing in the crystal lattice. A limitation of our *in vitro* studies is that they were performed in the absence of the ESCRT-III substrate, and further studies are needed to understand the effects of cofactor and substrate binding on the oligomerization state. The leading model is that substrates bind to the pore loops at the center of the Vps4 hexamer and, in doing so, impart asymmetry upon the hexamer. Visualizing the Vps4 structure that binds substrate and learning how its asymmetry is coupled to progression of ATP binding and hydrolysis in the different subunits will be fundamental in understanding Vps4 mechanism. Nevertheless, our finding that the yeast and archaeal Vps4 proteins oligomerize in a concentration-dependent manner using a conserved hexamerization interface and that the wild-type proteins form hexamers in the presence of ATP supports the model that Vps4 functions as a spastin-like [53] six-membered ring.

Materials and Methods

Protein expression and purification

S. cerevisiae Vps4p and Vta1p were expressed and purified as previously described [40,46]. The Vps4 gene (SSO0909) from *S. solfataricus* was amplified from genomic DNA (ATCC 35092D-5) and cloned into a pET151 vector (Invitrogen) encoding an N-terminal 6× His-tag followed by a PreScission protease (GE Healthcare) cleavage site. The Vps4 gene from *A. hospitalis* was synthesized by DNA2.0 (Menlo Park, CA, USA) with the same cleavable N-terminal 6× His-tag and cloned into pJexpress414 (DNA2.0). Mutations were introduced by QuikChange mutagenesis (Stratagene). Plasmids for protein expression were deposited at the DNASU Plasmid Repository† [76] (Supplementary Table 1).

SsoVps4 and AhosVps4 were expressed in *Escherichia coli* BL21(DE3) RIL cells (Stratagene) grown in ZY autoinduction media at 37 °C for 6 h and then at 19 °C overnight. Cells were pelleted by centrifugation, resuspended in lysis buffer [25 mM Tris–HCl (pH 7.4), 450 mM NaCl, 20 mM imidazole, 1 mg/ml lysozyme, and protease inhibitors], and incubated for 45 min on ice followed by sonication and clarification by centrifugation (15,000 rpm, 45 min, 4 °C). The supernatant was incubated at 75 °C for 15 min, precipitated protein was removed by centrifugation, and the soluble fraction was bound to Ni-NTA agarose equilibrated with 25 mM Tris–HCl (pH 7.4), 450 mM NaCl, and 20 mM imidazole. Following a wash with the same buffer, protein was eluted with 200 mM imidazole; dialyzed into 25 mM Tris–HCl (pH 7.4), 150 mM NaCl, 1 mM ethylenediaminetetraacetic acid, and 1 mM DTT; and incubated with 1 mg His-tagged PreScission protease per 100 mg of protein overnight at 4 °C to remove the N-terminal His-tag. Uncleaved protein and the protease were removed by batch-binding to Ni-NTA agarose. Cleaved Vps4 was further purified by size-exclusion chromatography in 25 mM Tris–HCl (pH 7.4) and 100 mM NaCl using a Superdex S200 column. Yields were typically 25 mg of pure protein per liter of bacterial culture.

Structure determination

Crystals were grown in the absence of nucleotide by sitting-drop vapor diffusion at 20 °C using protein in the size-exclusion chromatography buffer. Selenomethionine-substituted SsoVps4(85–372, E206Q) crystals grew in drops composed of 1 μl of a 7 mg/ml protein stock solution and 2 μl of reservoir solution [70% (v/v) methyl-2,4-pentanediol and 100 mM Hepes (pH 7.5)]. AhosVps4 crystals grew in drops composed of 1.5 μl of 10 mg/ml protein mixed with 1.5 μl of reservoir solution [0.2 M $MgCl_2$, 0.1 M Hepes (pH 7.5), and 30% (v/v) polyethylene glycol 400]. In both cases, crystals were cryo-cooled for data collection by plunging into liquid nitrogen directly from the mother liquor.

Diffraction data were collected at beamlines 11-1 (AhosVps4) and 7-1 [SsoVps4(85–372, E206Q)] of the Stanford Synchrotron Radiation Lightsource (SSRL) and processed using the HKL2000 suite [77]. Phases for SsoVps4(85–372, E206Q) were determined by the single-wavelength anomalous diffraction method using SOLVE [78]. The AhosVps4 structure was determined by molecular

replacement using PHASER [79] and the refined structure of SsoVps4(85–372, E206Q) as a search model. Both models were refined using Refmac [80] and Phenix with rounds of rebuilding in Coot [81].

Interfaces were analyzed using PISA [82] and structures superimposed using secondary structure matching [83] as implemented in the CCP4 package [84]. Figures of molecular structures were prepared in PyMOL [85].

Analytical size-exclusion chromatography

Size-exclusion chromatography was performed at 4 °C unless otherwise stated. A Superdex 200 size-exclusion column (GE Healthcare) was calibrated with molecular mass standards (Biorad). Protein samples at a concentration of 100 µM (unless indicated otherwise) were used for size-exclusion chromatography in 25 mM Tris–HCl (pH 7.4) and 100 mM NaCl or in the same buffer supplemented with 2 mM magnesium chloride and 1 mM ATP, 1 mM ADP, or 0.2 mM ATPγS. For yeast proteins, the buffer was supplemented with 1 mM DTT. Archaeal proteins were analyzed in the absence of reductant because they contain only a single cysteine that is not exposed on the surface. Vps4 proteins were preincubated with the respective nucleotide at the concentration used in the size-exclusion chromatography buffer for 5 min on ice prior to analysis.

Analytical ultracentrifugation

AUC experiments were performed using absorbance optics for nucleotide-free experiments and Rayleigh interference optics in the presence of nucleotides to avoid complications from nucleotide absorbance. Equilibrium sedimentation experiments on SsoVps4(E206Q) in the absence of nucleotide were performed at 4 °C using an XL-A analytical ultracentrifuge (Beckman Coulter). Sample cells with a six-channel centerpiece were filled with 120 µl of the protein sample at concentrations ranging from 2.5 µM to 10 µM, and 125 µl of size-exclusion chromatography buffer was loaded into the reference sectors. Absorbance scans at 280 nm were taken at equilibrium after centrifugation at 3500 rpm and 5000 rpm.

Sedimentation equilibrium experiments in the presence of nucleotides were performed using an XL-I analytical ultracentrifuge (Beckman Coulter). External loading cells with a two-channel centerpiece were loaded with 140 µl of water and aged by alternate cycles of centrifugation at 8000 rpm and re-torquing until the cells were mechanically stable, after which blank scans were then taken at all speeds used for the experiment following a procedure described by Cole *et al.* [86]. The water was then exchanged for 120 µl of protein samples at concentrations ranging from 10 to 50 µM in 25 mM Tris–HCl (pH 7.4), 100 mM NaCl, and 2 mM magnesium chloride supplemented with 1 mM ATP, ATPγS, or ADP with the corresponding buffer in the reference cell. Interference data were collected at 4 °C and rotor speeds of 3000 and 5000 rpm and were analyzed using the Heteroanalysis Software (version 1.1.56) [87]. Theoretical molecular masses and partial specific volumes were calculated in SEDNTERP (version 1.09) [88] based on the amino acid sequence. To fit interference data, we converted the extinction coefficient at 280 nm to a refractive index increment using a factor of 2.75.

ATPase activity

ATPase activity of Vps4 proteins was measured as described for human VPS4A [66]. Reactions containing 0.1–0.5 µM Vps4 in 25 mM Tris–HCl (pH 7.4), 100 mM NaCl, 5 mM $MgCl_2$, and 1 mM ATP in a total volume of 50 µl proceeded for at least 5 min at the temperature indicated (4, 37, or 60 °C). The reaction was then placed on ice and quenched with 100 µl of malachite green color reagent [14 mM ammonium molybdate, 1.3 M HCl, 0.1% (v/v) Triton X-100, and 1.5 mM malachite green] and 50 µl of 21% (w/v) citric acid. The green complex formed by malachite green, molybdate, and free phosphate was detected by absorbance at 650 nm using a plate reader. A sodium phosphate standard curve was used to estimate the amount of phosphate released during ATP hydrolysis. Error bars denote standard deviations from three independent samples.

GFP-CPS sorting in yeast cells

Vacuolar cargo sorting assays were performed as previously described [36]. Confocal microscopy was used to image *vps4pΔ* yeast cells in a SEY6210 genetic background harboring pRS415MET + GFP-CPS and either pRS416 + Vps4p (wild type or mutant) or an empty control plasmid. For each data set, 100 cells were scored for GFP fluorescence in the vacuolar lumen in three independent experiments. Limiting vacuolar membranes were stained with FM4-64.

Accession numbers

Atomic coordinates and structure factors have been deposited in the Protein Data Bank with accession codes 4LGM for SsoVps4(E206Q, 85–372) and 4LCB for AhosVps4.

Acknowledgements

We thank Markus Babst (University of Utah) and Janet Shaw (University of Utah) for antibody reagents. Portions of this work were performed in Core Facilities at the University of Utah, which were supported by P30CA042014 from the National Cancer Institute. Portions of this research were performed at the SSRL, a national user facility operated by Stanford University on behalf of the US Department of Energy, Office of Basic Energy Sciences. The SSRL Structural Molecular Biology Program is supported by the Department of Energy, Office of Biological and Environmental Research, and the National Institutes of Health; National Center for Research Resources; Biomedical Technology Program; and the National Institute of General Medical Sciences. N.M. was supported by grants PBZHP3-135952 and PBZHP3-141465 from

the Swiss National Science Foundation. This work was supported by National Institutes of Health grant P50 GM082545 to C.P.H. and W.I.S.

Appendix A. Supplementary data

Supplementary data to this article can be found online at http://dx.doi.org/10.1016/j.jmb.2013.09.043.

Received 14 August 2013;
Received in revised form 26 September 2013;
Accepted 30 September 2013
Available online 23 October 2013

Keywords:
multivesicular body;
HIV budding;
ESCRT;
AAA ATPase;
protein oligomerization

Present address: M. D. Gonciarz, Lilly Corporate Center, Indianapolis, IN 46285, USA.
† http://dnasu.org/DNASU/

Abbreviations used:
EM, electron microscopy; AUC, analytical ultracentri fugation; GFP, green fluorescent protein; CPS, carboxypeptidase S; SSRL, Stanford Synchrotron Radiation Lightsource.

References

[1] Carlton JG, Martin-Serrano J. Parallels between cytokinesis and retroviral budding: a role for the ESCRT machinery. Science 2007;316:1908–12.
[2] Morita E, Sandrin V, Chung HY, Morham SG, Gygi SP, Rodesch CK, et al. Human ESCRT and ALIX proteins interact with proteins of the midbody and function in cytokinesis. EMBO J 2007;26:4215–27.
[3] Caballe A, Martin-Serrano J. ESCRT machinery and cytokinesis: the road to daughter cell separation. Traffic 2011;12:1318–26.
[4] Babst M, Sato TK, Banta LM, Emr SD. Endosomal transport function in yeast requires a novel AAA-type ATPase, Vps4p. EMBO J 1997;16:1820–31.
[5] Bishop N, Woodman P. ATPase-defective mammalian VPS4 localizes to aberrant endosomes and impairs cholesterol trafficking. Mol Biol Cell 2000;11:227–39.
[6] Finken-Eigen M, Rohricht RA, Kohrer K. The VPS4 gene is involved in protein transport out of a yeast pre-vacuolar endosome-like compartment. Curr Genet 1997;31:469–80.
[7] Fujita H, Yamanaka M, Imamura K, Tanaka Y, Nara A, Yoshimori T, et al. A dominant negative form of the AAA ATPase SKD1/VPS4 impairs membrane trafficking out of endosomal/lysosomal compartments: class E vps phenotype in mammalian cells. J Cell Sci 2003;116:401–14.
[8] Yoshimori T, Yamagata F, Yamamoto A, Mizushima N, Kabeya Y, Nara A, et al. The mouse SKD1, a homologue of yeast Vps4p, is required for normal endosomal trafficking and morphology in mammalian cells. Mol Biol Cell 2000;11:747–63.
[9] Hanson PI, Cashikar A. Multivesicular body morphogenesis. Annu Rev Cell Dev Biol 2012;28:337–62.
[10] Deatherage BL, Cookson BT. Membrane vesicle release in bacteria, eukaryotes, and archaea: a conserved yet underappreciated aspect of microbial life. Infect Immun 2012;80:1948–57.
[11] Nabhan JF, Hu R, Oh RS, Cohen SN, Lu Q. Formation and release of arrestin domain-containing protein 1-mediated microvesicles (ARMMs) at plasma membrane by recruitment of TSG101 protein. Proc Natl Acad Sci U S A 2012;109:4146–51.
[12] Wehman AM, Poggioli C, Schweinsberg P, Grant BD, Nance J. The P4-ATPase TAT-5 inhibits the budding of extracellular vesicles in *C. elegans* embryos. Curr Biol 2011;21:1951–9.
[13] Bieniasz PD. Late budding domains and host proteins in enveloped virus release. Virology 2006;344:55–63.
[14] Fujii K, Hurley JH, Freed EO. Beyond Tsg101: the role of Alix in "ESCRTing" HIV-1. Nat Rev Microbiol 2007;5:912–6.
[15] Morita E, Sundquist WI. Retrovirus budding. Annu Rev Cell Dev Biol 2004;20:395–425.
[16] Welsch S, Muller B, Krausslich HG. More than one door—budding of enveloped viruses through cellular membranes. FEBS Lett 2007;581:2089–97.
[17] Weiss ER, Gottlinger H. The role of cellular factors in promoting HIV budding. J Mol Biol 2011;410:525–33.
[18] Martin-Serrano J, Neil SJ. Host factors involved in retroviral budding and release. Nat Rev Microbiol 2011;9:519–31.
[19] Bodon G, Chassefeyre R, Pernet-Gallay K, Martinelli N, Effantin G, Hulsik DL, et al. Charged multivesicular body protein 2B (CHMP2B) of the endosomal sorting complex required for transport-III (ESCRT-III) polymerizes into helical structures deforming the plasma membrane. J Biol Chem 2011;286:40276–86.
[20] Effantin G, Dordor A, Sandrin V, Martinelli N, Sundquist WI, Schoehn G, et al. ESCRT-III CHMP2A and CHMP3 form variable helical polymers *in vitro* and act synergistically during HIV-1 budding. Cell Microbiol 2013;15:213–26.
[21] Hanson PI, Roth R, Lin Y, Heuser JE. Plasma membrane deformation by circular arrays of ESCRT-III protein filaments. J Cell Biol 2008;180:389–402.
[22] Henne WM, Buchkovich NJ, Emr SD. The ESCRT pathway. Dev Cell 2011;21:77–91.
[23] Hurley JH. The ESCRT complexes. Crit Rev Biochem Mol Biol 2010;45:463–87.
[24] Hill CP, Babst M. Structure and function of the membrane deformation AAA ATPase Vps4. Biochim Biophys Acta 2012;1823:172–81.
[25] McCullough J, Colf LA, Sundquist WI. Membrane fission reactions of the mammalian ESCRT pathway. Annu Rev Biochem 2013;82:663–92.
[26] Hobel CF, Albers SV, Driessen AJ, Lupas AN. The *Sulfolobus solfataricus* AAA protein Sso0909, a homologue of the eukaryotic ESCRT Vps4 ATPase. Biochem Soc Trans 2008;36:94–8.

[27] Makarova KS, Yutin N, Bell SD, Koonin EV. Evolution of diverse cell division and vesicle formation systems in Archaea. Nat Rev Microbiol 2010;8:731–41.
[28] Lindas AC, Karlsson EA, Lindgren MT, Ettema TJ, Bernander R. A unique cell division machinery in the Archaea. Proc Natl Acad Sci U S A 2008;105:18942–6.
[29] Samson RY, Obita T, Freund SM, Williams RL, Bell SD. A role for the ESCRT system in cell division in archaea. Science 2008;322:1710–3.
[30] Snyder JC, Young MJ. Potential role of cellular ESCRT proteins in the STIV life cycle. Biochem Soc Trans 2011;39: 107–10.
[31] Snyder JC, Samson RY, Brumfield SK, Bell SD, Young MJ. Functional interplay between a virus and the ESCRT machinery in archaea. Proc Natl Acad Sci U S A 2013;110:10783–7.
[32] Frickey T, Lupas AN. Phylogenetic analysis of AAA proteins. J Struct Biol 2004;146:2–10.
[33] Iyer LM, Leipe DD, Koonin EV, Aravind L. Evolutionary history and higher order classification of AAA+ ATPases. J Struct Biol 2004;146:11–31.
[34] Ogura T, Wilkinson AJ. AAA+ superfamily ATPases: common structure–diverse function. Genes Cells 2001;6:575–97.
[35] Kieffer C, Skalicky JJ, Morita E, De Domenico I, Ward DM, Kaplan J, et al. Two distinct modes of ESCRT-III recognition are required for VPS4 functions in lysosomal protein targeting and HIV-1 budding. Dev Cell 2008;15:62–73.
[36] Stuchell-Brereton MD, Skalicky JJ, Kieffer C, Karren MA, Ghaffarian S, Sundquist WI. ESCRT-III recognition by VPS4 ATPases. Nature 2007;449:740–4.
[37] Scott A, Gaspar J, Stuchell-Brereton MD, Alam SL, Skalicky JJ, Sundquist WI. Structure and ESCRT-III protein interactions of the MIT domain of human VPS4A. Proc Natl Acad Sci U S A 2005;102:13813–8.
[38] Obita T, Saksena S, Ghazi-Tabatabai S, Gill DJ, Perisic O, Emr SD, et al. Structural basis for selective recognition of ESCRT-III by the AAA ATPase Vps4. Nature 2007;449: 735–9.
[39] Azmi I, Davies B, Dimaano C, Payne J, Eckert D, Babst M, et al. Recycling of ESCRTs by the AAA-ATPase Vps4 is regulated by a conserved VSL region in Vta1. J Cell Biol 2006;172:705–17.
[40] Scott A, Chung HY, Gonciarz-Swiatek M, Hill GC, Whitby FG, Gaspar J, et al. Structural and mechanistic studies of VPS4 proteins. EMBO J 2005;24:3658–69.
[41] Yang D, Hurley JH. Structural role of the Vps4-Vta1 interface in ESCRT-III recycling. Structure 2010;18:976–84.
[42] Lottridge JM, Flannery AR, Vincelli JL, Stevens TH. Vta1p and Vps46p regulate the membrane association and ATPase activity of Vps4p at the yeast multivesicular body. Proc Natl Acad Sci U S A 2006;103:6202–7.
[43] Xiao J, Xia H, Zhou J, Azmi IF, Davies BA, Katzmann DJ, et al. Structural basis of Vta1 function in the multivesicular body sorting pathway. Dev Cell 2008;14:37–49.
[44] Azmi IF, Davies BA, Xiao J, Babst M, Xu Z, Katzmann DJ. ESCRT-III family members stimulate Vps4 ATPase activity directly or via Vta1. Dev Cell 2008;14:50–61.
[45] Babst M, Wendland B, Estepa EJ, Emr SD. The Vps4p AAA ATPase regulates membrane association of a Vps protein complex required for normal endosome function. EMBO J 1998;17:2982–93.
[46] Gonciarz MD, Whitby FG, Eckert DM, Kieffer C, Heroux A, Sundquist WI, et al. Biochemical and structural studies of yeast Vps4 oligomerization. J Mol Biol 2008;384:878–95.
[47] Hartmann C, Chami M, Zachariae U, de Groot BL, Engel A, Grutter MG. Vacuolar protein sorting: two different functional states of the AAA-ATPase Vps4p. J Mol Biol 2008;377: 352–63.
[48] Landsberg MJ, Vajjhala PR, Rothnagel R, Munn AL, Hankamer B. Three-dimensional structure of AAA ATPase Vps4: advancing structural insights into the mechanisms of endosomal sorting and enveloped virus budding. Structure 2009;17:427–37.
[49] Xiao J, Xia H, Yoshino-Koh K, Zhou J, Xu Z. Structural characterization of the ATPase reaction cycle of endosomal AAA protein Vps4. J Mol Biol 2007;374:655–70.
[50] Hanson PI, Whiteheart SW. AAA+ proteins: have engine, will work. Nat Rev Mol Cell Biol 2005;6:519–29.
[51] Lupas AN, Martin J. AAA proteins. Curr Opin Struct Biol 2002;12:746–53.
[52] Inoue M, Kamikubo H, Kataoka M, Kato R, Yoshimori T, Wakatsuki S, et al. Nucleotide-dependent conformational changes and assembly of the AAA ATPase SKD1/VPS4B. Traffic 2008;9:2180–9.
[53] Roll-Mecak A, Vale RD. Structural basis of microtubule severing by the hereditary spastic paraplegia protein spastin. Nature 2008;451:363–7.
[54] Davies JM, Brunger AT, Weis WI. Improved structures of full-length p97, an AAA ATPase: implications for mechanisms of nucleotide-dependent conformational change. Structure 2008;16:715–26.
[55] Dreveny I, Kondo H, Uchiyama K, Shaw A, Zhang X, Freemont PS. Structural basis of the interaction between the AAA ATPase p97/VCP and its adaptor protein p47. EMBO J 2004;23:1030–9.
[56] Huyton T, Pye VE, Briggs LC, Flynn TC, Beuron F, Kondo H, et al. The crystal structure of murine p97/VCP at 3.6A. J Struct Biol 2003;144:337–48.
[57] Zhang X, Shaw A, Bates PA, Newman RH, Gowen B, Orlova E, et al. Structure of the AAA ATPase p97. Mol Cell 2000;6:1473–84.
[58] Yu Z, Gonciarz MD, Sundquist WI, Hill CP, Jensen GJ. Cryo-EM structure of dodecameric Vps4p and its 2:1 complex with Vta1p. J Mol Biol 2008;377:364–77.
[59] Story RM, Steitz TA. Structure of the recA protein–ADP complex. Nature 1992;355:374–6.
[60] Wendler P, Ciniawsky S, Kock M, Kube S. Structure and function of the AAA+ nucleotide binding pocket. Biochim Biophys Acta 2012;1823:2–14.
[61] Moriscot C, Gribaldo S, Jault JM, Krupovic M, Arnaud J, Jamin M, et al. Crenarchaeal CdvA forms double-helical filaments containing DNA and interacts with ESCRT-III-like CdvB. PLoS One 2011;6:e21921.
[62] Brock TD, Brock KM, Belly RT, Weiss RL. Sulfolobus: a new genus of sulfur-oxidizing bacteria living at low pH and high temperature. Arch Mikrobiol 1972;84:54–68.
[63] Janin J, Bahadur RP, Chakrabarti P. Protein–protein interaction and quaternary structure. Q Rev Biophys 2008;41:133–80.
[64] Wang Q, Song C, Irizarry L, Dai R, Zhang X, Li CC. Multifunctional roles of the conserved Arg residues in the second region of homology of p97/valosin-containing protein. J Biol Chem 2005;280:40515–23.
[65] Davies BA, Azmi IF, Payne J, Shestakova A, Horazdovsky BF, Babst M, et al. Coordination of substrate binding and ATP hydrolysis in Vps4-mediated ESCRT-III disassembly. Mol Biol Cell 2010;21:3396–408.

[66] Merrill SA, Hanson PI. Activation of human VPS4A by ESCRT-III proteins reveals ability of substrates to relieve enzyme autoinhibition. J Biol Chem 2010;285:35428–38.
[67] Erzberger JP, Berger JM. Evolutionary relationships and structural mechanisms of AAA+ proteins. Annu Rev Biophys Biomol Struct 2006;35:93–114.
[68] Akoev V, Gogol EP, Barnett ME, Zolkiewski M. Nucleotide-induced switch in oligomerization of the AAA+ ATPase ClpB. Protein Sci 2004;13:567–74.
[69] Zhang F, Hu M, Tian G, Zhang P, Finley D, Jeffrey PD, et al. Structural insights into the regulatory particle of the proteasome from *Methanocaldococcus jannaschii*. Mol Cell 2009;34:473–84.
[70] Smith DM, Kafri G, Cheng Y, Ng D, Walz T, Goldberg AL. ATP binding to PAN or the 26S ATPases causes association with the 20S proteasome, gate opening, and translocation of unfolded proteins. Mol Cell 2005;20:687–98.
[71] Henderson JN, Hazra S, Dunkle AM, Salvucci ME, Wachter RM. Biophysical characterization of higher plant Rubisco activase. Biochim Biophys Acta 2013;1834:87–97.
[72] Stotz M, Mueller-Cajar O, Ciniawsky S, Wendler P, Hartl FU, Bracher A, et al. Structure of green-type Rubisco activase from tobacco. Nat Struct Mol Biol 2011;18:1366–70.
[73] Enemark EJ, Joshua-Tor L. Mechanism of DNA translocation in a replicative hexameric helicase. Nature 2006;442:270–5.
[74] Thomsen ND, Berger JM. Running in reverse: the structural basis for translocation polarity in hexameric helicases. Cell 2009;139:523–34.
[75] Diemand AV, Lupas AN. Modeling AAA+ ring complexes from monomeric structures. J Struct Biol 2006;156:230–43.
[76] Cormier CY, Park JG, Fiacco M, Steel J, Hunter P, Kramer J, et al. PSI:Biology-materials repository: a biologist's resource for protein expression plasmids. J Struct Funct Genomics 2011;12:55–62.
[77] Otwinowski Z, Minor W. Processing of X-ray diffraction data collected in oscillation mode. In: Carter JCW, Sweet RM, editors. Methods Enzymol, Vol. 276. New York, NY: Academic Press; 1997. p. 307–26.
[78] Terwilliger TC, Berendzen J. Automated MAD and MIR structure solution. Acta Crystallogr Sect D Biol Crystallogr 1999;55:849–61.
[79] McCoy AJ, Grosse-Kunstleve RW, Storoni LC, Read RJ. Likelihood-enhanced fast translation functions. Acta Crystallogr Sect D Biol Crystallogr 2005;61:458–64.
[80] Murshudov GN, Vagin AA, Dodson EJ. Refinement of macromolecular structures by the maximum-likelihood method. Acta Crystallogr Sect D Biol Crystallogr 1997;53:240–55.
[81] Emsley P, Cowtan K. Coot: model-building tools for molecular graphics. Acta Crystallogr Sect D Biol Crystallogr 2004;60:2126–32.
[82] Krissinel E, Henrick K. Inference of macromolecular assemblies from crystalline state. J Mol Biol 2007;372:774–97.
[83] Krissinel E, Henrick K. Secondary-structure matching (SSM), a new tool for fast protein structure alignment in three dimensions. Acta Crystallogr Sect D Biol Crystallogr 2004;60:2256–68.
[84] Winn MD, Ballard CC, Cowtan KD, Dodson EJ, Emsley P, Evans PR, et al. Overview of the CCP4 suite and current developments. Acta Crystallogr Sect D Biol Crystallogr 2011;67:235–42.
[85] DeLano WL. The PyMOL molecular graphics system. San Carlos, CA: DeLano Scientific; 2002.
[86] Cole JL, Lary JW, Moody T, Laue TM. Analytical ultracentrifugation: sedimentation velocity and sedimentation equilibrium. Methods Cell Biol 2008;84:143–79.
[87] Cole JL. Analysis of heterogeneous interactions. Methods Enzymol 2004;384:212–32.
[88] Laue TM, Shah BD, Ridgeway TM, Pelletier SL. In: Harding S, Rowe A, Horton J, editors. Analytical ultracentrifugation in biochemistry and polymer science. Cambridge, UK: Royal Society of Chemistry; 1992. p. 90–125.

CHAPTER 3

CRYSTALLOGRAPHIC EFFORTS TOWARDS THE VPS4 OLIGOMER STRUCTURE

Introduction

Vps4 contains an N-terminal MIT domain and a C-terminal AAA+ ATPase cassette [1; 2]. The MIT domain can selectively bind MIM motifs on ESCRT-III proteins [3; 4; 5]. The structures of MIT domains and monomeric AAA+ ATPase cassettes have been reported by several groups [1; 6; 7; 8; 9]. Like other proteins within the AAA+ ATPase family, Vps4 functions as an oligomer [10]. The details of Vps4 oligomerization have been controversial, and several very different molecular models from EM or Cryo-EM reconstructions have been proposed [7; 11; 12]. Vps4p with a mutation on the Walker B motif (E233Q) has been reported to form a dodecamer [1; 10], which is consistent with the model from EM or Cryo-EM reconstruction of Vps4p(E233Q) [11; 12]. Recently, we found that wild type Vps4 can form a hexamer in the presence of ATP, and concluded that Vps4 is active as a hexamer (Chapter 2). I have pursued four different strategies in an attempt to obtain crystals of the Vps4 oligomer suitable for structure determination: (1) crystallization of Vps4 homologs from different Crenarchaeal species, (2)

crystallization of the Vps4p:VSL complex, (3) crystallization of the templated-Vps4p hexamer, and (4) crystallization of the Vps4p:substrate complex.

Crystallization of Vps4 homologs from different Crenarchaeal species

ESCRT-III and Vps4 have been highly conserved throughout evolution, and function in the final stages of cell division in eukaryotes and the Crenarchaea [13; 14]. Crenarchaeal Vps4 displays the MIT domain and ATPase cassette of the eukaryotic proteins, but lack the beta-domain [15]. Consistent with this, there is no gene encoding a homolog of Vta1p apparent in Crenarchaea [15; 16]. Unlike the Vps4p of *Saccharomyces cerevisiae*, some Crenarchaeal Vps4 enzymes do not require ATP for oligomerization [17]. Moreover, negative stain EM imaging of the Vps4 homolog from the hyperthermophilic archaeon *Metallospherae sedula* indicated a ring-like structure [17]. Therefore, Crenarchaeal Vps4 homologs seemed like good candidates for crystallization of a Vps4 oligomer.

Co-crystallization of a Vps4p:VSL complex

The VSL domain of Vta1p has been reported to stabilize Vps4p oligomerization and stimulate Vps4p ATPase activity [18; 19]. The structure of the complex of the Vta1p VSL domain with the beta and the C-terminal domain of Vps4 has been reported [20]. Surprisingly, however, this structure does not support the model that the Vps4 beta domain interaction with the Vta1p VSL stabilizes single Vps4 oligomer [20]. Instead, it suggests that the dimeric VSL domain can cross-link different Vps4 oligomers into a network [20]. Recently, we found that the

VSL domain does not change the oligomerization of wild type Vps4p in the presence of ATP (Chapter 2), which supports the first model that VSL domain stabilizes single Vps4 oligomer. We also found that the ATPase cassette of Vps4p can form a stable hexamer in the presence of the Vta1p VSL and ADP·AlF_x, an ATP analog that can mimick a range of nucleotide states experienced during the ATP hydrolytic cycle (Chapter 4). I therefore tried to co-crystallize the Vps4 ATPase cassette of Vps4p with the VSL domain of Vta1p in the presence of ADP·AlF_x.

Crystallization of the templated-Vps4p hexamer

Because we are confident that Vps4 is active as a hexamer that roughly approximates p97 D1 (Chapter 2), I designed a fusion with the stable hexameric protein CCMK4 [21]that is expected to preserve the stable Vps4 association. The lab previously used this approach successfully to crystallize hexameric HIV CA protein [22].

Crystallization of Vps4p:substrate complex

The most informative AAA+ ATPase structure is that of the Papillomavirus E1 helicase, whose success depended upon co-crystallization with nucleic acid substrate in the central pore [23]. Although not an AAA+ ATPase, the highly informative rho helicase structure similarly depended upon co-crystallization with a central substrate [24]. Moreover, we have shown that active Vps4p is an asymmetric hexamer that is stabilized by binding of substrate protein in the

central pore (Chapter 4). I therefore tried to use the same strategy to crystallize Vps4 hexamer in complex with a substrate Vps2/ESCRT-III helix 5 peptide that binds the Vps4 pore (Chapter 4).

Materials and methods

Plasmids

Plasmids encoding different Vps4 homologs from Crenarchaeal species, except *Sulfolobus solfataricus,* were synthesized by DNA2.0 (Menlo Park, CA, USA) with a cleavable N-terminal 6xHis-tag and cloned into pJexpress414 (DNA2.0). A prescission protease cleavage site was placed between the His-tag and the Vps4 coding region. The gene encoding *Sulfolobus solfataricus* Vps4 was amplified from the genome (ATCC 35092D-5) and inserted into the vector pET151D-topo. The TEV cleavage site between the His-tag and the *Sulfolobus solfataricus* Vps4 was replaced by a prescission protease cleavage site. Genes encoding *Saccharomyces cerevisiae* Vps4p and the VSL domain of Vta1p were also inserted into the vector pET151D-topo. These different mutations or truncations of Vps4p were created by Quikchange mutagenesis (Stratagene).

Protein expression and purification

All of the proteins were expressed in BL21 Condon+ *E.coli* cells in ZY autoinduction media at 37°C until OD600 of 0.5 and then overnight at 21°C. The harvested cells were lysed in lysis buffer (20mM imidazole, 300mM NaCl, 25mM Tris) containing 10mg/ml lysozyme and protease inhibitors (PMSF (0.2mg/ml),

aprotinin (1.0μg/ml), leupeptin (1.0μg/ml), pepstatin (1.0μg/ml)) at 4°C for 1 hour followed by sonication. The pH of lysis buffer is different for different proteins. For Crenarchaeal Vps4 homologs, pHs from 6 to 9 were tried, and the optimal pH for each homolog is listed in Table 3.1. All of the twelve Vps4 homologs tested were soluble except the protein from *Staphylothermus hellenicus*. For Vps4p, its variants and the VSL domain of Vta1p, lysis buffer of pH7.4 was used.

After sonication, cell lysate of Crenarchaeal Vps4 homologs were incubated at 75°C for 15min. Cell lysates were centrifuged at 35,000g for 45min. The supernatants were collected and incubated with Ni-NTA agarose for 1 hour. The Ni-NTA agarose bound with protein was washed by at least 10x volume of lysis buffer, then eluted by elution buffer (400mM imidazole, 300mM NaCl, 25mM Tris, pH 7.5). The eluted proteins were incubated with TEV protease (~1mg/100mg, for Vps4p, its variants, and Vta1p VSL) or precision protease (~1mg/100mg, for Crenarchaeal Vps4) in cleavage buffer (150mM NaCl, 1mM EDTA, 1mM DTT, 25mM Tris, pH 7.5) for 20 hours at 4°C to cleave the histidine tag. After cleavage, the samples were run through the Ni-NTA agarose column to remove the uncleaved proteins. The flow-through containing the purified proteins was collected. For Vps4p and its variants, a further step of purification on a Q column was applied. Specifically, Vps4p in buffer A (100mM NaCl, 20mM HEPES, pH 7.5) was loaded onto the HiTrap Q HP (GE Healthcare Life Sciences). The column was washed with 5x volume of buffer A, and the protein eluted by a gradient (0-35%) of buffer B (1M NaCl, 20mM HEPES, pH 7.5). For Crenarchaeal Vps4 homologs, a further step of purification by size exclusion

Table 3.1. Different Crenarchaeal Vps4 homologs tested for expression.

Name	Length[AA]	Mw[Da]	Theoretical pI	Solubility Screen (pH)
Sulfolobus solfataricus Vps4	372	42247	6.28	7.4
Sulfolobus tokodaii Vps4	369	42268	6.82	7.4
Acidianus hospitalis Vps4	365	42043	5.64	7.4
Aeropyrum pernix Vps4	384	43849	8.34	7.4
Acidilobus saccharovorans Vps4	385	43802	5.63	8, 9
Ignicoccus hospitalis Vps4	366	41370	7.67	9
Hyperthermus butylicus Vps4	370	42387	8.39	9
Ignicoccus aggregans Vps4	382	43777	6.83	9
Staphylothermus hellenicus Vps4	379	43376	9.03	Not soluble
Desulfurococcus kamchatkensis Vps4	390	44202	5.91	9
Thermosphaera aggregans Vps4	381	43997	6.05	9
Sulfolobus acidocaldarius Vps4	374	42523	7.93	9

chromatography with SD200 column was applied. The purified proteins were dialysed into low salt buffer (100mM NaCl, 10mM $MgCl_2$, 1mM DTT, 20mM HEPES, pH 7.5), and concentrated to proper concentrations for biochemical assay or crystallization using an Amicon concentrator.

Peptides

Peptides were synthesized in Dr. Kay's lab at the Biochemistry department, University of Utah. The crude materials were purified by reverse phase C18 HPLC and confirmed by Mass Spectrometry at the University of Utah Core Facility.

Analytical size exclusion chromatography

A Superdex200 column was equilibrated in running buffer (10mM $MgCl_2$, 100mM NaCl, 20mM HEPES, pH7.0). 1mM ADP·AlF_x or ATP was added to the running buffer if needed. When there was ADP·AlF_x or ATP in the running buffer, the nucleotide was added to the Vps4 sample and the sample was incubated at 4°C overnight before loading onto the column. The column was calibrated by protein standards (Biorad), and the predicted positions of the Vps4 dodecamer, hexamer, and dimer on chromatogram were calculated from the protein standards.

ATPase assay

Malachite green, which forms a green complex with the free phosphate released from ATP hydrolysis, was used to measure the ATPase activity of Vps4p. Vps4p or its variants (final concentration 0.3μM) was mixed with 2μM ATP in reaction buffer (100mM NaCl, 10mM $MgCl_2$, 1mM DTT, 20mM HEPES, pH 7.5). The mixture was incubated for 10min at 37°C. Addition of 2x volume of malachite green solution (14 mM ammonium molybdate, 1.3 M HCl, 1.5 mM malachite green) was followed by adding the same volume of 21% citric acid to stop the reaction. Absorbance at 650nm was measured by a plate reader. The concentration of the free phosphate released from ATP hydrolysis was calculated according to a sodium phosphate standard.

Crystallization

The purified proteins or protein complexes were concentrated to from 5mg/ml to 15mg/ml. ADP·AlF_x was added into proteins or protein complexes to 1mM. The sitting drop method was used for the initial broad screens. The crystallization conditions from eight commercial crystallization screens were used: Hampton Crystal Screen HT 1&2, Hampton Index, Hampton Salt, Hampton Natrix, Hampton Lite, Jena Bioscience Screen HTS1, Qiagen JCSG+, Qiagen PACT. Three different temperatures were tried: 4°C, 13°C, and 20°C. Initial hits were optimized by altering the pH, precipitants, concentration of precipitants, additives, and centration of additives.

Data collection

The diffraction data were collected at our home X-ray source or at a synchrotron (SSRL or NSLS). A cryo-protectant that allowed the crystals to freeze clear, usually 15-20% glycerol or mineral oil, was added to the drops when necessary. Crystals were cooled by plunging into liquid N_2 prior to data collection at 100K.

Data analysis

Collected data were indexed by d*TREK [25] or DENZO [26]. The possible number of molecules in each asymmetric unit and the corresponding solvent content was determined by Matthew's Probability Calculator (http://www.ruppweb.org/mattprob/). If a complete data set was collected, the

data were scaled by SCALEPACK [26]. Self-rotation functions were calculated using [27]. To determine whether a crystal contains a hexamer, two criteria were set. First, a 6-fold noncrystallographic or crystallographic symmetry was expected. If the data allowed calculation of a self-rotation function, it was inspected for the presence of a 6-fold symmetry peak, although we were cognizant of the potential for an asymmetric hexamer to give only weak or no signal by this criterion. Crystallographic symmetry was considered to determine if it might be coincident with the axis of a Vps4 hexamer. For example, if the crystal contains one molecule in each asymmetric unit, there must be a 6-fold crystallographic symmetry, and the 6-fold symmetric axis cannot be a screw axis. If there are two molecules in each asymmetric unit, there must be a 3-fold crystallographic symmetry. If there are three molecules in each asymmetric unit, there must be a 2-fold crystallographic symmetry. Another fundamental criterion is that the unit cell must be big enough to accommodate a p97-like Vps4 hexamer [1; 6]. To accommodate the p97-like hexamer model, the length of two of three edges of a unit cell must be larger than 130Å (Figure 3.1). For the crystal of the Vps4:peptide complex, the extra very convenient criterion is that the crystal must be green since the peptide contains a fluorescein.

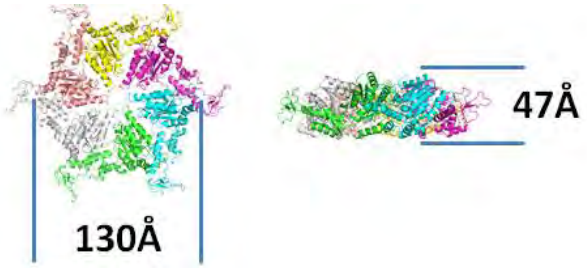

Figure 3.1. Dimension of p97-like Vps4 hexamer

Structure determination

The structure of one crystal form of *Sulfolobus solfataricus* Vps4 was solved by SAD-MR. SAD data were collected on a Sel-Met crystal of *Sulfolobus solfataricus* Vps4. SHELX [28] was used to phase the data to get the initial electron density map. Molecular replacement was applied to search the *Sulfolobus solfataricus* Vps4 monomer model in the electron density map by Molrep [29].

Results

Crystallization of Crenarchaeal Vps4 homologs

Twelve different Vps4 homologs from different Crenarchaeal species were cloned, expressed, and purified. For those homologs that purified as a soluble protein, oligomerization was tested in the absence or presence of ATP by analytical size-exclusion chromatography (Table 3.2). The oligomerization of Vps4 homologs from *Sulfolobus solfataricus, Sulfolobus tokodaii,* and *Acidianus hospitalis* was confirmed by analytical ultracentrifugation.

The Vps4 homologs from *Sulfolobus solfataricus, Sulfolobus tokodaii, Sulfolobus acidocaldarius, Acidianus hospitalis, Ignicoccus hospitalis, Ignisphaera aggregans, Acidilobus saccharovorans, Thermosphaera aggregans, Desulfurococcus kamchatkensis* were subjected to crystallization trials with and without ADP·AlF_x . Initial hits were optimized and screened (Table 3.3). Two structures of the AAA+ ATPase cassette from *Sulfolobus solfataricus* and *Acidianus hospitalis*, both in the monomeric state, were determined (see Chapter 2).

Table 3.2. Oligomerization of Crenarchaeal Vps4 homologs

Vps4 homolog from	Identify with *Sulfolobus solfataricus* Vps4 (100%)	Oligomerization without ATP	Oligomerization with ATP
Sulfolobus solfataricus	100	Dodecamer	Hexamer-Dimer Equilibrium
Sulfolobus tokodaii	76	Dodecamer	> Hexamer
Acidianus hospitalis	76	> Dodecamer	> Hexamer
Aeropyrum pernix	56	Polydisperse	Not Done
Acidilobus saccharovorans	55	Dimer	Dimer
Ignicoccus hospitalis	53	> Hexamer	>Hexamer
Hyperthermus butylicus	58	Polydisperse	Not Done
Ignicoccus aggregans	52	Polydisperse	Polydisperse
Desulfurococcus kamchatkensis	45	Hexamer	Aggregate
Thermosphaera aggregans	46	Dodecamer	Aggregate
Sulfolobus acidocaldarius	73	Hexamer	Dimer

One crystal from *Sulfolobus solfataricus* Vps4(E206Q) in the presence of ADP·AlF_x (the first crystal form on Table 3.3) was a good candidate to contain a p97-like Vps4 hexamer based on its self-rotation function (Figure 3.2 A). The six-fold noncrystallographic symmetry revealed by the self-rotation function indicates there might be a hexamer in the crystal. Optimization efforts on this crystal form, including trying different concentrations of precipitant, different precipitants, different pH, different concentration of additives, different additives and surface entropy reduction mutants, did not result in a crystal with resolution higher than 4Å. The structure was solved by SAD-MR. The initial map was calculated by SAD, and then molecular replacement was applied using the structure of *Sulfolobus solfataricus* Vps4 as the search model. Two Vps4 monomers were found in each asymmetric unit according to the SAD-MR solution (Figure 3.2 C),

Table 3.3. Characterized crystal hits of Crenarchaeal Vps4 homologs.

Protein	Nucleotide	Space Group	Hexamer or Not	Picture of Crystal
Sulfolobus solfataricus Vps4(E206Q)	ADP·AlFx	$C222_1$, 150Å, 183Å, 114Å	No hexamer. Structure was solved by SAD	
Sulfolobus solfataricus Vps4(E206Q)	ADP·AlFx	P422, 156Å, 156Å, 152Å	No hexamer confirmed. Hexamer can be packed in the unit cell, but no high resolution crystal(better than 10 Å) can be obtained to solve the structure	
Sulfolobus solfataricus Vps4	ADP·AlFx	$P6_322$, 168Å, 168Å, 96Å,	No hexamer. 6-fold screw axis	
Sulfolobus solfataricus Vps4	ADP·AlFx	P422, 154Å, 154Å, 155Å	No hexamer. No 6-fold symmetry on self-rotation function	
Sulfolobus solfataricus Vps4	ADP·AlFx	P3/P6, 74Å, 74Å, 153Å	No hexamer. Hexamer cannot be packed into the unit cell	
Sulfolobus tokodaii Vps4	ADP·AlFx	P222, 81Å, 103Å, 345Å	No hexamer. Hexamer cannot be packed into the unit cell	
Sulfolobus tokodaii Vps4	ADP·AlFx	$P6_2$, 79Å, 79Å, 104Å	No hexamer. 6-fold screw axis	
Acidianus hospitalis Vps4	No nucleotide	$P6_5$, 96Å, 96Å, 78Å	No hexamer. Structure was solved (see Chapter 3)	
Acidianus hospitalis Vps4	ADP·AlFx	$P3_221$, 120Å, 120Å, 180Å.	No hexamer. Hexamer cannot be packed into the unit cell. 3-fold screw axis	
Sulfolobus acidocaldarius Vps4	ADP·AlFx	P3/6, 109Å, 109Å, 516Å	No hexamer. Hexamer cannot be packed into the unit cell	
Sulfolobus acidocaldarius Vps4	ADP·AlFx	P3/6, 112Å, 112Å, 534Å	No hexamer. Hexamer cannot be packed into the unit cell	
Ignicoccus hospitalis Vps4	ADP·AlFx	P222, 121Å, 126Å, 279Å	No hexamer. No 6-fold symmetry on self-rotation function	
Ignicoccus aggregans Vps4	ADP·AlFx	P3/6, 89Å, 89Å, 152Å	No hexamer. Hexamer cannot be packed into the unit cell	
Ignicoccus aggregans Vps4	ADP·AlFx	P3/6, 96Å, 96Å, 71Å	No hexamer. Hexamer cannot be packed into the unit cell	
Acidilobus saccharovorans Vps4	ADP·AlFx	P3/6, 91Å, 91Å, 99Å	No hexamer. Hexamer cannot be packed into the unit cell	
Acidilobus saccharovorans Vps4	No nucleotide	P3/6, 98Å, 98Å, 92Å	No hexamer. Hexamer cannot be packed into the unit cell	
Thermosphaera aggregans Vps4	No nucleotide	P222, 22Å, 34Å, 98Å	No hexamer. Crystal of proteolyzed or degraded product	
Desulfurococcus kamchatkensis Vps4			No hits with resolution high enough for characterization	

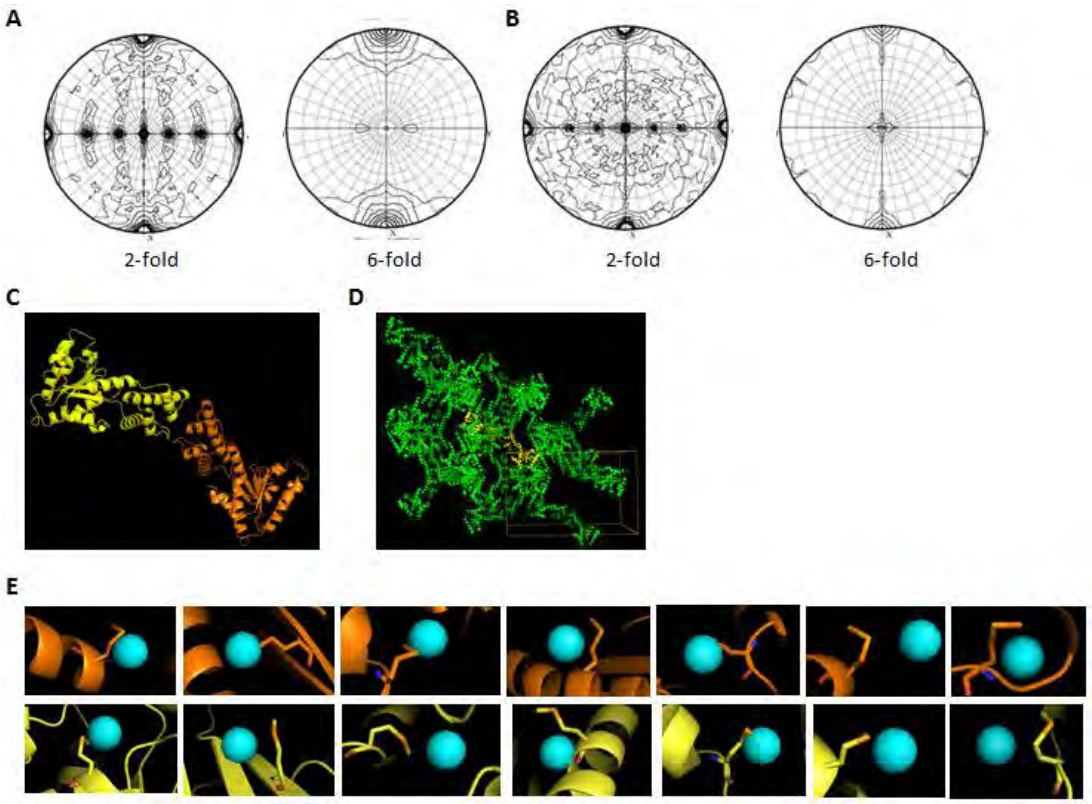

Figure 3.2. Analysis of a crystal form of *Sulfolobus solfataricus* Vps4.
A: Observed self-rotation function of the diffraction data set collected from the crystal. There is a 6-fold noncrystallographic symmetric axis parallel to the edge a of the unit cell and 6 2-fold symmetric axes perpendicular to the 6-fold symmetric axis. B: Calculated self-rotation function of the solution model, which is similar to the observed self-rotation function. C: Molecular replacement solution of this crystal form. Two monomers in one symmetric unit were colored yellow and orange. D: No hexamer can be formed when crystallographic symmetry was applied. E. Every Se atom in the substructure is close to a methionine in the solution model.

and the solution was validated by the positions of selenium atoms in a heavy atom derivative, which were very close to methionine residues in the solution model (Figure 3.2 E) and that the calculated self-rotation function of the solution model was very similar to the self-rotation function of the collected data (Figure 3.2 A, B). Unfortunately, however, the crystal lattice did not generate a hexamer (Figure 3.2 D).

Co-crystallization of Vps4p:VSL complex

The C-terminal VSL domain of Vta1p has been shown to stimulate the ATPase activity of Vps4 and to stabilize Vps4 oligomer [18; 19]. To co-crystallize Vps4p with the VSL domain, the VSL domain was expressed in *E. coli* and purified. Figure 3.3 indicates that the purified VSL domain can stabilize a Vps4 hexamer.

VSL domain was copurified with ΔMIT-Vps4p by size-exclusion chromatography in the presence of ADP·AlF_x. The purified samples were analyzed by SDS-PAGE electrophoresis. VSL domain can be copurified with ΔMIT-Vps4p as a complex (Figure 3.4). The Vps4p-VSL complex was collected and concentrated to 10m/ml. Crystallization of the concentrated sample led to several hits. Two of them could be characterized after optimization. Unfortunately, however, neither of them contains a Vps4p hexamer (Table 3.4).

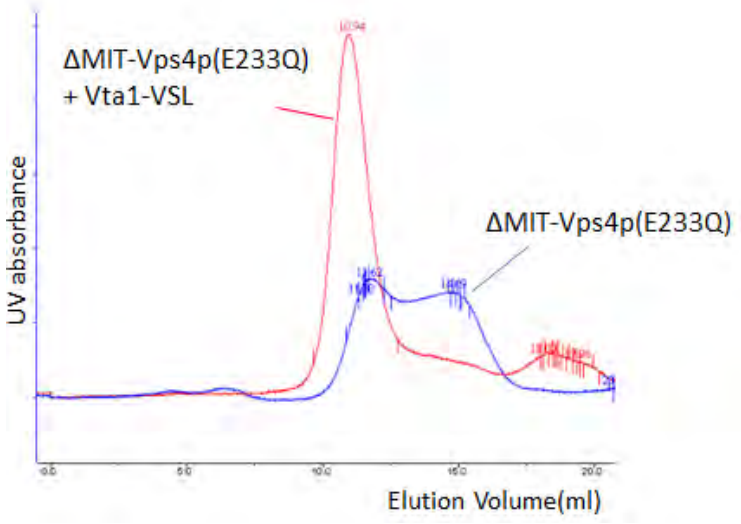

Figure 3.3. Vta1p-VSL domain can stabilize Vps4p hexamer.

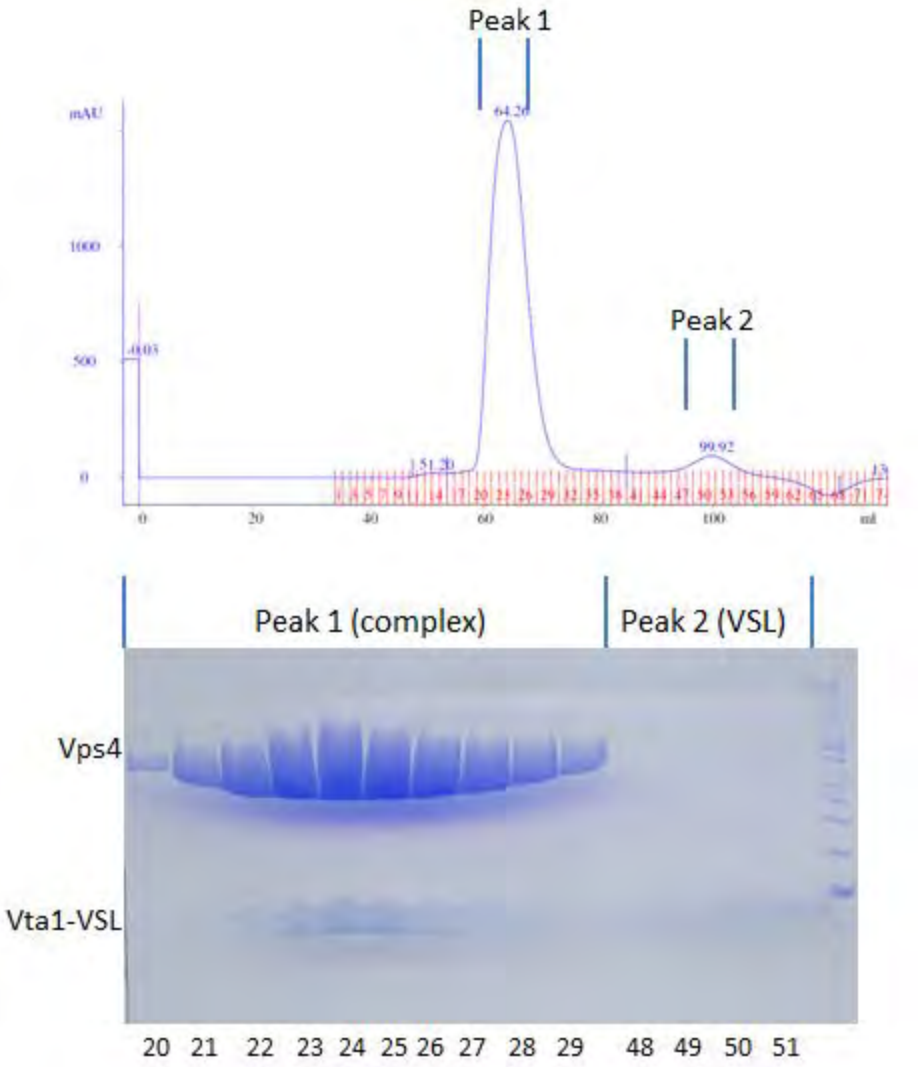

Figure 3.4. Purification of Vps4p:VSL complex.
ΔMIT-Vps4p was mixed with Vta1p VSL with a ratio of 6:3 and was loaded onto the SD200 column equilibrated with ADP·AlF_x buffer. There are two peaks on the chromatogram. Analysis with SDS-PAGE electrophoresis indicated that peak1 is the complex composed of ΔMIT-Vps4p and Vta1p-VSL and peak2 is extra Vta1p-VSL.

Table 3.4. Characterized crystal hits of the Vps4p:VSL complex.

Protein	Nucleotide	Space Group	Hexamer or Not	Picture of Crystal
Saccharomyces cerevisiae Vps4p(101-437) + Vta1p(280-330)	ADP·AlFx	C222, 89Å, 116Å, 87Å	No hexamer. Hexamer cannot be packed into the unit cell	
Saccharomyces cerevisiae Vps4p(101-437) + Vta1p(280-330)	ADP·AlFx	$P6_522$, 108Å, 108Å, 173Å	No hexamer. Hexamer cannot be packed into the unit cell	

Crystallization of templated Vps4 hexamer

To stabilize the Vps4 hexamer, a template molecule that exists as a highly stable hexamer was fused to the C-terminus of the Vps4p AAA+ ATPase domain. CCMK4, which can form stable hexamer in vitro [21] and has been used as the template for crystallizing HIV CA protein hexamer [22], was chosen as the template to be fused to the C-terminus of the Vps4p AAA+ ATPase cassette. Guided by the CCMK4 crystal structure and p97 D1 homology model, a $(G_4S)_3$ linker was inserted between Vps4p and CCMK4. Analytical size-exclusion chromatography was used to demonstrate that the fused protein is a stable oligomer in the absence of nucleotide (Figure 3.5 B). To test whether the fusion protein can form the properly assembled Vps4 hexamer, the ATPase activity of the fusion protein was used as the indicator because the ATPase activity required assembled Vps4. Without the MIT domain and the whole linker region between the MIT domain and the AAA+ ATPase cassette, the Vps4p AAA+ ATPase domain alone cannot hydrolyze ATP by itself, and adding VSL domain can activate the ATPase activity (Figure 3.5 A). This is consistent with the role of VSL domain to stabilize the

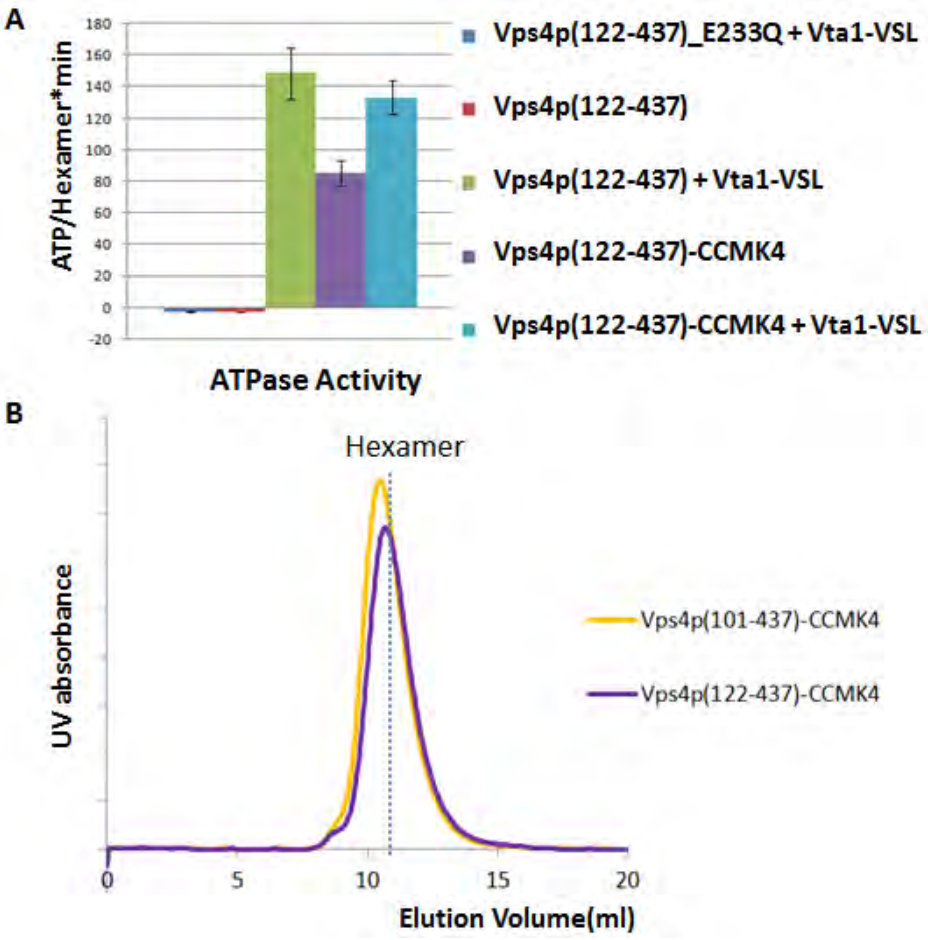

Figure 3.5. Vps4p-CCMK4 oligomerized properly.
A: ATPase activity of Vps4p-AAA+ ATPase cassette and the Vps4p-CCMK4 fusion protein. Vps4p(122-437)-CCMK4 can hydrolyze ATP, and the activity can be boosted by VSL domain of Vta1p. B: Analysis of the oligomerization of Vps4p-CCMK4 by analytical size-exclusion chromatography. The dotted line indicates the predicted position of the peak of fusion protein hexamer.

Vps4 oligomer. When the AAA+ ATPase cassette was fused to the N-terminus of CCMK4, ATPase activity was observed (Figure 3.5 A). The ATPase activity of the fusion protein can be further enhanced by adding VSL (Figure 3.5 A). This indicated that the Vps4p AAA+ ATPase cassette can oligomerize properly when it was fused to CCMK4, and the oligomerization can be further stabilized by the VSL domain.

Two fusion proteins were generated with this template: Vps4p(101-437)-CCMK4 and Vps4p(122-437)-CCMK4. The fusion protein was crystallized together with the VSL domain. Two crystal hits grew about one month after the crystallization trays were set up (Table 3.5). However, neither of them contained a unit cell big enough to hold p97-like Vps4 hexamer (Table 3.5).

Crystallization of Vps4p:substrate complex

The peptide corresponding to helix5 of Vps2, an ESCRT-III subunit from *Saccharomyces cerevisiae*, bound to the pore loops of Vps4p hexamer (Figure 3.6 A, C and Chapter 4). A construct of ΔMIT-Vps4p carrying pore loop mutations E243A and E247A was found to interact with the peptide with much higher affinity than wild type ΔMIT-Vps4p (Figure 3.6 B, C and Chapter 4). The peptide was used in co-crystallization trials with wild type ΔMIT-Vps4p and ΔMIT-Vps4p(E243A, E247A) in the presence of VSL and ADP·AlF_x . Several crystal hits were obtained, optimized, and screened. Some of these crystal diffracted to better than 10Å resolution and were indexed and analyzed. Unfortunately, none of these hits contained a Vps4p hexamer (Table 3.6). Several hits had very low

Table 3.5. Characterized crystal hits of Vps4p-CCMK4.

Protein	Nucleotide	Space Group	Hexamer or Not	Picture of Crystal
Vps4p(122-437)-CCMK4 + Vta1p(280-330)	ADP·AlFx	P6, 59Å, 59Å, 159Å	No hexamer. Crystal of proteolyzed or degraded product.	
Vps4p(101-437)-CCMK4 + Vta1p(280-330)	ADP·AlFx	C2, 121Å, 70Å, 102Å	No hexamer. Hexamer cannot be packed into the unit cell	

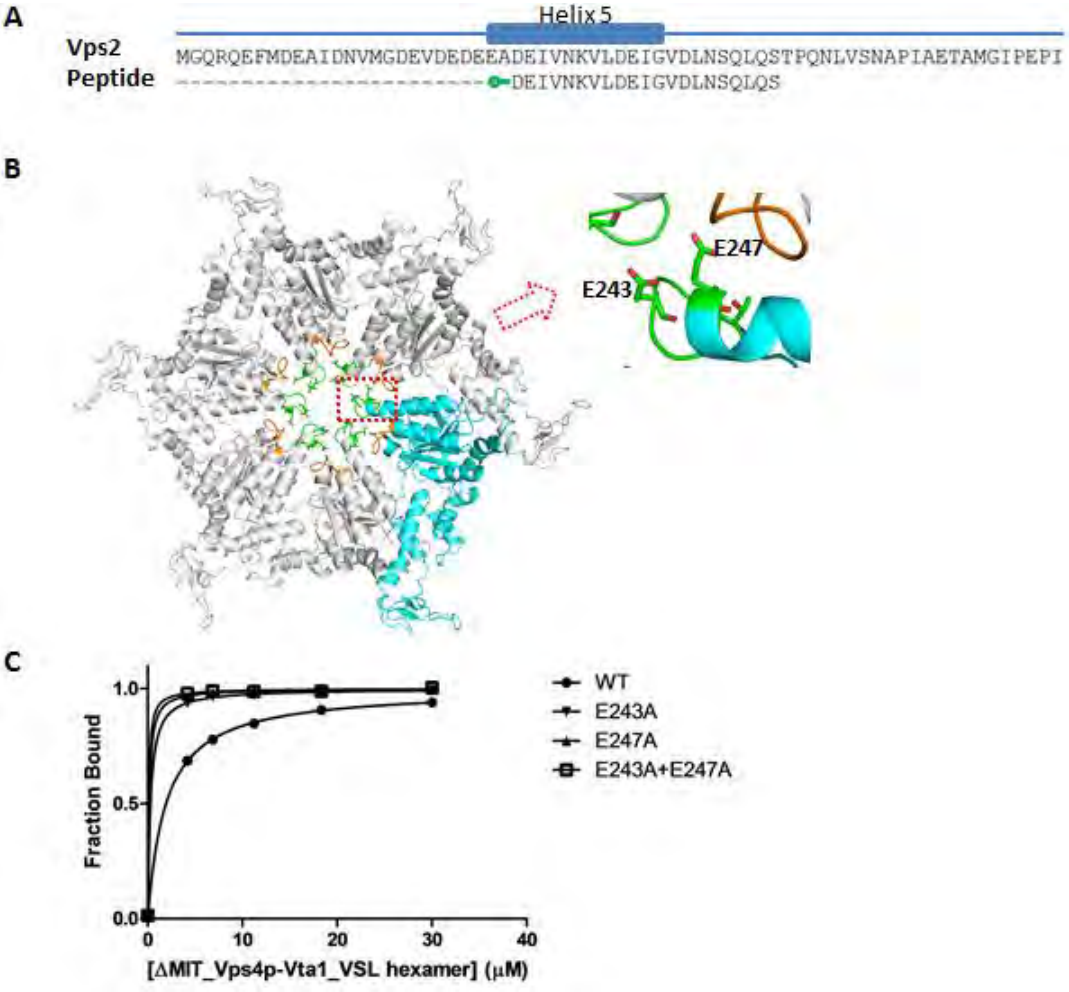

Figure 3.6. Peptide corresponding to the predicted helix 5 of Vps2 binds to Vps4p hexamer.
A: Sequence of the peptide. A fluorescein molecule is attached to the N-terminus of the peptide. B: Important residues on pore loop 2. A p97-like Vps4p hexamer was shown on the left. Pore loop 2 is colored green and pore loop 1 is colored orange. Alanine replacement on E243 and E247 (shown as sticks) increased the affinity between Vps4p hexamer and the peptide. C: The ΔMIT-Vps4p hexamer can bind to the peptide. Pore loop 2 mutations E243A and E247 can increase the binding affinity.

Table 3.6. Characterized crystal hits of Vps4p:peptide complex.

Protein	Nucleotide	Space Group	Hexamer or Not	pH of crystallization buffer	Color of Crystal	Picture of Crystal
Vps4p(101-437) + Vta1p(280-330) + Peptide	ADP·AlF_x	P3/P6 114Å, 114Å, 126Å	No hexamer. Hexamer cannot be packed into the unit cell.	5.0	Colorless	
Vps4p(101-437) + Vta1p(280-330) + Peptide	ADP·AlF_x	$P6_4$ 135Å, 135Å, 65Å	No hexamer. 6-fold screw axis.	6.0	Colorless	
Vps4p(101-437) + Vta1p(280-330) + Peptide	ADP·AlF_x	$P6_522$ 109Å, 109Å, 172Å,	No hexamer. 6-fold screw axis	5.5	Colorless	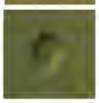
Vps4p(101-437) + Vta1p(280-330) + Peptide	ADP·AlF_x	Can not be decided due to low resolution	Can not be decided	7.0	Yellow-green	
Vps4p(101-437) (E243A +E247A) Vta1p(280-330) + Peptide	ADP·AlF_x	$P2_12_12_1$ 76Å, 120Å, 152Å	No hexamer. Hexamer cannot be packed into the unit cell	4.6	Colorless	
Vps4p(101-437) (E243A +E247A) Vta1p(280-330) + Peptide	ADP·AlF_x	Can not be decided due to low resolution	Can not be decided	6.5	Yellow-green	
Vps4p(101-437) (E243A +E247A) Vta1p(280-330) + Peptide	ADP·AlF_x	Can not be decided due to low resolution	Can not be decided	7.5	Yellow-green	

resolution and did not give useable data, but did display a green color, which indicated that they might contain Vps4p:peptide complex.

Discussion

Although Vps4 forms an oligomer in solution in the presence of ATP or ATP analogs, crystallization of Vps4 proteins from different species always resulted in Vps4 monomers packed in the crystals like a spiral [6; 30]. The crystallographic interface between two monomers along one spiral is conserved among all of the published crystal forms of Vps4 [1; 6; 7; 8; 9; 30].

The conserved crystallographic interface is similar to the hexameric interface in the p97-like hexamer model of Vps4 [6; 30]. One possible reason why a hexamer cannot be crystallized is that the hexamer is asymmetric, and the previous crystallization efforts did not start with a stable asymmetric hexamer.

To stabilize the asymmetric hexamer, the ATP analog ADP·AlF_x, which can mimic different states of ATP during ATP hydrolysis, were used. Stable hexamer can be obtained in the solution with ADP·AlF_x, but high resolution crystals containing Vps4 hexamer were not obtained. Another method used to stabilize the asymmetric hexamer was to form a complex with a peptide substrate (see Chapter 4). Crystallization efforts with the currently used peptide have not yet led to high resolution crystals containing Vps4 hexamer. Efforts to create new peptides which have higher affinity to Vps4 hexamer should be one of the future directions. Peptide with higher affinity might be obtained by introducing mutations to the current peptide, which will be better crystallization partners for Vps4 hexamer. At the same time, more constructs of Vps4p with different truncations on the N-terminus or with surface entropy reduction mutations should also be made to be co-crystallized together with the peptide.

References

1. Scott, A., Chung, H. Y., Gonciarz-Swiatek, M., Hill, G. C., Whitby, F. G., Gaspar, J., Holton, J. M., Viswanathan, R., Ghaffarian, S., Hill, C. P. & Sundquist, W. I. (2005). Structural and mechanistic studies of VPS4 proteins. *EMBO J* **24**, 3658-69.

2. Scott, A., Gaspar, J., Stuchell-Brereton, M. D., Alam, S. L., Skalicky, J. J. & Sundquist, W. I. (2005). Structure and ESCRT-III protein interactions of the MIT domain of human VPS4A. *Proc Natl Acad Sci U S A* **102**, 13813-8.

3. Kieffer, C., Skalicky, J. J., Morita, E., De Domenico, I., Ward, D. M., Kaplan, J. & Sundquist, W. I. (2008). Two distinct modes of ESCRT-III recognition are required for VPS4 functions in lysosomal protein targeting and HIV-1 budding. *Dev Cell* **15**, 62-73.

4. Stuchell-Brereton, M. D., Skalicky, J. J., Kieffer, C., Karren, M. A., Ghaffarian, S. & Sundquist, W. I. (2007). ESCRT-III recognition by VPS4 ATPases. *Nature* **449**, 740-4.

5. Obita, T., Saksena, S., Ghazi-Tabatabai, S., Gill, D. J., Perisic, O., Emr, S. D. & Williams, R. L. (2007). Structural basis for selective recognition of ESCRT-III by the AAA ATPase Vps4. *Nature* **449**, 735-9.

6. Gonciarz, M. D., Whitby, F. G., Eckert, D. M., Kieffer, C., Heroux, A., Sundquist, W. I. & Hill, C. P. (2008). Biochemical and structural studies of yeast Vps4 oligomerization. *J Mol Biol* **384**, 878-95.

7. Hartmann, C., Chami, M., Zachariae, U., de Groot, B. L., Engel, A. & Grutter, M. G. (2008). Vacuolar protein sorting: two different functional states of the AAA-ATPase Vps4p. *J Mol Biol* **377**, 352-63.

8. Inoue, M., Kamikubo, H., Kataoka, M., Kato, R., Yoshimori, T., Wakatsuki, S. & Kawasaki, M. (2008). Nucleotide-dependent conformational changes and assembly of the AAA ATPase SKD1/VPS4B. *Traffic* **9**, 2180-9.

9. Xiao, J., Xia, H., Yoshino-Koh, K., Zhou, J. & Xu, Z. (2007). Structural characterization of the ATPase reaction cycle of endosomal AAA protein Vps4. *J Mol Biol* **374**, 655-70.

10. Babst, M., Wendland, B., Estepa, E. J. & Emr, S. D. (1998). The Vps4p AAA ATPase regulates membrane association of a Vps protein complex required for normal endosome function. *EMBO J* **17**, 2982-93.

11. Yu, Z., Gonciarz, M. D., Sundquist, W. I., Hill, C. P. & Jensen, G. J. (2008). Cryo-EM structure of dodecameric Vps4p and its 2:1 complex with Vta1p. *J Mol Biol* **377**, 364-77.

12. Landsberg, M. J., Vajjhala, P. R., Rothnagel, R., Munn, A. L. & Hankamer, B. (2009). Three-dimensional structure of AAA ATPase Vps4: advancing structural insights into the mechanisms of endosomal sorting and enveloped virus budding. *Structure* **17**, 427-37.

13. Samson, R. Y., Obita, T., Freund, S. M., Williams, R. L. & Bell, S. D. (2008). A role for the ESCRT system in cell division in archaea. *Science* **322**, 1710-3.

14. Ghazi-Tabatabai, S., Obita, T., Pobbati, A. V., Perisic, O., Samson, R. Y., Bell, S. D. & Williams, R. L. (2009). Evolution and assembly of ESCRTs. *Biochem Soc Trans* **37**, 151-5.

15. Hobel, C. F., Albers, S. V., Driessen, A. J. & Lupas, A. N. (2008). The Sulfolobus solfataricus AAA protein Sso0909, a homologue of the eukaryotic ESCRT Vps4 ATPase. *Biochem Soc Trans* **36**, 94-8.

16. Ellen, A. F., Albers, S. V., Huibers, W., Pitcher, A., Hobel, C. F., Schwarz, H., Folea, M., Schouten, S., Boekema, E. J., Poolman, B. & Driessen, A. J. (2009). Proteomic analysis of secreted membrane vesicles of archaeal Sulfolobus species reveals the presence of endosome sorting complex components. *Extremophiles* **13**, 67-79.

17. Moriscot, C., Gribaldo, S., Jault, J. M., Krupovic, M., Arnaud, J., Jamin, M., Schoehn, G., Forterre, P., Weissenhorn, W. & Renesto, P. (2011). Crenarchaeal CdvA forms double-helical filaments containing DNA and interacts with ESCRT-III-like CdvB. *PLoS One* **6**, e21921.

18. Azmi, I. F., Davies, B. A., Xiao, J., Babst, M., Xu, Z. & Katzmann, D. J. (2008). ESCRT-III family members stimulate Vps4 ATPase activity directly or via Vta1. *Dev Cell* **14**, 50-61.

19. Azmi, I., Davies, B., Dimaano, C., Payne, J., Eckert, D., Babst, M. & Katzmann, D. J. (2006). Recycling of ESCRTs by the AAA-ATPase Vps4 is regulated by a conserved VSL region in Vta1. *J Cell Biol* **172**, 705-17.

20. Yang, D. & Hurley, J. H. (2010). Structural role of the Vps4-Vta1 interface in ESCRT-III recycling. *Structure* **18**, 976-84.

21. Kerfeld, C. A., Sawaya, M. R., Tanaka, S., Nguyen, C. V., Phillips, M., Beeby, M. & Yeates, T. O. (2005). Protein structures forming the shell of primitive bacterial organelles. *Science* **309**, 936-8.

22. Pornillos, O., Ganser-Pornillos, B. K., Kelly, B. N., Hua, Y., Whitby, F. G., Stout, C. D., Sundquist, W. I., Hill, C. P. & Yeager, M. (2009). X-ray structures of the hexameric building block of the HIV capsid. *Cell* **137**, 1282-92.

23. Enemark, E. J. & Joshua-Tor, L. (2006). Mechanism of DNA translocation in a replicative hexameric helicase. *Nature* **442**, 270-5.

24. Thomsen, N. D. & Berger, J. M. (2009). Running in reverse: the structural basis for translocation polarity in hexameric helicases. *Cell* **139**, 523-34.

25. Pflugrath, J. W. (1999). The finer things in X-ray diffraction data collection. *Acta Crystallogr D Biol Crystallogr* **55**, 1718-25.

26. Otwinowski, Z. & Minor, W. (1997). Processing of X-ray diffraction data collected in oscillation mode. *Methods in Enzymology, part A* **276**, 307-326.

27. Tong, L. & Rossmann, M. G. (1997). Rotation function calculations with GLRF program. *Methods Enzymol* **276**, 594-611.

28. Sheldrick, G. M. (2008). A short history of SHELX. *Acta Crystallogr A* **64**, 112-22.

29. Vagin, A. & Teplyakov, A. (1997). MOLREP: an Automated Program for Molecular Replacement. *Journal of Applied Crystallography* **30**, 1022-1025.

30. Monroe, N., Han, H., Gonciarz, M. D., Eckert, D. M., Karren, M. A., Whitby, F. G., Sundquist, W. I. & Hill, C. P. (2013). The oligomeric state of the active Vps4 AAA ATPase. *J Mol Biol*.

CHAPTER 4

ESCRT-III HELIX 5 BINDS THE VPS4 HEXAMER CENTRAL PORE IN AN INTERACTION THAT IS AUTOINHIBITED BY THE VPS4 MIT DOMAIN

Abstract

Vps4 is a hexameric AAA ATPase that functions with the ESCRT-III complex to drive reverse topology membrane fission events during several cellular processes, including cytokinesis, MVB biogenesis, and HIV budding. Vps4 contains an N-terminal MIT domain that binds the C-terminal MIM motifs of ESCRT-III subunits, although it is not known how the mechanism progresses from this initial recognition to ATP-driven disassembly of ESCRT-III complexes. Here, we report that Vps4p lacking the MIT domain can form a hexamer that binds residues from helix 5 of the Vps2p/ESCRT-III subunit. Mutagenesis experiments map this interaction to the central pore of the Vps4p hexamer, and the observed 6:1 Vps4p:Vps2p binding stoichiometry indicates that the functional Vps4p hexamer is asymmetric. These data support a model that the ESCRT-III complexes are disassembled by pulling the helix 5 of ESCRT-III through/into the central pore of Vps4 hexamer. Our finding that a sequence preceding Vps2p

helix 5 does not bind the Vps4p pore suggests that “stop translocation” sequences regulate the extent to which substrates pass through the Vps4p pore. We also report that binding of the Vps2p/ESCRT-III peptide is autoinhibited by the MIT domain of full-length Vps4p, and that this inhibition is alleviated when the MIT engages a MIM motif, thereby indicating a mechanism to ensure specificity of substrate selection while allowing a variety of ESCRT-III substrates to be processed.

Introduction

The cellular Endosomal Sorting Complexes Required for Transport (ESCRT) pathway functions in reverse topology membrane fission events, including the sorting of ubiquitylated cargo proteins into multivesicular bodies (MVB) [1; 2; 3; 4; 5], the abscission step of cytokinesis [6; 7], and the budding of many retroviruses, including HIV budding [8; 9; 10; 11; 12]. It comprises multiple protein complexes: ESCRT-0, I, II, III, and the Vps4 complex; plus a number of accessory proteins [13; 14]. ESCRT complexes are recruited sequentially to the site of membrane fission [13; 14; 15; 16]. ESCRT-0 functions in ubiquitylated cargo sorting, and ESCRT-I & II drive membrane deformation. When ESCRT-III proteins are recruited to the membrane, they form a lattice structure that is thought to constrict the membrane neck [3]. The AAA ATPase Vps4 is then recruited to the membrane neck before fission occurs, and it subsequently disassembles the ESCRT-III lattice [16; 17; 18; 19; 20]. ESCRT-III complexes can be disassembled by Vps4 in vitro [20], although the mechanism of ESCRT-III disassembly by Vps4 is not yet established.

Vps4 includes an N-terminal MIT domain that forms a three helices bundle that serves as the primary substrate recognition module by binding the C-terminal MIT-Interacting Motifs (MIMs) of ESCRT-III subunits [21; 22; 23; 24]. There are seven members (Vps2p0, Snf7, Vps2p4, Vps2p0, Did2, Vps60, and Ist1) of the ESCRT-III family in S. cerevisiae [14], three of which (Vps2p, Did2, and Ist1) contain MIM motifs that interact directly with Vps4 [24; 25]. Two different types of Vps4-interacting MIM (MIM1 and MIM2) have been characterized, including structures of MIM1:MIT and MIM2:MIT complexes [21; 23; 24]. Only MIM1 has been identified in the ESCRT-III subunits from *S. cerevisiae* [24; 25]. Structures of the CHMP3(hVp24) and Ist1 subunits show that the different ESCRT-III family members display a conserved four helices core domain followed by unstructured sequences and at least two additional helices [26; 27; 28]. The four helices core appears to mediate ESCRT-III lattice formation, while the 5th α-helix can bind to the core domain to stabilize the soluble unassembled state and inhibit lattice formation [26].

The Vps4 MIT domain is followed by a ~40-residue linker and a single AAA+ ATPase cassette that is responsible for ATP hydrolysis, oligomerization, and presumably substrate (ESCRT-III proteins) processing [1; 29; 30; 31]. Multiple crystal structures of Vps4 ATPase cassettes in the monomeric state have been reported [30; 31; 32; 33; 34]. Although the subunit stoichiometry of the active Vps4 ATPase has been controversial [32; 35; 36], we have recently shown that Vps4, like most characterized AAA+ ATPases [37; 38], functions as a hexameric ring (see Chapter 2). Our working model for the Vps4 hexamer is based on the structure of the p97

D1 ATPase cassette hexamer, and is supported by mutational analysis of proposed hexamer interface residues [30; 31; 39]. This model features two pore loops: pore loop 1 and pore loop 2 that, similar to other AAA+ ATPases, line the central pore of the hexamer [30; 31; 39]. Pore loops of AAA+ ATPase hexamers form the substrate binding/processing motifs, as demonstrated for the unfoldase ClpX and the papillomavirus E1 helicase [40; 41; 42; 43]. Pore loop 1 of Vps4 displays an Ar-Φ loop that includes an aromatic residue followed by a hydrophobic residue, which is conserved among many AAA+ ATPases that have polypeptide substrates [30], and has been shown to be able to grip the substrate in Clpx and spastin [40; 44]. Mutations on both pore loops of Vps4 have been shown to restrict HIV-1 budding [30; 31].

Motivated by observations that C-terminal fragments of overexpressed ESCRT-III subunits CHMP2A and CHMP1B are required for their co-sedimentation with VPS4B_E235Q from cell lysate [45] and that C-terminal fragments of ESCRT-III proteins activate the ATP hydrolysis activity of VPS4A [46], we characterized the Vps4-ESCRT-III interaction using purified recombinant yeast proteins Vps4p and Vps2p, which is the yeast homolog of CHMP2. We found that the AAA+ ATPase cassette of Vps4p can form a stable hexamer with the nonhydrolyzable ATP analogs ADP·AlF_x or ADP·BeF_x and the VSL domain of the Vta1p cofactor, and that this hexameric complex directly binds a single peptide of Vps2p helix 5 in an interaction that is mediated by the Vps4p pore loop residues. Moreover, we found that binding of the α-helix 5 of Vps2p to the ATPase domain was autoinhibited by the MIT domain, and that this inhibition is

alleviated by MIM-MIT interaction. These observations support the model that ESCRT-III complexes are disassembled by pulling the helix 5 of ESCRT-III through or into the central pore of the Vps4p hexamer in a manner that is initially primed and activated by binding of MIT domains to ESCRT-III MIM sequences.

Materials and methods

Cloning

DNA encoding full-length Vps4p, full-length Vps2p, and full-length Vta1p was cloned into the E.coli expression vector pET151 as described previously [30; 31; 36]. The mutations or deletions were introduced into pET151-Vps4p, pET151-Vps2p, and pET151-Vta1p constructs by Quikchange mutagenesis and verified by DNA sequencing.

Peptides and proteins

Peptides were synthesized in Dr. Kay's lab at the Biochemistry department, University of Utah. The crude materials were purified by reverse phase C18 HPLC and the mass was confirmed by mass spectrometry (MS) at the University of Utah Peptide Synthesis Core.

Vps4p and Vta1p proteins were purified as described [30; 31; 36]. Briefly, proteins were expressed in BL21 RIL codon+ *E.coli* cells in ZY autoinduction media at 37°C until OD600 of 0.5 and then overnight at 21°C. Cells were harvested by centrifugation and lysed by incubation with 10 mg/ml lysozyme in lysis buffer (20mM imidazole, 300mM NaCl, 25mM Tris, pH 7.5, and protease

inhibitors including PMSF, aprotinin, leupeptin, pepstatin) at 4°C for 1 hour, followed by sonication. Cell lysates were clarified by centrifugation at 35,000 g for 45min, and the supernatant was incubated with Ni-NTA agarose for 1 hour and then washed with at least 10x volume of lysis buffer. For Vps2p proteins, the Ni-NTA wash was performed in high salt buffer (20mM imidazole, 1M NaCl, 25mM Tris, pH 7.5, and protease inhibitors including PMSF, aprotinin, leupeptin, pepstatin). Protein was eluted with elution buffer (400mM imidazole, 300mM NaCl, 25mM Tris, pH 7.5), and incubated with TEV protease (~1mg/100mg) in cleavage buffer (150mM NaCl, 1mM EDTA, 1mM DTT, 25mM Tris, pH 7.5) for 20 hours at 4°C followed by passage through a Ni-NTA agarose column to remove the cleaved affinity tag and unprocessed proteins. For Vps4p and Vta1p proteins, a subsequent Q chromatography step was applied. Specifically, Vps4p in buffer A (100mM NaCl, 20mM HEPES, pH 7.5) was loaded onto a HiTrap Q HP (GE Healthcare Life Sciences). The column was washed with 5x volume of buffer A. Then the protein was eluted with a gradient (0-35%) of buffer B (1M NaCl, 20mM HEPES, pH 7.5). Purified proteins were dialyzed into low salt buffer (100mM NaCl, 10mM $MgCl_2$, 1mM DTT, 20mM HEPES, pH 7.5) for biochemical experiments.

Analytical size-exclusion chromatography

A superdex200 column was equilibrated in running buffer (2mM ADP·AlF_x or ADP·BeF_x 10mM MgCl2, 100mM NaCl, 20mM HEPES, pH7.0). Vps4p or its variants were preincubated with Vta1p-VSL in running buffer at 4°C for at least 2

hours. The samples were filtered before being loaded onto the column. The column was calibrated by protein standards (Biorad).

Fluorescence anisotropy

A series of different concentrations of Vps4p (or its variants):Vta1p-VSL complexes were incubated with peptides (1nM) at 25°C for at least 3 hours. The fluorescence anisotropy value was measured at 25°C. The binding affinity was obtained by fitting the data to a 1:1 interaction model using GraphPad Prism5.

GST pull-down assay

Purified ΔMIT-Vps4p or full-length Vps4p (240 μM) and GST fusion proteins (40μM) were mixed with or without ADP·AlF_x. A 50 μl portion of glutathione agarose (Amersham) was preincubated with the protein samples for 2 hours at 4°C. Unbound proteins were removed by washing with wash buffer (10mM $MgCl_2$, 100mM NaCl, 20mM HEPES, pH7.0) containing 2mM ADP·AlF_x or not. Bound proteins were eluted by boiling in SDS–PAGE buffer and detected by SDS–PAGE.

ATPase assay

Malachite green, which forms a green complex with free phosphate released upon ATP hydrolysis, was used to measure the ATPase activity of Vps4p. Full-length Vps4p:Vta1p-VSL complex (final concentration 0.15μM) or ΔMIT-Vps4p:Vta1p-VSL complex (final concentration 0.3μM) was mixed with

2μM ATP in reaction buffer (100mM NaCl, 10mM MgCl2, 1mM DTT, 20mM HEPES, pH 7.5). Peptides or Vps2p were added as indicated. The mixture was incubated for 10min at 37 4°C. Then 2 volumes of malachite green solution (14 mM ammonium molybdate, 1.3 M HCl, 1.5 mM malachite green) were added into the reaction, followed by adding 21% citric acid of the same volume of malachite green solution. Absorbance at 650nm was measured using a plate reader. The concentration of the free phosphate released from ATP hydrolysis was calculated according to a sodium phosphate standard.

Results

Vps2p peptides bind the ATPase cassette
of an asymmetric Vps4p hexamer

To determine if Vps2p/ESCRT-III sequences preceding the MIM motif directly contact the Vps4p ATPase cassette, we used a Vps4p construct that lacks the N-terminal MIT domain in a fluorescence anisotropy assay with two overlapping fluorescein-labeled peptides, peptide A and peptide B, and peptide C corresponding to the sequence shared between peptides A and B (Figure 4.1). Although the full-length Vps4p hexamer exists as a concentration-dependent equilibrium of dimers and hexamers (Chapter 2), we found that ΔMIT-Vps4p (81-437) in complex with the VSL domain of Vta1p formed a stable hexamer in the presence of ADP·AlF_x or ADP·BeF_x over the concentration range used for the titration experiment (Figure 4.1). An interaction was observed in the presence of ADP·AlF_x or ADP·BeF_x, but not ATP, ADP, AMPPNP, or ATPγS (Figure 4.1). The

Figure 4.1. Vps2p helix 5 binds the Vps4p cassette.
A: Sequence alignment of helix 5 and nearby loops from ESCRT-III proteins. Peptides A, B, C were labeled with an N-terminal fluorescein. Peptides A2, B2, and C2 were labeled on the C-terminus. The acidic residues patch is indicated by a red rectangle.
B: Peptides A, B, and C bind to ΔMIT-Vps4p in the presence of ADP·AlFx or ADP·BeFx but not in the presence of other nucleotides tested.
C: ΔMIT-Vps4p forms a stable hexamer in the presence of Vta1p-VSL and ADP·AlFx or ADP·BeFx. ΔMIT-Vps4p at 200 μM (solid) and 50 μM (dotted) was run on a gel-filtration column in the presence of Vta1p-VSL and different nucleotides. Virtical dotted lines indicate calculated elution volume of the ΔMIT-Vps4p hexamer and dimer relative to standards.

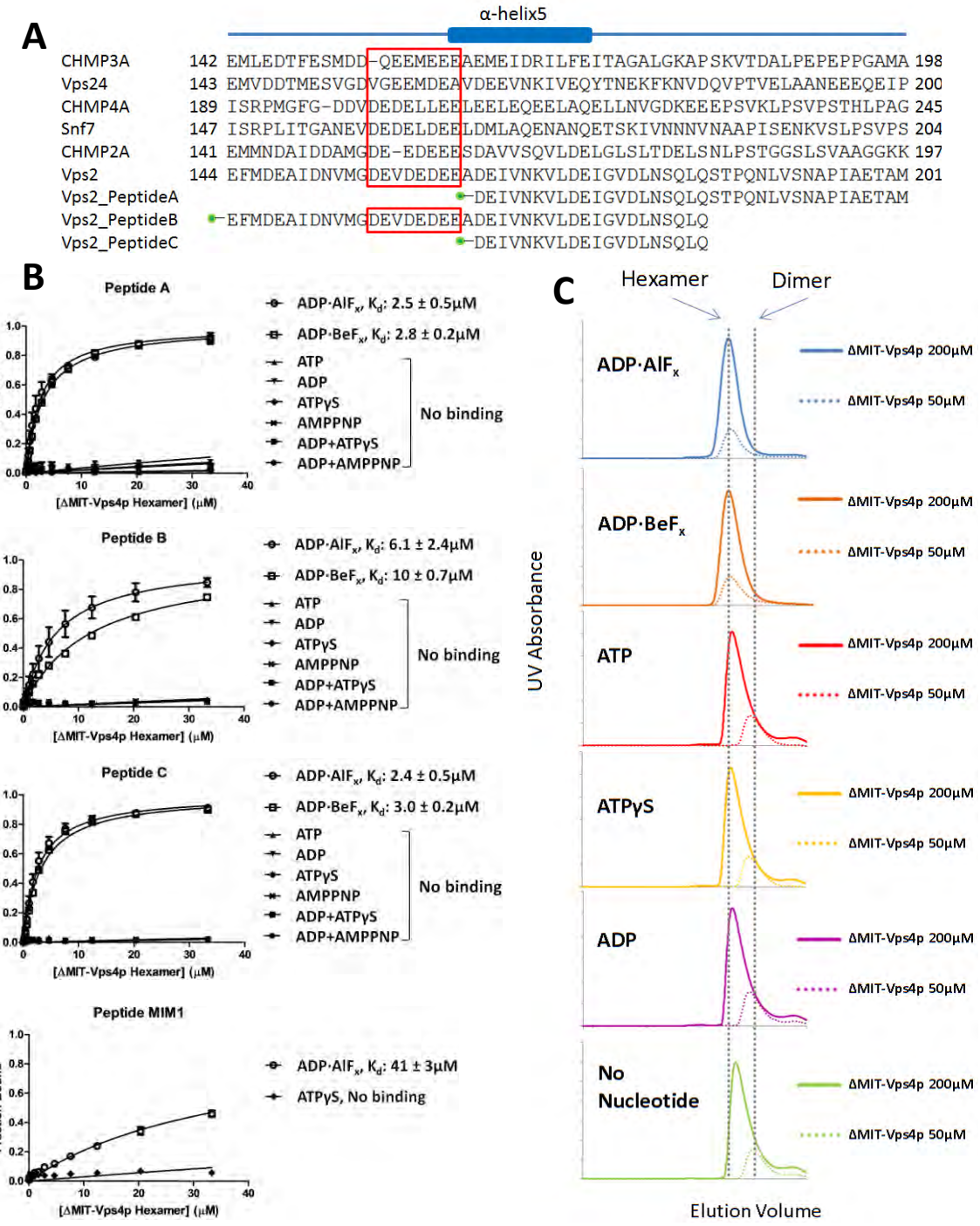
A
α-helix5
CHMP3A 142 EMLEDTFESMDD-QEEMEEEAEMEIDRILFEITAGALGKAPSKVTDALPEPEPPGAMA 198
Vps24 143 EMVDDTMESVGDVGEEMDEAVDEEVNKIVEQYTNEKFKNVDQVPTVELAANEEEQEIP 200
CHMP4A 189 ISRPMGFG-DDVDEDELLEELEELEQEELAQELLNVGDKEEEPSVKLPSVPSTHLPAG 245
Snf7 147 ISRPLITGANEVDEDELDEELDMLAQENANQETSKIVNNNVNAAPISENKVSLPSVPS 204
CHMP2A 141 EMMNDAIDDAMGDE-EDEEESDAVVSQVLDELGLSLTDELSNLPSTGGSLSVAAGGKK 197
Vps2 144 EFMDEAIDNVMGDEVDEDEEADEIVNKVLDEIGVDLNSQLQSTPQNLVSNAPIAETAM 201
Vps2_PeptideA DEIVNKVLDEIGVDLNSQLQSTPQNLVSNAPIAETAM
Vps2_PeptideB EFMDEAIDNVMGDEVDEDEEADEIVNKVLDEIGVDLNSQLQ
Vps2_PeptideC DEIVNKVLDEIGVDLNSQLQ
B
Peptide A
ADP·AlFx, Kd: 2.5 ± 0.5μM
ADP·BeFx, Kd: 2.8 ± 0.2μM
ATP
ADP
ATPγS
AMPPNP
ADP+ATPγS
ADP+AMPPNP
No binding
Fraction Bound
[ΔMIT-Vps4p Hexamer] (μM)
Peptide B
ADP·AlFx, Kd: 6.1 ± 2.4μM
ADP·BeFx, Kd: 10 ± 0.7μM
ATP
ADP
ATPγS
AMPPNP
ADP+ATPγS
ADP+AMPPNP
No binding
Fraction Bound
[ΔMIT-Vps4p Hexamer] (μM)
Peptide C
ADP·AlFx, Kd: 2.4 ± 0.5μM
ADP·BeFx, Kd: 3.0 ± 0.2μM
ATP
ADP
ATPγS
AMPPNP
ADP+ATPγS
ADP+AMPPNP
No binding
Fraction Bound
[ΔMIT-Vps4p Hexamer] (μM)
Peptide MIM1
ADP·AlFx, Kd: 41 ± 3μM
ATPγS, No binding
Fraction Bound
[ΔMIT-Vps4p Hexamer] (μM)
C
Hexamer
Dimer
UV Absorbance
ADP·AlFx
ADP·BeFx
ATP
ATPγS
ADP
No Nucleotide
ΔMIT-Vps4p 200μM
ΔMIT-Vps4p 50μM
Elution Volume

failure to detect binding with ATP is consistent with transient interactions in the presence of productive substrate cycling. The ability of ADP·AlF_x and ADP·BeF_x to support binding may reflect their ability to mimic multiple states, including ATP, ADP, and transition state bound nucleotide complexes, and a requirement for different subunits of the Vps4p hexamer to adopt different conformation to generate an asymmetric substrate binding surface.

The binding affinity between the ΔMIT-Vps4p:Vta1p-VSL hexamer and the peptides in the presence of ADP·AlF_x was calculated assuming that one Vps4p hexamer binds one peptide (below). Peptide A (K_d = 2.5 ± 0.5 μM) bound to the Vps4p hexamer more tightly than peptide B (K_d = 6.1 ± 2.4 μM). Peptide C bound with the same affinity as peptide A (K_d = 2.4 ± 0.5 μM) (Figure 4.1). The Vps2p MIM1 motif (218-232), a negative control that has a similar length to peptide C, was found to bind with an affinity 20 times lower than peptide C (Figure 4.1).

We also test the interaction between the Vps4p hexamer and the C-terminally labeled peptides of the same sequences (peptide A2, B2, and C2). Peptide A2 and peptide A have similar affinity to Vps4p the hexamer (~2-fold difference) (Figure 4.2). However, peptide B2 and C2 have much lower affinity (> 5-fold) towards Vps4p hexamer compared with peptide B and C, respectively (Figure 4.2). Peptide B2 and C2 have the fluorescein attached to the same residue (Gln184), so this residue or nearby residue(s) may be important for interaction with Vps4p hexamer. Atomic details of this interaction are required to understand how different residues contribute to the substrate binding to Vps4p hexamer.

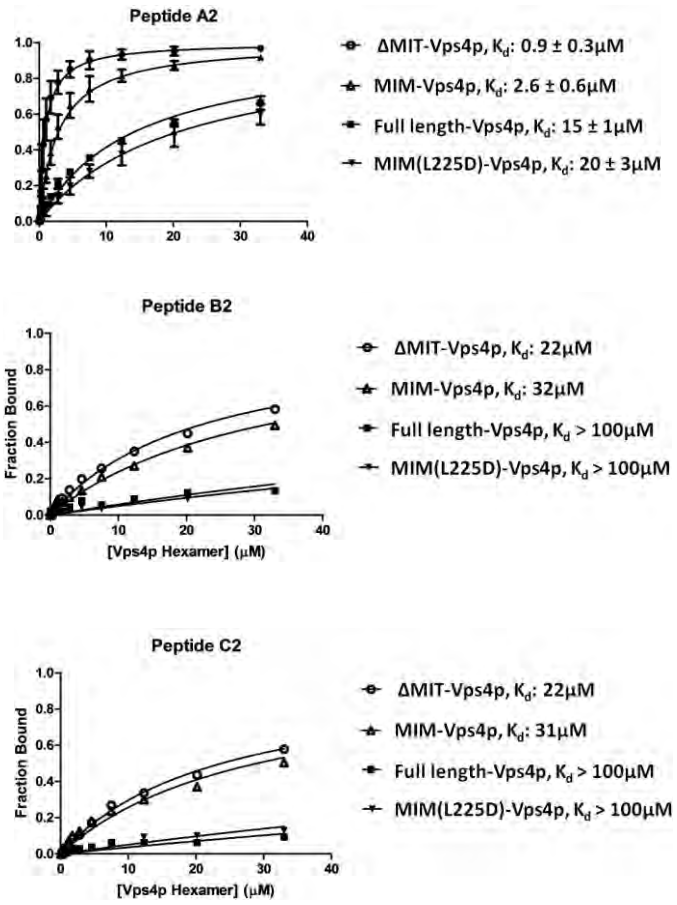

Figure 4.2. Binding of C-terminally labeled peptides to Vps4p hexamer.
C-terminally fluorescein labeled peptide A2, B2, and C2 have the same sequences as peptide A, B, and C, respectively. Fluorescence anisotropy assay was used to measure the binding affinity between the peptides and Vps4p or its variants in the presence of ADP·AlFx.

The Vps4p hexamer binds a single peptide

To verify the stoichiometry of this interaction, peptide C of high concentration (~20-fold above the K_d) was titrated with ΔMIT-Vps4p hexamers in the presence of ADP·AlF_x. Peptide binding was saturated when the stoichiometry was close to 1 (Figure 4.3). This is consistent with the model that only the asymmetric Vps4p hexamer is capable of forming binding sites for ESCRT-III substrates on their ATPase domains and one peptide binding site is

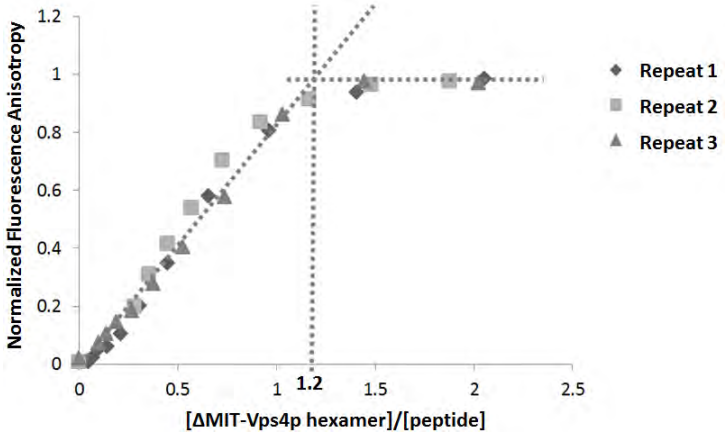

Figure 4.3. One ΔMIT-Vps4p hexamer binds one Vps2p-helix 5.
Fluorescence anisotropy was measured during titration of 50μM (~25-fold of K_d) peptide C with the ΔMIT-Vps4p:Vta1p-VSL hexamer. Saturation of the signal occurs at when the stoichiometry of the complex is close to 1:1.

formed within one hexamer. This model is appealing because the AAA ATPases E1 helicase [41] and Rho helicase [42] have been visualized binding their DNA and RNA substrates in this manner in their central pores. Other AAA ATPases, including ClpX [40], ClpB [47], and spastin [44], also appear to bind their substrate in the central hexamer pore, and are therefore also expected to have a stoichiometry of one substrate per hexamer.

Pore loop residues are important for binding of Vps2p-derived peptides

Our working hexamer model positions Vps4p pore loop 1 and pore loop 2 at the central pore [30; 31; 39]. To determine if residues in these loops contribute to binding, we tested peptide binding to pore loop mutants that have been previously shown to restrict HIV budding in the human homologs. These residues

correspond to S. cerevisiae Vps4p W206A on pore loop 1, R241A on pore loop 2, and R251A adjacent to pore loop 2 [30; 31]. Consistent with the model, none of these point mutants bind peptides with appreciable affinity (Figure 4.4 A).

Although these pore loop mutants did not bind to peptide, the hexamer stability of these mutants was reduced compared to wild type protein at low concentrations (Figure 4.4 B), which raises concern that the effect may be due to loss of assembly rather than loss of peptide binding *per se*. To find mutations that do not destabilize the Vps4p hexamer, we substituted pore loop residues with alanine and assayed oligimerization by analytical size exclusion chromatography. Out of ten residues tested, three were found not to impair

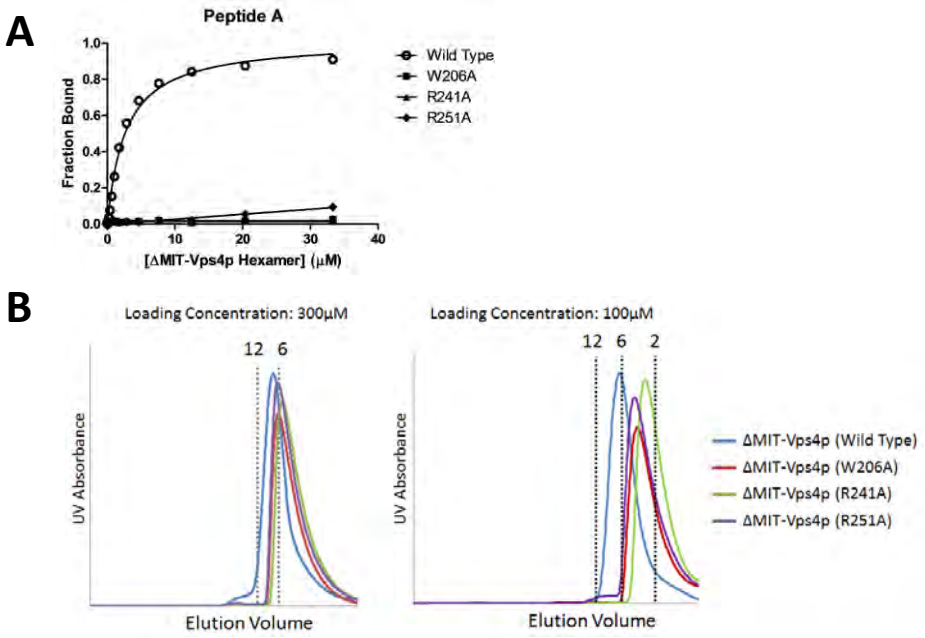

Figure 4.4. A conserved aromatic residue on pore loop 1 and both Arg residues on pore loop 2 of Vps4p hexamer are crucial for binding Vps2p-helix 5.
A: ΔMIT-Vps4p carrying a single mutation of these residues cannot bind the Vps2p-derived peptide.
B: Mutant ΔMIT-Vps4p cannot form stable hexamers compared to wild type Vps4p in the presence of ADP·AlFx.

oligomerization: T240 (pore loop 2), E243 (pore loop 2), and E247 (pore loop 2) (Figure 4.5A). Additional mutations at these positions were therefore made and tested for peptide binding. Of particular interest, the T240K, E243A, and E247A variants increased the binding affinity to Vps2p-helix 5 derived peptideC by 2-, 3-, and 4-fold, respectively (Figure 4.5). The double mutant, ΔMIT-Vps4p (E243A, E247A) bound 5-fold (peptide C) or 10-fold (peptide B) more tightly than wild type Vps4p (Figure 4.5). Because several different mutations on the pore loops of Vps4p can increase or reduce peptide binding affinity without apparently changing the hexamerization state, we conclude that the Vps4p substrates bind to the pore loops.

Charge-charge repulsion limits the Vps4p-Vps2p interaction

Peptide B, but not peptide C, displays a larger fluorescence anisotropy value when bound to ΔMIT-Vps4p (E243A, E247A) than wild type ΔMIT-Vps4p (Figure 4.5). This implies that the peptide B fluorophore tumbles more slowly when bound to ΔMIT-Vps4p (E243A, E247A) than wild type ΔMIT-Vps4p, and suggests that the fluorophore is closer to the ΔMIT-Vps4p (E243A, E247A) binding site than to the wild type ΔMIT-Vps4p binding site. Compared to peptide C, peptide B has several additional acidic residues between the N-terminal fluorescein and their common binding motif (Figure 4.5). Because the mutated Vps4p pore loop residues are also acidic (E243, E247), we propose that the charge-charge repulsion between acidic residues of Vps4p pore loop 2 and Vps2p helix 5 limits the interaction and cause the N-terminal fluorophore of

Figure 4.5 Negatively charged residues on pore loop 2 of the Vps4p hexamer regulate binding to Vps2p-helix 5.
A: ΔMIT-Vps4p hexamer model based on the p97 D1 hexamer structure. Pore loops 1 and 2 are highlighted in orange and green, respectively. T240, E243, and E247 are shown as sticks.
B: ΔMIT-Vps4p carrying point mutations T240A, E243A, or E247A on pore loop 2 can oligomerize into a hexamer in the presence of Vta1p-VSL and ADP·AlFx. Oligomerization of ΔMIT-Vps4p at loading concentration of 50μM was measured by gel filtration in the presence of Vta1p-VSL and ADP·AlFx. The column was calibrated using molecular weight standard proteins. The two dotted lines indicate the calculated elution volumes of hexamer and dimer.
C: ΔMIT-Vps4p or its variants carrying mutations on T240, including T240A, T240F, T240K, were tested for binding to peptide C by fluorescence anisotropy assay. All of the three mutations can change the binding affinity slightly.
D: ΔMIT-Vps4p or its variants carrying mutations on E243 and/or E247 were tested for binding to peptide B and C by fluorescence anisotropy assay. Double mutation E243A+E247A on pore loop 2 can increase both the binding affinity between ΔMIT-Vps4p and peptide B and the saturated fluorescence anisotropy value of ΔMIT-Vps4p bound peptide B significantly. The fluorescence anisotropy (FA) value or the bound fraction of peptide is shown on the y-axis.

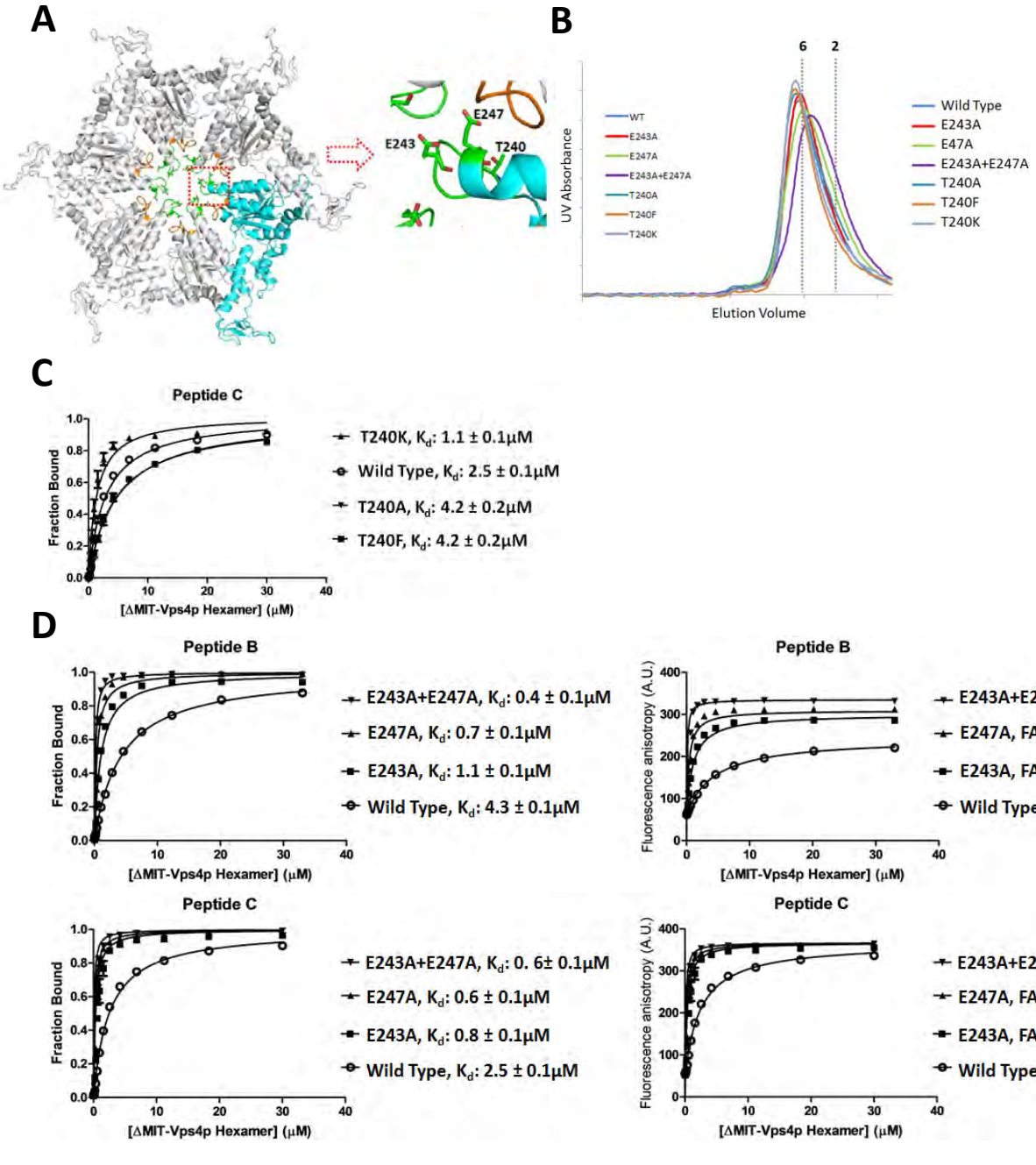
A
E247
E243
T240
B
6
2
WT
E243A
E247A
E243A+E247A
T240A
T240F
T240K
UV Absorbance
Elution Volume
Wild Type
E243A
E47A
E243A+E247A
T240A
T240F
T240K
C
Peptide C
Fraction Bound
[ΔMIT-Vps4p Hexamer] (μM)
T240K, Kd: 1.1 ± 0.1μM
Wild Type, Kd: 2.5 ± 0.1μM
T240A, Kd: 4.2 ± 0.2μM
T240F, Kd: 4.2 ± 0.2μM
D
Peptide B
Fraction Bound
[ΔMIT-Vps4p Hexamer] (μM)
E243A+E247A, Kd: 0.4 ± 0.1μM
E247A, Kd: 0.7 ± 0.1μM
E243A, Kd: 1.1 ± 0.1μM
Wild Type, Kd: 4.3 ± 0.1μM
Peptide B
Fluorescence anisotropy (A.U.)
[ΔMIT-Vps4p Hexamer] (μM)
E243A+E247A, FA :335
E247A, FA: 310
E243A, FA: 300
Wild Type, FA: 243
Peptide C
Fraction Bound
[ΔMIT-Vps4p Hexamer] (μM)
E243A+E247A, Kd: 0. 6± 0.1μM
E247A, Kd: 0.6 ± 0.1μM
E243A, Kd: 0.8 ± 0.1μM
Wild Type, Kd: 2.5 ± 0.1μM
Peptide C
Fluorescence anisotropy (A.U.)
[ΔMIT-Vps4p Hexamer] (μM)
E243A+E247A, FA: 367
E247A, FA: 367
E243A, FA: 367
Wild Type, FA: 367

peptide B to be held away from Vps4p.

The continuous negatively charged residues preceding helix 5 of Vps2p are conserved among several ESCRT-III proteins, including three of the four core ESCRT-III proteins: Snf7/CHMP4, Vps24/CHMP3, and Vps2/CHMP2 (Figure 4.1A). The negatively charged pore loop 2 residues are also conserved between *S. cerevisiae* Vps4p and the two human isoforms, VPS4A and VPS4B (Figure 4.6A). There are three acidic residues on pore loop 2 for each subunit. Mutation on the middle one (E245 on Vps4p) can severely affect the oligomerization of Vps4, so only two acidic residues (E243, E247 on Vps4p) can be mutated without significantly affect the oligomerization of Vps4. To test the biological importance of the negatively charged collar in human cells, we introduced the corresponding mutations (E245A, E249A) into VPS4B, and expressed the mutant VPS4B in VPS4A/B depleted cells. Expression of exogenous wild type VPS4B or VPS4B with a single collar mutation rescued HIV budding in this context, whereas VPS4B carrying double mutations on the pore loop 2 (E245A + E249A) led to a ~2-fold reduction in virus titer of the released viruses (compare lane 3 and lane 8 in Figure 4.6C). The relatively weak affect (only ~2-fold reduction) may be because there is still one more acidic residue kept on pore loop 2 of all of the subunits within a Vps4 hexamer. Thus, the negatively charged collar on pore loop 2 plays a role in HIV budding. However, because these corresponding mutations also impair the ATPase activity of Vps4p (Figure 4.6D), it is not clear whether reduced HIV budding results from impaired regulatory function of pore loop 2 or from the impaired ATPase activity.

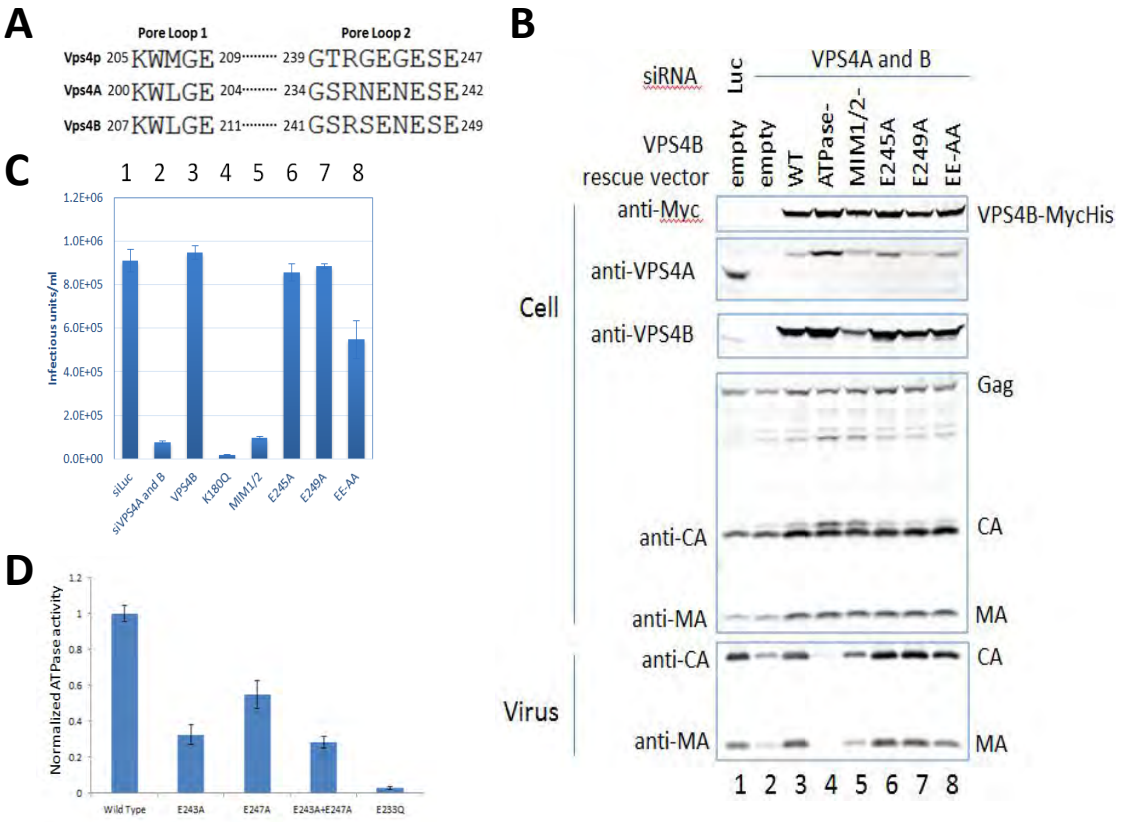

Figure 4.6 The acidic residues of Vps4 pore loop 2 contribute to efficient HIV budding.

A: Acidic residues on pore loop 2 are conserved among Vps4p, VPS4A, and VPS4B.

B: Western blots showing detection of Vps4 and viral proteins in cells and viral proteins of the harvested virus from the culture supernatants. (It seems there is some difference for the MA protein of the released viruses between lane 3 and 8, which support the virus budding is limited. But CA protein did not show difference between land 3 and 8)

C: Infectivity of the harvested virus from the culture supernatants. RNAi depletion of endogenous Vps4A/B (lane 2) restrict HIV budding. Expression of exogenous wild type Vps4B rescues HIV budding (lane 3). Expressing an ATPase deficient Vps4B mutant did not rescue HIV budding (lane 4). Single residue mutations on pore loop 2 (lane 6 and 7) did not impair the function of Vps4B in HIV budding process, whereas a double mutation (lane 8) led to ~2-fold reduction in HIV budding and virus titer of the culture supernatants.

D: Mutations of the acidic residues on pore loop 2 of Vps4p impaired the ATPase activity of Vps4p. ATPase activities of wild type and mutated ΔMIT-Vps4p in complex with the Vta1p-VSL domain were measured at 37°C. Double mutation (E243A+E247A) on the negatively charged collar reduced the ATPase activity by ~70% compared with wild type Vps4p.

Peptide binding stimulates ΔMIT-Vps4p ATPase activity and stabilizes the hexamer

Motivated by a report that the C-terminal portion of ESCRTIII proteins covering the MIM motif and helix 5 activates VPS4A ATPase activity [46], we determined if the same was true for the much shorter peptide C. Peptide C at different concentrations was added to the ΔMIT-Vps4p:Vta1p-VSL complex, and the ATPase activity was measured at 37°C. As shown in Figure 4.7, adding peptide C increased ATPase activity, demonstrating that this short Vps2p-helix 5 peptide can bind and activate the ATPase cassette of Vps4p.

An attractive explanation for this observation is that peptide binding stabilizes the ΔMIT-Vps4p hexamer. To test this possibility, we characterized the oligomerization of ΔMIT-Vps4p:Vta1p-VSL with or without peptide C by analytical gel filtration in the presence of ADP·AlF_x at a concentration where the complex dissociates, which is closer to the concentration at which ATPase activity is assayed. By itself, ΔMIT-Vps4p:Vta1p-VSL did not elute as a single peak corresponding to the hexamer (Figure 4.7B) at a concentration of 10 μM. However, when the protein complex was pre-incubated with peptide C, the majority of the protein eluted as a single peak corresponding to the hexamer (Figure 4.7B). This validates the hypothesis that the activation of ATPase activity of ΔMIT-Vps4p by peptide C is due, at least partially, to the stabilization of ΔMIT-Vps4p hexamer by peptide C.

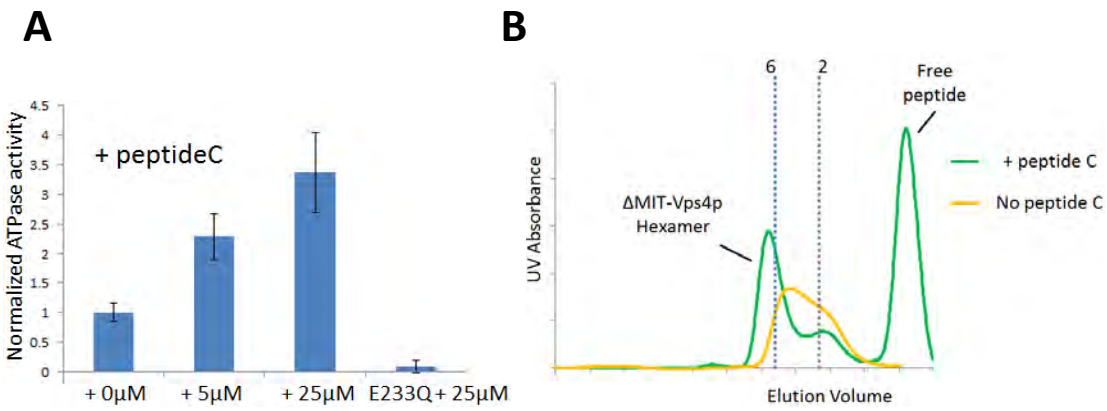

Figure 4.7, Vps2p-helix 5 can activate the ATPase activity of Vps4p and stabilize the Vps4p hexamer.
A: Peptide C can activate the ATPase activity of Vps4p. ATPase activity of the ΔMIT-Vps4p:Vta1p-VSL complex was measured in the presence of different concentrations of peptide C. Adding peptides can increase the ATPase activity of Vps4p.
B: Peptide C can stabilize ΔMIT-Vps4p hexamer. Oligomerization of ΔMIT-Vps4p (10μM) was measured by gel-filtration in the presence of Vta1p-VSL (10μM) and ADP·AlFx. Blue and black dotted lines are calculated positions of ΔMIT-Vps4p hexamer and dimer. More hexamer was formed when peptide C was added (green).

ESCRT-III binding to pore loops is inhibited by the MIT domain in the absence of a MIM interaction

Recruitment of Vps4 to the membrane is mediated by MIT domain binding to MIM sequences of ESCRT-III substrates [23; 24]. To determine if the MIT domain also influences binding of the ESCRT-III helix 5 to the Vps4p pore, we measured the binding affinity between the full-length Vps4p and the Vps2p-helix 5 derived peptide. The affinity of the interaction between the full-length Vps4p and the peptide was ~10 times lower than that between ΔMIT-Vps4p and the peptide (Figure 4.8B), indicating that the MIT domain has an inhibitory effect on binding at the Vps4p pore. Consistent with this, the pull down assay also showed that

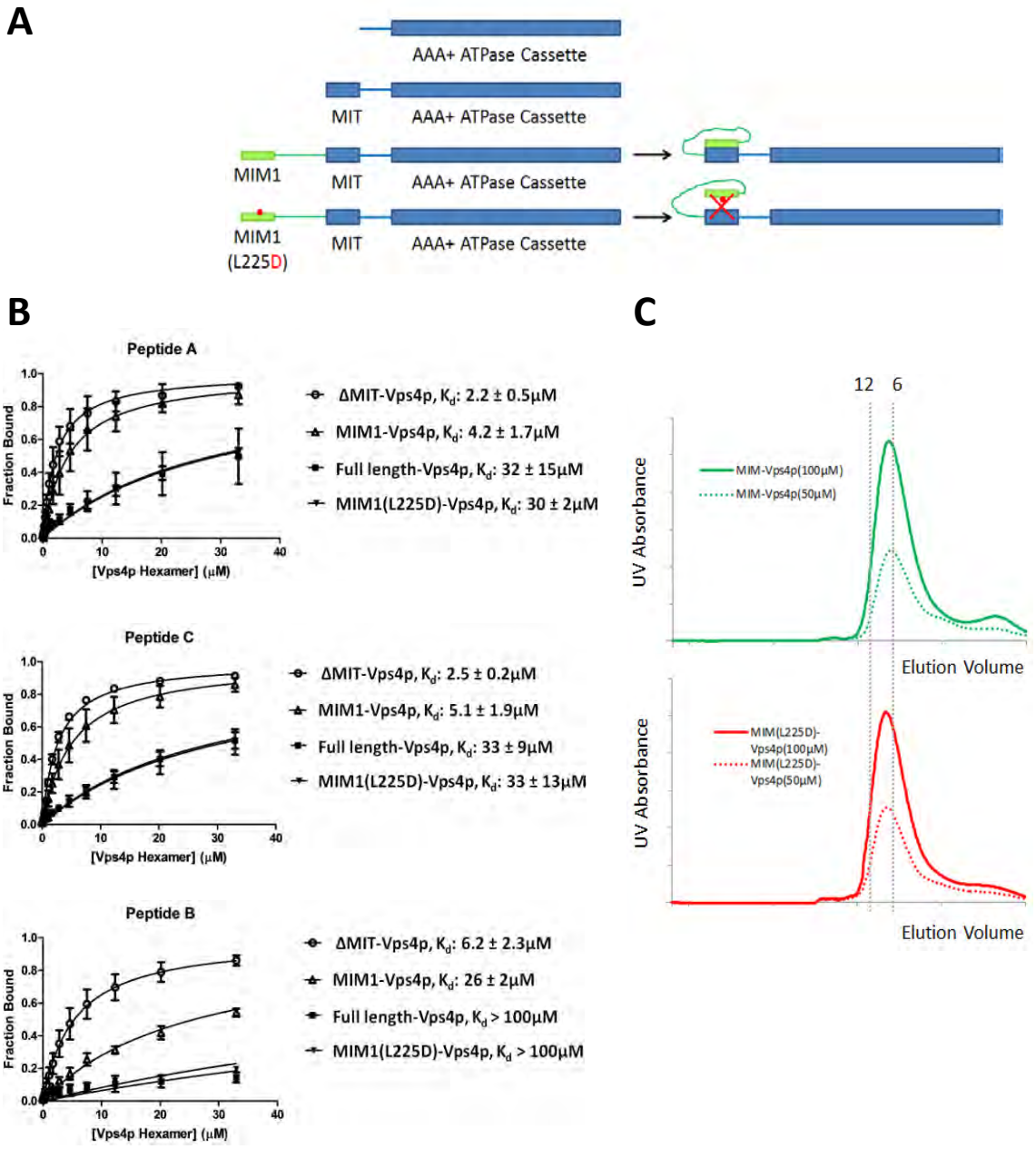

Figure 4.8. MIM-MIT regulation of Vps2p-helix 5 binding to the Vps4p AAA+ ATPase cassette.
A: Vps4p constructs were used in the binding experiments.
B: Full-length Vps4p and MIM1(L225D)-Vps4p binding the Vps2p-helix 5 derived peptides with ~10-fold lower Kd than ΔMIT-Vps4p and MIM1-Vps4p.
C: MIM1-Vps4p oligomerizes similarly to MIM1(L225D)-Vps4p

Vps2p-helix 5 derived peptide fused to GST has higher affinity to ΔMIT-Vps4p than to the full-length Vps4p (Figure 4.9).

We subsequently tested whether binding of MIM1 to the MIT domain can alleviate the inhibitory effect from the MIT domain. To test this hypothesis, we inspected the reported MIM1:MIT structure [24] to design an N-terminal extension to full-length Vps4p that encoded the MIM1 motif of Vps2p and a $(GGGGS)_3$ linker that was long enough to allow the MIM1-MIT interaction (Figure 4.8A). MIM1(L225D)-Vps4p was used as the negative control because this mutation disrupts the interaction between MIM1 and MIT [24]. The MIM1-Vps4p fusion protein bound peptide C ~10 times more tightly than full-length Vps4p, while the binding affinity of MIM1(L225D)-Vps4p towards peptide was similar to the affinity of full-length Vps4p (Figure 4.8B). GST-pull down assay also confirms that MIM-Vps4p had similar GST-peptide binding affinity to that of ΔMIT-Vps4p, which was much higher than that of the full length Vps4p. This supports the model that binding of MIM1 to the MIT domain alleviates the inhibitory effect on substrate engagement in the Vps4p hexamer pore.

I also tried to determine the mechanism of the regulation of peptide binding by the MIT domain and MIM1 motif. One possibility is that the MIT domain has a negative impact on the oligomerization of Vps4p that can be alleviated by the MIT-MIM1 interaction. Arguing against this possibility, however, the size of the MIM1-Vps4p and MIM1(L225D)-Vps4p oligomers showed no significant difference in the analytical gel-filtration assay in the presence of $ADP{\cdot}AlF_x$ (Figure 4.8C).

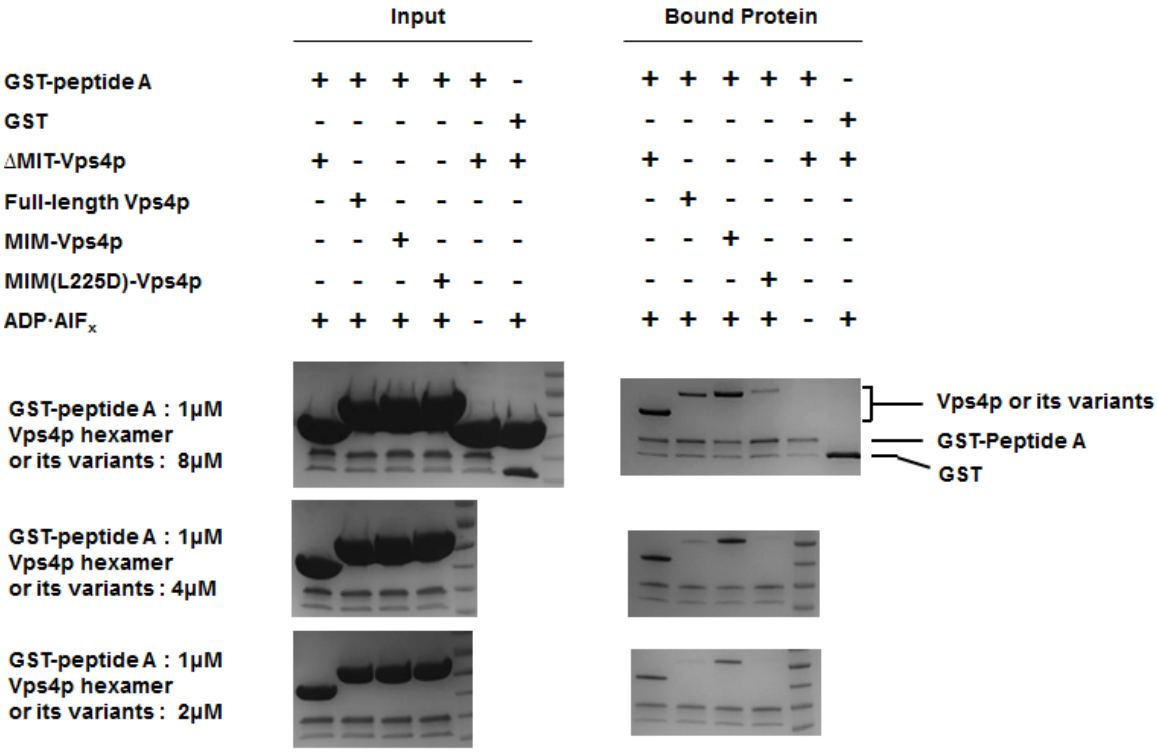

Figure 4.9. GST-peptide A can bind ΔMIT-Vps4p and full-length Vps4p in the presence of ADP·AlFx as demonstrated by pull-down assay. With equivalent input levels of full-length Vps4p or ΔMIT-Vps4p, GST-peptide A pulls down more ΔMIT-Vps4p

Discussion

Motivated by reports that co-sedimentation of Vps4B(E235Q) with overexpressed ΔMIM-CHMP2A is dependent on helix 5 and nearby loops of CHMP2A [45], and that C-terminal sequences of ESCRT-III proteins covering helix 4, helix 5, and C-terminal MIM, activate the ATPase activity of Vps4A [46], we mapped this interaction using *S. cerevisiae* Vps4p and Vps2p (homolog of human CHMP2). Using fluorescence anisotropy, we found that a 20-residue peptide derived from Vps2p-helix 5 binds the Vps4p ATPase cassette with the same affinity as a longer 28-residue construct. This peptide also stimulates

ATPase activity, at least in part by stabilizing the Vps4p hexamer. Mutagenesis data indicate that the peptide directly contacts that Vps4p pore loops. We further demonstrated that this interaction is regulated by the MIT domain and its interaction with the Vps2p MIM residues. These observations support a model that ESCRT-III complexes are disassembled by pulling the helix 5 of ESCRT-III through/into the central pore of the Vps4 hexamer in a manner that is initially primed and activated by binding of MIT domains to ESCRT-III MIM sequences.

There are 12 different ESCRT-III proteins in human cells and 7 different ESCRT-III proteins in *S. cerevisiae*. In addition to CHMP2A (hVps2p), C-terminal sections of overexpressed ESCRT-III subunits CHMP1B are also important for its co-sedimentation with VPS4B_E235Q from cell lysate [45]. The C-terminal fragments of several different ESCRT-III proteins, including CHMP2A, CHMP1B, CHMP3, CHMP4A, CHMP6, and CHMP5, can activate the ATP hydrolysis activity of Vps4A [46]. We therefore propose that other ESCRT-III subunits make equivalent interactions with Vps4 through analogous interactions to those of helix 5 of Vps2p.

The interaction between ΔMIT-Vps4p and Vps2p-helix 5 was dependent upon the presence of ADP·AlF_x or ADP·BeF_x, which are nonhydrolyzable ATP analogs that can mimic binding of ATP, ADP, and the transition state. Because the interaction was not observed in the presence of other nonhydrolyzable ATP analogs, ATP, ADP, or an ATP/ADP mixture, we conclude that cycling ATP induces transient interactions, consistent with substrate cycling, and that the functional Vps4p hexamer is asymmetric with a requirement for different

nucleotide bound conformations at different subunits. This is consistent with models of other ring-like ATPases, including the F1 ATPase [48], the E1 helicase [41] and the Rho helicase [42], in which crystal structures have demonstrated different nucleotide states correlating with subunit pore loop conformations and binding in the central pore.

Many AAA+ ATPases that process polypeptide substrates display an aromatic residue followed by a hydrophobic residue on pore loop 1 [30]. This Ar-Φ motif has been shown to grip the substrate in Clpx and spastin [40; 44]. Vps4 also contains this conserved Ar-Φ loop on pore loop 1 (Figure 4.6A). Mutation of this aromatic residue of human Vps4 homologs (W201 of VPS4A and W208 of VPS4B) inhibits HIV-1 release [30]. Consistent with this model, we found that Vps4p carrying the mutation on the corresponding aromatic residue (W206A) of *S. cerevisiae* cannot bind to Vps2p-helix 5 (Figure 4.4). A caveat, however, is that the Vps4p(W206A) hexamer was not as stable as the wild type hexamer (Figure 4.4), which raised the possibility that failure of Vps4p(W206A) to bind Vps2p-helix 5 was indirectly due to weaker assembly. Thus, while the model that Vps4 pore loop 1 contacts substrate directly is very attractive, more evidence is needed to provide definite confirmation.

Vps4 displays three conserved acidic residues on pore loop 2 and the downstream helix that form an acidic collar (Figure 4.5). We found that alanine substitution on two of these three acidic residues (E243A, E247A) increases binding affinity between Vps4p and peptides derived from Vps2p, further supporting the model that pore loop 2 is a binding site for Vps2p-helix 5 (Figure

4.5). Peptide B contained an extra continuous acidic-residue-patch preceding helix 5 compared with peptide C (Figure 4.1A), suggesting that repulsion between the acidic-residue-patch preceding helix 5 and the acidic residues on pore loop 2 (E243, E247) prevent the Vps4p hexamer binding to the upstream sequence of helix 5. Thus, Vps4p pore loop 2 functions in both substrate binding and the regulation of substrate binding.

Our findings that the MIT domain inhibits peptide binding to the central pore and that this inhibition is alleviated by binding of an MIM sequence suggests a mechanism to prevent nonspecific substrate binding and processing. Because the sequences of ESCRT-III subunits are not conserved, it is likely that the Vps4p central pore is able to bind and translocate a wide variety of peptides, but the requirement for prior binding of an MIM will exclude engagement of inappropriate substrates.

Our data support a two-step model of Vps4-mediated ESCRT-III lattice disassembly (Figure 4.10). Before interacting with ESCRT-III, the Vps4 hexamer central pore has low binding affinity to peptides because of autoinhibition by the MIT domain. Following recruitment of Vps4 to the membrane neck by MIT-MIM interaction, the substrate-binding potential of the Vps4 pore loops will be unmasked, leading to engagement of ESCRT-III helix 5. We further speculate that ESCRT-III lattice disassembly results when the C-terminal region of ESCRT-III is translocated into the central Vps4 pore, and that the negatively charged collar of pore loop 2 prevents passage of ESCRT-III beyond the acidic-residue-patch N-terminal to helix 5.

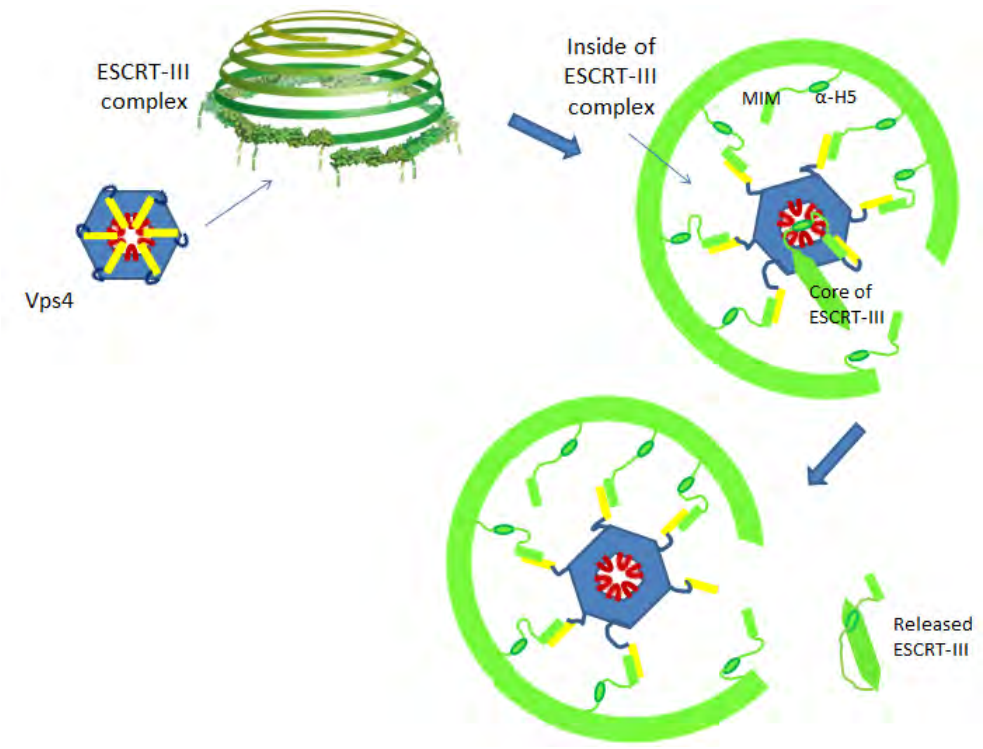

Figure 4.10: Model: Disassembly of the ESCRT-III complex by Vps4.

Important future goals include determining a structure of a Vps4-substrate complex in order to visualize molecular details of the Vps4 hexamer assembly and pore loop-substrate interaction. Another important goal is to understand the MIT domain interactions that inhibit substrate binding and how they are alleviated by MIM binding. Additionally, more data are needed to verify the extent to which ESCRT-III translocates through the central pore, and how this is coupled to disassembly of the ESCRT-III lattice. Finally, it is important to explore the extent to which this mechanism is conserved. The C-terminal region of several different ESCRT-III proteins have been shown to activate the ATPase activity of Vps4 [46]. Sequences of helix 5 from different ESCRT-III subunits are not very well conserved, but several ESCRT-III subunits contain the patch of acidic residues

N-terminal to helix 5 (Figure 2A). Systematic work to find out which ESCRT-III subunits use this strategy to interact with Vps4 will be important.

References

1. Babst, M., Sato, T. K., Banta, L. M. & Emr, S. D. (1997). Endosomal transport function in yeast requires a novel AAA-type ATPase, Vps4p. *EMBO J* **16**, 1820-31.

2. Katzmann, D. J., Babst, M. & Emr, S. D. (2001). Ubiquitin-dependent sorting into the multivesicular body pathway requires the function of a conserved endosomal protein sorting complex, ESCRT-I. *Cell* **106**, 145-55.

3. Babst, M., Katzmann, D. J., Estepa-Sabal, E. J., Meerloo, T. & Emr, S. D. (2002). Escrt-III: an endosome-associated heterooligomeric protein complex required for mvb sorting. *Dev Cell* **3**, 271-82.

4. Babst, M., Katzmann, D. J., Snyder, W. B., Wendland, B. & Emr, S. D. (2002). Endosome-associated complex, ESCRT-II, recruits transport machinery for protein sorting at the multivesicular body. *Dev Cell* **3**, 283-9.

5. Katzmann, D. J., Stefan, C. J., Babst, M. & Emr, S. D. (2003). Vps27 recruits ESCRT machinery to endosomes during MVB sorting. *J Cell Biol* **162**, 413-23.

6. Carlton, J. G. & Martin-Serrano, J. (2007). Parallels between cytokinesis and retroviral budding: a role for the ESCRT machinery. *Science* **316**, 1908-12.

7. Morita, E., Sandrin, V., Chung, H. Y., Morham, S. G., Gygi, S. P., Rodesch, C. K. & Sundquist, W. I. (2007). Human ESCRT and ALIX proteins interact with proteins of the midbody and function in cytokinesis. *EMBO J* **26**, 4215-27.

8. Garrus, J. E., von Schwedler, U. K., Pornillos, O. W., Morham, S. G., Zavitz, K. H., Wang, H. E., Wettstein, D. A., Stray, K. M., Cote, M., Rich, R. L., Myszka, D. G. & Sundquist, W. I. (2001). Tsg101 and the vacuolar protein sorting pathway are essential for HIV-1 budding. *Cell* **107**, 55-65.

9. Pornillos, O., Higginson, D. S., Stray, K. M., Fisher, R. D., Garrus, J. E., Payne, M., He, G. P., Wang, H. E., Morham, S. G. & Sundquist, W. I. (2003). HIV Gag mimics the Tsg101-recruiting activity of the human Hrs protein. *J Cell Biol* **162**, 425-34.

10. Martin-Serrano, J., Zang, T. & Bieniasz, P. D. (2001). HIV-1 and Ebola virus encode small peptide motifs that recruit Tsg101 to sites of particle assembly to facilitate egress. *Nat Med* **7**, 1313-9.

11. VerPlank, L., Bouamr, F., LaGrassa, T. J., Agresta, B., Kikonyogo, A., Leis, J. & Carter, C. A. (2001). Tsg101, a homologue of ubiquitin-conjugating (E2) enzymes, binds the L domain in HIV type 1 Pr55(Gag). *Proc Natl Acad Sci U S A* **98**, 7724-9.

12. Votteler, J. & Sundquist, W. I. (2013). Virus budding and the ESCRT pathway. *Cell Host Microbe* **14**, 232-41.

13. McCullough, J., Colf, L. A. & Sundquist, W. I. (2013). Membrane fission reactions of the mammalian ESCRT pathway. *Annu Rev Biochem* **82**, 663-92.

14. Hanson, P. I. & Cashikar, A. (2012). Multivesicular body morphogenesis. *Annu Rev Cell Dev Biol* **28**, 337-62.

15. Wollert, T. & Hurley, J. H. (2010). Molecular mechanism of multivesicular body biogenesis by ESCRT complexes. *Nature* **464**, 864-9.

16. Wollert, T., Wunder, C., Lippincott-Schwartz, J. & Hurley, J. H. (2009). Membrane scission by the ESCRT-III complex. *Nature* **458**, 172-7.

17. Baumgartel, V., Ivanchenko, S., Dupont, A., Sergeev, M., Wiseman, P. W., Krausslich, H. G., Brauchle, C., Muller, B. & Lamb, D. C. (2011). Live-cell visualization of dynamics of HIV budding site interactions with an ESCRT component. *Nat Cell Biol* **13**, 469-74.

18. Elia, N., Sougrat, R., Spurlin, T. A., Hurley, J. H. & Lippincott-Schwartz, J. (2011). Dynamics of endosomal sorting complex required for transport (ESCRT) machinery during cytokinesis and its role in abscission. *Proc Natl Acad Sci U S A* **108**, 4846-51.

19. Jouvenet, N., Zhadina, M., Bieniasz, P. D. & Simon, S. M. (2011). Dynamics of ESCRT protein recruitment during retroviral assembly. *Nat Cell Biol* **13**, 394-401.

20. Lata, S., Schoehn, G., Jain, A., Pires, R., Piehler, J., Gottlinger, H. G. & Weissenhorn, W. (2008). Helical structures of ESCRT-III are disassembled by VPS4. *Science* **321**, 1354-7.

21. Kieffer, C., Skalicky, J. J., Morita, E., De Domenico, I., Ward, D. M., Kaplan, J. & Sundquist, W. I. (2008). Two distinct modes of ESCRT-III

recognition are required for VPS4 functions in lysosomal protein targeting and HIV-1 budding. *Dev Cell* **15**, 62-73.

22. Scott, A., Gaspar, J., Stuchell-Brereton, M. D., Alam, S. L., Skalicky, J. J. & Sundquist, W. I. (2005). Structure and ESCRT-III protein interactions of the MIT domain of human VPS4A. *Proc Natl Acad Sci U S A* **102**, 13813-8.

23. Stuchell-Brereton, M. D., Skalicky, J. J., Kieffer, C., Karren, M. A., Ghaffarian, S. & Sundquist, W. I. (2007). ESCRT-III recognition by VPS4 ATPases. *Nature* **449**, 740-4.

24. Obita, T., Saksena, S., Ghazi-Tabatabai, S., Gill, D. J., Perisic, O., Emr, S. D. & Williams, R. L. (2007). Structural basis for selective recognition of ESCRT-III by the AAA ATPase Vps4. *Nature* **449**, 735-9.

25. Dimaano, C., Jones, C. B., Hanono, A., Curtiss, M. & Babst, M. (2008). Ist1 regulates Vps4 localization and assembly. *Mol Biol Cell* **19**, 465-74.

26. Bajorek, M., Schubert, H. L., McCullough, J., Langelier, C., Eckert, D. M., Stubblefield, W. M., Uter, N. T., Myszka, D. G., Hill, C. P. & Sundquist, W. I. (2009). Structural basis for ESCRT-III protein autoinhibition. *Nat Struct Mol Biol* **16**, 754-62.

27. Muziol, T., Pineda-Molina, E., Ravelli, R. B., Zamborlini, A., Usami, Y., Gottlinger, H. & Weissenhorn, W. (2006). Structural basis for budding by the ESCRT-III factor CHMP3. *Dev Cell* **10**, 821-30.

28. Xiao, J., Chen, X. W., Davies, B. A., Saltiel, A. R., Katzmann, D. J. & Xu, Z. (2009). Structural basis of Ist1 function and Ist1-Did2 interaction in the multivesicular body pathway and cytokinesis. *Mol Biol Cell* **20**, 3514-24.

29. Babst, M., Wendland, B., Estepa, E. J. & Emr, S. D. (1998). The Vps4p AAA ATPase regulates membrane association of a Vps protein complex required for normal endosome function. *EMBO J* **17**, 2982-93.

30. Scott, A., Chung, H. Y., Gonciarz-Swiatek, M., Hill, G. C., Whitby, F. G., Gaspar, J., Holton, J. M., Viswanathan, R., Ghaffarian, S., Hill, C. P. & Sundquist, W. I. (2005). Structural and mechanistic studies of VPS4 proteins. *EMBO J* **24**, 3658-69.

31. Gonciarz, M. D., Whitby, F. G., Eckert, D. M., Kieffer, C., Heroux, A., Sundquist, W. I. & Hill, C. P. (2008). Biochemical and structural studies of yeast Vps4 oligomerization. *J Mol Biol* **384**, 878-95.

32. Hartmann, C., Chami, M., Zachariae, U., de Groot, B. L., Engel, A. & Grutter, M. G. (2008). Vacuolar protein sorting: two different functional states of the AAA-ATPase Vps4p. *J Mol Biol* **377**, 352-63.

33. Inoue, M., Kamikubo, H., Kataoka, M., Kato, R., Yoshimori, T., Wakatsuki, S. & Kawasaki, M. (2008). Nucleotide-dependent conformational changes and assembly of the AAA ATPase SKD1/VPS4B. *Traffic* **9**, 2180-9.

34. Xiao, J., Xia, H., Yoshino-Koh, K., Zhou, J. & Xu, Z. (2007). Structural characterization of the ATPase reaction cycle of endosomal AAA protein Vps4. *J Mol Biol* **374**, 655-70.

35. Landsberg, M. J., Vajjhala, P. R., Rothnagel, R., Munn, A. L. & Hankamer, B. (2009). Three-dimensional structure of AAA ATPase Vps4: advancing structural insights into the mechanisms of endosomal sorting and enveloped virus budding. *Structure* **17**, 427-37.

36. Yu, Z., Gonciarz, M. D., Sundquist, W. I., Hill, C. P. & Jensen, G. J. (2008). Cryo-EM structure of dodecameric Vps4p and its 2:1 complex with Vta1p. *J Mol Biol* **377**, 364-77.

37. Erzberger, J. P. & Berger, J. M. (2006). Evolutionary relationships and structural mechanisms of AAA+ proteins. *Annu Rev Biophys Biomol Struct* **35**, 93-114.

38. Hanson, P. I. & Whiteheart, S. W. (2005). AAA+ proteins: have engine, will work. *Nat Rev Mol Cell Biol* **6**, 519-29.

39. Monroe, N., Han, H., Gonciarz, M. D., Eckert, D. M., Karren, M. A., Whitby, F. G., Sundquist, W. I. & Hill, C. P. (2013). The oligomeric state of the active Vps4 AAA ATPase. *J Mol Biol*.

40. Martin, A., Baker, T. A. & Sauer, R. T. (2008). Pore loops of the AAA+ ClpX machine grip substrates to drive translocation and unfolding. *Nat Struct Mol Biol* **15**, 1147-51.

41. Enemark, E. J. & Joshua-Tor, L. (2006). Mechanism of DNA translocation in a replicative hexameric helicase. *Nature* **442**, 270-5.

42. Thomsen, N. D. & Berger, J. M. (2009). Running in reverse: the structural basis for translocation polarity in hexameric helicases. *Cell* **139**, 523-34.

43. Lyubimov, A. Y., Strycharska, M. & Berger, J. M. (2011). The nuts and bolts of ring-translocase structure and mechanism. *Curr Opin Struct Biol* **21**, 240-8.

44. Roll-Mecak, A. & Vale, R. D. (2008). Structural basis of microtubule severing by the hereditary spastic paraplegia protein spastin. *Nature* **451**, 363-7.

45. Shim, S., Merrill, S. A. & Hanson, P. I. (2008). Novel interactions of ESCRT-III with LIP5 and VPS4 and their implications for ESCRT-III disassembly. *Mol Biol Cell* **19**, 2661-72.

46. Merrill, S. A. & Hanson, P. I. (2010). Activation of human VPS4A by ESCRT-III proteins reveals ability of substrates to relieve enzyme autoinhibition. *J Biol Chem* **285**, 35428-38.

47. Schlieker, C., Weibezahn, J., Patzelt, H., Tessarz, P., Strub, C., Zeth, K., Erbse, A., Schneider-Mergener, J., Chin, J. W., Schultz, P. G., Bukau, B. & Mogk, A. (2004). Substrate recognition by the AAA+ chaperone ClpB. *Nat Struct Mol Biol* **11**, 607-15.

48. Abrahams, J. P., Leslie, A. G., Lutter, R. & Walker, J. E. (1994). Structure at 2.8 A resolution of F1-ATPase from bovine heart mitochondria. *Nature* **370**, 621-8.

CHAPTER 5

SUMMARY AND FUTURE DIRECTIONS

Summary

My thesis aimed to understand two aspects of the Vps4 mechanism: how the Vps4 oligomer is formed and how Vps4 processes its substrate. Using several different biochemical and structural methods, some important progress was made. First, we found that Vps4p works as a hexamer in the presence of ATP. Second, structures were determined of two Crenarchaeal Vps4 AAA+ ATPase cassettes. The similarity between these two structures and the structure of eukaryotic Vps4 proteins indicated that the Vps4 3D structure is conserved during evolution. Third, the active Vps4 hexamer was found to be asymmetric, and the pore loops of the asymmetric hexamer were shown to bind residues of helix 5 from the ESCRT-III protein Vps2. The interaction seems to be limited to helix 5 due to repulsion between the acidic patch preceding the N-terminus of helix 5 of ESCRT-III and the acidic collar on the pore loop 2 of the Vps4 hexamer. Fourth, we found that the interaction with Vps2 helix 5 is inhibited by the N-terminal MIT domain of Vps4, and that this inhibition can be relieved by the MIT-MIM1 interaction. All of these data are consistent with a two-step model of ESCRT-III complex disassembly in which the MIT-MIM interaction recruits the

Vps4 hexamer and relieves autoinhibition to facilitate substrate binding by Vps4 pore loops, followed by translocation of ESCRT-III subunits into the central pore of the Vps4 hexamer and concomitant ESCRT-III lattice disassembly. To validate and understand the atomic details of this model, more research will be required to determine the structure of active Vps4 and understand the mechanism of ESCRT-III lattice disassembly.

Future Directions

Crystallization of Vps4 hexamer

Although homology modeling based on the p97 D1 structure has provided a useful model for active Vps4 [1; 2; 3], a high resolution experimental structure of the Vps4 hexamer would be very informational, especially as a complex with an ESCRT-III substrate. This structure would provide insight to how Vps4 disassembles the ESCRT-III complexes and guide future studies. There are three different models about the working mechanism of ring-like ATPase: a concerted model, a stochastic model, and a rotary model [4]. Current structures of ring-like ATPases containing the substrate in the central pore support a rotary model [5; 6], although both of these structures are ring-like helicases that act on nucleic acids: rho helicase from *E.coli* and E1 helicase from papillomavirus [5; 6]. There are currently no high resolution structures of AAA+ ATPases bound with their corresponding protein/peptide substrate. Our green crystals of Vps4p and peptide, although still only diffracting to very low resolution, are attractive targets for future optimization because they seem likely to contain a Vps4p hexamer with

a peptide in the central pore (see Chapter 3). The current biochemical data suggest that one functional Vps4 hexamer displays multiple ATP-bound states, including ATP-bound, ADP-bound, and possibly intermediate and empty states. A high resolution structure might support the rotary model of Vps4 function and explain how ATP binding and hydrolysis are coordinated with peptide binding/processing.

I have tried many different strategies to crystallize the Vps4 hexamer. However, Vps4 monomers from multiple species have always crystallized in spirals. Although the Vps4 hexamer can be obtained in the presence of ADP·AlF_x and peptide derived from helix 5 of Vps2, this complex has not yet yielded good crystals. One approach that could be tried would be to obtain more stable Vps4-peptide complex for crystallization. Another attractive strategy would be to focus on the peptide and ADP·AlFx complex using a variety of truncations on the N-terminus and surface entropy reduction mutants of Vps4p.

One possible approach to finding a tighter-binding peptide would be to screen variants of current peptide. For example, alanine screening of peptide C may identify variants with improved binding affinity, and a second round of mutations on selected residues further increase affinity. Another approach would be to sceen peptides from the helix 5 of other ESCRT III proteins. Yet another approach could be to truncate the peptide with highest affinity to identify the shortest peptide that maintains high affinity, because removing regions that are inherently flexible (not binding) can increase the chance of crystallization.

ESCRT-III disassembly by Vps4

Several questions need to be addressed in order to understand how binding of ESCRT-III helix 5 leads to disassembly. First, we have to determine the role of helix 5 in ESCRT-III assembly. Helix 5 has been suggested to be the autoinhibitory because it folds back against the N-terminal helix core in structures of monomeric ESCRT-III subunits [7]. Although the role of helix 5 in the assembled ESCRT-III complexes is not yet established, preliminary cryo-EM studies of ESCRT-III tubes assembled in vitro in Dr. Frost's lab at University of Utah suggest that the helix 5 may serve as an intermolecule bridge in the assembled ESCRT-III complexes. If these findings hold-up, they will imply that disrupting helix 5 structure may be an effective way to trigger ESCRT-III disassembly by disrupting subunit-subunit interactions.

A second important question, is how does the Vps4 hexamer process different ESCRT-III subunits? There are seven different ESCRT-III and ESCRT-III-like proteins in yeast and twelve different proteins in human cells. Although the 3D-structures of different ESCRT-III proteins are predicted to be conserved [8], their sequences are not conserved. The C-terminal fragment of several different ESCRT-III subunits have been shown to activate the ATPase activity of Vps4 [9], which indicate Vps4 should be able to process ESCRT-III proteins of different sequences. The binding assay between the Vps4 hexamer and different ESCRT-III subunits will address the question that whether the Vps4 hexamer binds to certain sequence selectively.

Third, is the whole protein or only C-terminus of ESCRT-III proteins processed by Vps4 hexamer? There is a negatively charged residues patch preceding the N-terminus of helix 5 of Vps2. This patch is conserved among several other ESCRT-III subunits, and we propose that it functions as a stop sign to prevent the N-terminal four helices from being processed by Vps4 hexamer based on our fluorescence anisotropy assay (see Chapter 4). This question can be explored using ESCRT-III complex disassembly/unfolding assays with a variety of ESCRT-III constructs mutations on the negatively charged patch.

Fourth, how is the Vps4-ESCRT-III interaction regulated by the MIT domain? We have found that the interaction between the Vps4 hexamer and helix 5 of Vps2 is autoinhibited by the MIT domain, and that the inhibition can be relieved by an MIM1-MIT interaction. The MIT domain may inhibit the proper hexamerization of Vps4 or physically block the substrate-binding site. Cryo-EM experiment on different wild type Vps4 constructs, including full length Vps4p, ΔMIT-Vps4p, MIM1-Vps4p, MIM1(L225D)-Vps4p, may help to explore the conformational changes induced by the MIT domain and the MIM1-MIT interaction. Another possibility would be to use hydrogen exchange experiments of MIM1-Vps4p and MIM1(L225D)-Vps4p fusion proteins in the presence of $ADP{\cdot}AlF_x$ to identify a possible interface between the MIT domain and the AAA+ ATPase cassette. Cross-linking and mutagenesis experiments might be used to confirm this interface if it can be identified by hydrogen exchange.

Besides MIM1, some of the ESCRT-III proteins that can also interact with the Vps4 MIT domain display a distinctly different MIM2 motif, and the MIM2-MIT

interaction has been shown to be important for HIV budding [10]. The MIM motif of Crenarchaeal ESCRT-III protein interacts with the MIT domain of crenarchaeal Vps4 in a similar way as MIM2 [11]. So, one possibility is to determine if MIT domains are autoinhibitory in archaeal Vps4, and if so, determine if inhibition can be relieved by an MIM2-MIT.

References

1. Gonciarz, M. D., Whitby, F. G., Eckert, D. M., Kieffer, C., Heroux, A., Sundquist, W. I. & Hill, C. P. (2008). Biochemical and structural studies of yeast Vps4 oligomerization. *J Mol Biol* **384**, 878-95.

2. Monroe, N., Han, H., Gonciarz, M. D., Eckert, D. M., Karren, M. A., Whitby, F. G., Sundquist, W. I. & Hill, C. P. (2013). The oligomeric state of the active Vps4 AAA ATPase. *J Mol Biol*.

3. Scott, A., Chung, H. Y., Gonciarz-Swiatek, M., Hill, G. C., Whitby, F. G., Gaspar, J., Holton, J. M., Viswanathan, R., Ghaffarian, S., Hill, C. P. & Sundquist, W. I. (2005). Structural and mechanistic studies of VPS4 proteins. *EMBO J* **24**, 3658-69.

4. Lyubimov, A. Y., Strycharska, M. & Berger, J. M. (2011). The nuts and bolts of ring-translocase structure and mechanism. *Curr Opin Struct Biol* **21**, 240-8.

5. Thomsen, N. D. & Berger, J. M. (2009). Running in reverse: the structural basis for translocation polarity in hexameric helicases. *Cell* **139**, 523-34.

6. Enemark, E. J. & Joshua-Tor, L. (2006). Mechanism of DNA translocation in a replicative hexameric helicase. *Nature* **442**, 270-5.

7. Bajorek, M., Schubert, H. L., McCullough, J., Langelier, C., Eckert, D. M., Stubblefield, W. M., Uter, N. T., Myszka, D. G., Hill, C. P. & Sundquist, W. I. (2009). Structural basis for ESCRT-III protein autoinhibition. *Nat Struct Mol Biol* **16**, 754-62.

8. McCullough, J., Colf, L. A. & Sundquist, W. I. (2013). Membrane fission reactions of the mammalian ESCRT pathway. *Annu Rev Biochem* **82**, 663-92.

9. Merrill, S. A. & Hanson, P. I. (2010). Activation of human VPS4A by ESCRT-III proteins reveals ability of substrates to relieve enzyme autoinhibition. *J Biol Chem* **285**, 35428-38.

10. Kieffer, C., Skalicky, J. J., Morita, E., De Domenico, I., Ward, D. M., Kaplan, J. & Sundquist, W. I. (2008). Two distinct modes of ESCRT-III recognition are required for VPS4 functions in lysosomal protein targeting and HIV-1 budding. *Dev Cell* **15**, 62-73.

11. Samson, R. Y., Obita, T., Freund, S. M., Williams, R. L. & Bell, S. D. (2008). A role for the ESCRT system in cell division in archaea. *Science* **322**, 1710-3.